Deletion of *Cyfip1* in mouse microglia affects microglial actin dynamics, motility and functions, unveiling a dendritic spine maturation defect

Dissertation

zur **Erlangung des Doktorgrades (Dr. rer. Nat.)**

der **Mathematisch-Naturwissenschaftlichen Fakultät**

der **Rheinischen Friedrich-Wilhelms-Universität Bonn**

vorgelegt von

Shu-Farn Wan-Pollak

aus Taipeh, Taiwan

Bonn, 2024

Angefertigt mit Genehmigung der Mathematisch-Naturwissenschaftlichen Fakultät der
Rheinischen Friedrich-Wilhelms-Universität Bonn

Gutachter / Betreuer: Prof. Dr. Gabor Petzold
Gutachter: Prof. Dr. Walter Witke

Tag der Promotion: 2024.09.09
Erscheinungsjahr: 2024

Abstract

Microglia are the innate immune cells in the CNS, serving as the first line of defense in the brain parenchyma. During mouse embryogenesis, microglial progenitor cells originate from the yolk sac and migrate into the CNS via the circulatory system. As the developmental stage progresses, microglia develop ramified and motile processes which constantly survey the brain parenchyma. The high motility allows microglia to respond to insults by migrating to the affected sites, and clear up the pathogens and damage. Moreover, microglia also interact with neuronal synapses with their processes. Microglial motility is driven by the intracellular force generated by actin cytoskeleton rearrangement. Essential to this process is the cytoplasmic fragile-X mental messenger ribonucleoprotein (FMRP) interacting protein 1 (CYFIP1), an essential component of the WAVE regulatory complex (WRC), which activates the ARP2/3 complex to regulate branched actin networks.

In this study, we show that CYFIP1 is the sole CYFIP isoform in microglia, and is highly expressed compared to the other cell types in the CNS. We determine that microglia possess a unique WRC, which is composed of CYFIP1, HEM1, WAVE2 and ABI3, and that depleting CYFIP1 leads to the loss of all other WRC components. We then show that in the absence of CYFIP1, microglial branching is reduced and microglial homeostasis is impaired in the mouse brain. We also, for the first time, identify the molecular role of the CYFIP1-WRC in microglial actin dynamics, as a regulator of the dynamic filamentous actin formation, which is involved in microglial phagocytosis, migration and membrane ruffling. Indeed, the absence of the CYFIP1-WRC disrupted lamellipodium formation and impaired microglial directional migration. Interestingly, in the brain of *Cyfip1* conditional knockout mice, there was an unexpected alteration in dendritic spine maturation in layer V pyramidal neurons of the mouse cortex.

In summary, in this study we demonstrate the pivotal role of the CYFIP1-WRC in microglial homeostasis, motility and phagocytic function. Exploring the role of CYFIP1-dependent actin dynamics on the interaction of microglia with synapses and its significance for the establishment of neuronal circuits are intriguing topics for future research.

Table of Contents

List of Figures

List of Tables

List of Abbreviations

Ab	Antibody
ABI	Abl interactor
ABP	Actin binding protein
ADP	Adenosine diphosphate
ACM	Astrocyte-conditioned medium
ACSA2	Astrocyte cell surface antigen 2
AGM	Aorta-gonads-mesonephros
ANOVA	Analysis of variance
APS	Ammonium persulfate
ARP	Actin-related protein
ARPC	Actin-related protein 2/3 complex subunit
ASD	Autism spectrum disorder
ATP	Adenosine triphosphate
a.u.	Arbitrary units
BDNF	Brain-derived neurotrophic factor
bp	Base pairs
BSA	Bovine serum albumin
°C	Degree celsius
C_c	Critical concentration
CA1	Cornu Ammonis 1
CAPG	Capping protein, gelsolin-like
CD	Cluster of differentiation
CCL	CC-chemokine ligand
CNS	Central nervous system
COBL	Cordon-bleu
CR	Complement receptor
CSF1	Colony-stimulating factor 1
CSF1R	Colony-stimulating factor 1 receptor
CTRL	Control

CX3CL1	Chemokine (C-X3-C motif) ligand 1
CX3CR1	Chemokine (C-X3-C motif) receptor 1
CYFIP	Cytoplasmic FMR1 interacting protein
DAMP	Danger-associated molecular pattern
DAPI	4',6-diamidino-2-phenylindole
DISC1	Disrupted-in-schizophrenia 1
DIV	Days in vitro
DMEM	Dulbecco's modified Eagle medium
DMSO	Dimethyl sulfoxide
DNA	Deoxyribonucleic acid
dLGN	Dorsal lateral geniculate nucleus
dNTPs	Deoxynucleotide triphosphates
DPBS	Dulbecco's phosphate-buffered saline
E	Embryonic day
ECL	Enhanced chemical luminescence
E.coli	Escherichia coli
ECM	Extracellular matrix
EDTA	Ethylenediamine tetraacetic acid
EGTA	Ethylene glycol tetraacetic acid
eIF4E/A/G	Eukaryotic translation initiation factor 4E/A/G
EMP	Erythromyeloid progenitor
Et al	Et alii (and others)
FACS	Fluorescence-activated cell sorting
F-actin	Filamentous actin
FAK	Focal adhesion kinase
FBS	Fetal bovine serum
FH	Formin homology
flx	Floxed allele
Fmr1	Fragile X messenger ribonucleoprotein 1
FMRP	Fragile X messenger ribonucleoprotein

FXR1P	Fragile X related protein 1
G-actin	Globular actin
GFAP	Glial fibrillary acidic protein
GTP	Guanosine-5'-triphosphate
HBSS	Hank’s buffered saline solution
H&E	Hematoxylin and eosin
HEM1	Hematopoietic protein 1
HEPES	4-(2-hydroxyethyl)-1-piperazineethanesulfonic acid
hr	Hour
HRP	Horseradish peroxidase
HSC	Hematopoietic stem cell
HSP	Heat shock protein
HSPC300	Hematopoietic stem/progenitor cell protein 300
IBA1	Ionized calcium-binding adapter molecule 1
IFN	Interferon
Ig	Immunoglobulin
IGF	Insulin-like growth factor
IL	Interleukin
IRF8	Interferon regulatory factor 8
JMY	Junction-mediating and regulatory protein
KCl	Potassium chloride
kDa	Kilodalton
KO	Knockout
LCCM	L929 cell-conditioned medium
LMOD	Leimodin
LPS	Lipopolysaccharide
LSM	Laser scanning microscope

M1/M2	Classically activated macrophages/Alternatively activated macrophages
MACS	Magnetic-activated cell sorting
MeOH	Methanol
MBP	Myelin basic protein
MEF	Mouse embryonic fibroblast
mg	Milligram
ml	Milliliter
MHC	Major histocompatibility complex
MMP	Matrix metalloproteinase
mRNA	Messenger RNA
MP	Myeloid precursor
MYB	Myeloblastosis
NAP1	NCK-associated protein 1
NAP1L	NCK-associated protein 1 like
NeuN	Neuronal nuclear protein
NFκB	Nuclear factor 'kappa-light-chain-enhancer' of activated B-cells
NPF	Nucleation-promoting factor
NRG1	Neuregulin 1
N-WASP	Neural WASP
OH	Hydroxyl-
OPC	Oligodendrocyte precursor cell
P	Postnatal
PAGE	Polyacrylamide gel electrophoresis
PBS	Phosphate-buffered saline
PAMP	Pathogen-associated molecular pattern
PCD	Programmed cell death
PCR	Polymerase chain reaction

PFA	Paraformaldehyde
PHEM	PIPES, HEPES, EDTA, $MgCl_2$
P_i	Inorganic phosphate
PIPES	1,4-Piperazinediethanesulfonic acid
PIR121	p53-inducible RNA, 121F-specific
PLL	Poly-L-lysine hydrobromide
POP	Partner of profilin
P/S	Penicillin-streptomycin
PS	Phosphatidylserine
PSD	Postsynaptic density
PVDF	Polyvinylidene fluoride
RAC1	RAS-related C3 botulinum toxin substrate 1
RGC	Retinal ganglion cell
RHOA	RAS homolog gene family A
RNA	Ribonucleic acid
ROI	Region of interest
rpm	Revolutions per minute
SCZ	Schizophrenia
SDS	Sodium dodecyl sulfate
SIRP	Signal regulatory protein
SRA	Specifically RAC1-associated protein
ssRNA	Single-stranded RNA
STAT1	Signal transducer and activator of transcription 1
SVZ	Subventricular zone
TAE	Tris, acetic acid, EDTA (buffer)
TEMED	Tetramethylethylenediamine
TGF	Transforming growth factor
TLR	Toll-like receptor
TNF	Tumor necrosis factor
Tris	Tris(hydroxymethyl)aminomethane

Triton X-100	2-[4-(2,4,4-trimethylpentan-2-yl)phenoxy]ethanol
Tween-20	Poly(oxyethylene)20-sorbitan monolaurate
UDP	Uridine diphosphate
UTP	Uridine triphosphate
UV	Ultraviolet
VCA	veprolin-homology domain, cofilin-homology/central domain, acidic domain
VGLUT	Vesicular glutamate transporter
v/v	Volume/volume
WASH	Wiskott-Aldrich syndrome protein and SCAR homologue
WASP	Wiskott-Aldrich syndrome protein
WAVE	WASP family verprolin-homologous protein
WH2	WASP homology 2 (domain)
WRC	WAVE regulatory complex
WT	Wild-type
w/v	Weight/volume
YS	Yolk sac
μg	Microgram
μl	Microliter
μM	Micromolar

Chapter 1. Introduction

1.1. Microglia

The term “glia” came from the ancient Greek word for glue. Glia were originally believed to be matrix fibers which held neurons together, until in 1895 Michael von Lenhossek argued that glia were cells instead of matrix fibers and termed the glial cells astrocytes. In the second decade of the 20th century, Pío del Río-Hortega invented a novel ammoniacal silver carbonate staining technique. By using this staining technique, del Río-Hortega was the first person to identify microglia as well as the first to distinguish microglia from macroglial cells (astrocytes and oligodendrocytes) based on the small cell body size of microglia (Sierra *et al*, 2016). Del Río-Hortega proposed that microglia originated in the mesoderm and invaded the brain parenchyma during early development. In the mature brain, microglia displayed highly ramified cell morphology (Figure 1.1) and appeared to have their territory. He also stated that microglia had migratory and phagocytic ability (Kettenmann *et al*, 2011). Many of del Río-Hortega’s findings were confirmed afterwards (Barron, 1995; Kerschman, 1939; Rezaie & Male, 2002) and remain valid until today.

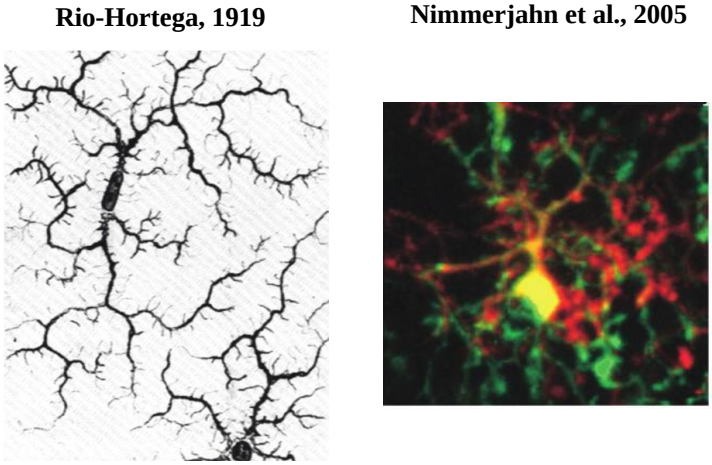

Figure 1.1: Del Río-Hortega’s illustration of microglial cells (left) and highly dynamic microglia in the homeostatic state in vivo shown by Nimmerjahn et al. (right)
In the image from Nimmerjahn et al., green color indicates microglial process elongation, whereas red color labels process retraction **(**Nimmerjahn *et al*, 2005**;** Sierra *et al.*, 2016**)**.

Nowadays, microglia are widely known as the predominant innate immune cells in the CNS. They constitute 0.5 - 16 % of the total cell population in the human brain **(**Mittelbronn *et al*, 2001**)** and roughly 10 % in the adult mouse brain **(**Lawson *et al*, 1992**)**. For a long time, microglia were thought to be the passive immune defender of the CNS. They express several

macrophage-related receptors and markers including CX3CR1, CD68, CD11b and IBA1 **(**Jurga *et al*, 2020**)**. In the healthy brain, homeostatic microglia with ramified morphology were assumed to be in a resting state. Upon sensing the pathogenic signals, microglia transform their morphology by shrinking their processes, migrate towards the insult, clear the pathogens or damaged cells, and repair the tissue **(**Vilhardt, 2005**)**. The theory of resting microglia was amended when Nimmerjahn et al. proved that ramified microglia, rather than resting in the healthy brain, actively inspect their microenvironment by constantly moving their motile processes back and forth **(**Nimmerjahn *et al.*, 2005). Microglia also participate in shaping neuronal circuits through interacting with dendritic spines of neurons in an experience-dependent manner **(**Paolicelli *et al*, 2011**;** Tremblay *et al*, 2010**;** Wake *et al*, 2009**)**.

1.1.1. Microglia origin

Since the discovery of microglia, their origin has been intensely debated. In the last decades, scientists have used different mouse models to address whether embryonic microglia originate from ectoderm or mesoderm **(**de Groot *et al*, 1992**;** Fedoroff *et al*, 1997**;** Hao *et al*, 1991**;** McKercher *et al*, 1996**)**. Among all, the *Spi1* (also known as *PU.1*) knock-out mouse model validated del Río-Hortega's mesodermal theory of microglia's origin **(**McKercher *et al.*, 1996**)**: mice with *Spi1* deletion were devoid of microglia **(**Beers *et al*, 2006**;** McKercher *et al.*, 1996**)**. Since SPI1/PU.1 is a transcription factor exclusively expressed in hematopoietic cells **(**Moreau-Gachelin, 1994**)**, this established the hematopoietic origin of microglia and indicated their ontogenetic relationship to macrophages.

Despite the consensus of hematopoietic (myeloid) origin of microglia, there were still many disputes regarding the exact nature of microglial progenitors. Many scientists, including del Río-Hortega, were unsure whether microglia emerged from primitive macrophages during embryonic development or from the circulating blood monocytes, which penetrated into the neonatal brain parenchyma (del Rio-Hortega, 1939). Perry et al., using histochemical methods, discovered that microglia in the brain of embryonic day 16 (E16), postnatal day 5 (P5) and adult mice expressed F4/80, a monocyte marker **(**Perry *et al*, 1985**)**. They identified circulating monocytes as the source of microglia, and proposed that dying neurons and axons during the development attracted monocytes to migrate into the brain. They believed that monocytes differentiated into microglia after they invaded the brain parenchyma. Although their hypothesis was later proven to be inaccurate, their discovery revealed that microglia already

reside in the brain before birth, indicating that microglial precursors originate from embryonic hematopoiesis rather than bone marrow hematopoiesis.

Mouse embryonic hematopoiesis

During mouse embryogenesis, hematopoiesis occurs in two locations: the extra-embryonic yolk sac (YS) for primitive hematopoiesis and fetal liver for definitive hematopoiesis (Figure 1.2) **(**Orkin & Zon, 2008**)**. Primitive hematopoiesis in mice takes place between E7.5 and E8. During this time period, primitive erythromyeloid progenitors (EMPs) are produced in the blood islands of the yolk sac **(**Bertrand *et al*, 2005**;** Palis *et al*, 1999**)**. After the circulatory system is established, at E9.5 to E10.5 EMPs differentiate into primitive macrophages, and migrate into several tissues through the blood vessels **(**McGrath *et al*, 2003**)**. Therefore, primitive macrophages invade and colonize the developing brain at mid-gestation, eventually transforming into embryonic microglia (Figure 1.2) **(**Alliot *et al*, 1999**;** Alliot *et al*, 1991**)**. Embryonic microglia express several myeloid markers such as C-X3-C motif chemokine receptor 1 (CX3CR1), F4/80, and colony-stimulating factor 1 receptor (CSF1R) **(**Kierdorf *et al*, 2013**)**. Embryonic microglia exhibit strong proliferative capacity, which contributes to the expansion of their local population in the brain parenchyma **(**Sorokin *et al*, 1992**)**.

Definitive hematopoiesis begins around E10.5 in the aorta-gonads-mesonephros (AGM) region and continues at E12.5 in fetal liver, which by then becomes the primary organ for hematopoiesis **(**Kumaravelu *et al*, 2002**;** Naito *et al*, 1990**)**. Hematopoietic stem cells (HSCs) generated from fetal liver differentiate into myeloid precursors (MPs), which eventually become monocytes. Monocytes entering the circulatory system populate all tissues, except the brain, due to the already formed blood brain barrier (Figure 1.2). However, it is believed that perivascular and choroid plexus macrophages in the CNS are derived from circulating monocytes **(**Ginhoux *et al*, 2013**;** Prinz & Priller, 2014**)**. Schulz et al. demonstrated that HSCs rely on the transcription factor MYB, whereas yolk sac macrophages do not, and the embryonic brains of mice lacking MYB have normal microglial density **(**Schulz *et al*, 2012**)**. This groundbreaking discovery highlighted the distinctions between primitive and definitive hematopoiesis, and confirmed that microglia are the progeny of yolk sac-derived macrophages **(**Schulz *et al.*, 2012**)**.

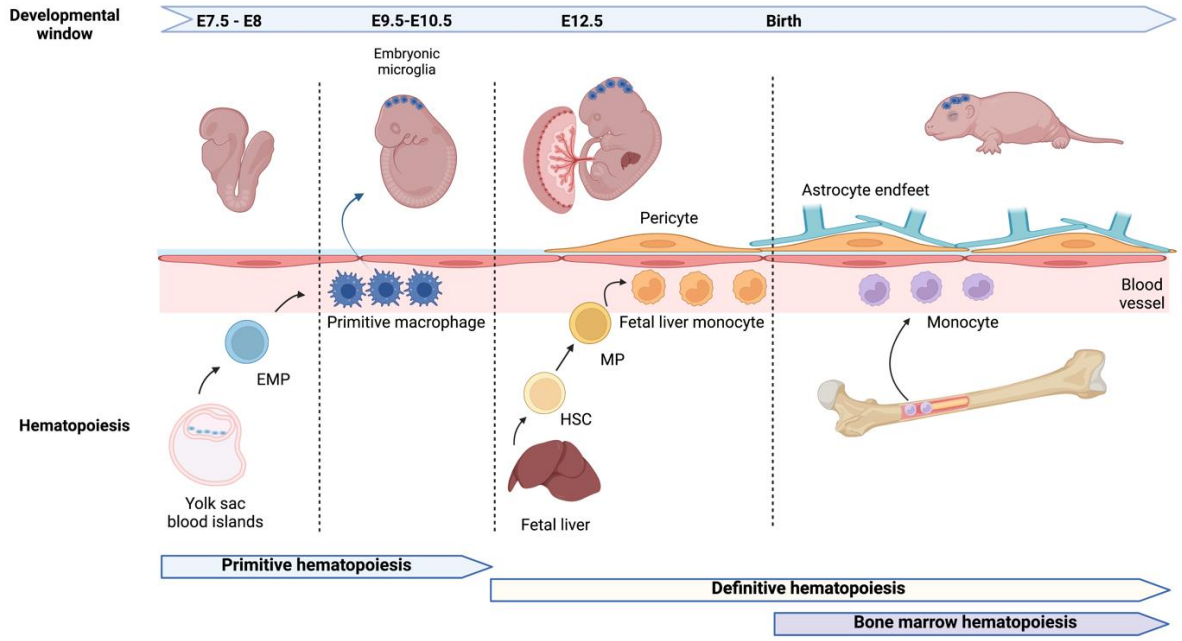

Figure 1.2: Microglial origin and hematopoietic development in mouse embryo
This figure illustrates the genesis of microglia as well as different sources of hematopoiesis during mouse embryonic and postnatal development. Primitive hematopoiesis happens between E7.5 and E10.5. During this period, erythromyeloid progenitors (EMPs) leave blood islands of the yolk sac and differentiate into primitive macrophages. Microglia are formed when primitive macrophages invade and colonize the embryonic brain via the circulatory system. Definitive hematopoiesis happens mainly in the fetal liver. At E12.5, myeloid precursors (MPs) derived from hematopoietic stem cells (HSCs) develop into monocytes and exit the fetal liver. Around the same time, the blood brain barrier develops in the embryonic brain, which restricts circulating monocytes from infiltrating into the brain parenchyma. After birth, the major hematopoietic site switches to bone marrow, where MPs and monocytes continue to be generated.

1.1.2. Microglia in the developing brain

As previously mentioned, microglial precursor cells (primitive macrophages) enter the brain through blood vessels and colonize the brain parenchyma through migration and proliferation. The process of their entry into the brain may be facilitated by the adhesion molecules on the endothelial cells of the blood vessels **(**Charabati *et al*, 2020**;** Mosser *et al*, 2017**)**. After entering the brain, embryonic microglia must proliferate and migrate to their final destination, where they mature into ramified microglia. Several signaling pathways have been identified as responsible for the chemotactic migration of embryonic and postnatal microglia. Microglia navigate to specific regions in the brain by following chemoattractant gradients such as CSF1, ATP, UDP and CX3CL1.The colony-stimulating factor 1 (CSF1) has been demonstrated to specifically bind to the CSF1 receptor (CSF1R), which in the brain is exclusively present on microglia. This pathway promotes the infiltration of embryonic microglia into the

subventricular zone of the cortex and facilitates the proliferation of embryonic microglia in the cerebral parenchyma **(**Lelli *et al*, 2013**;** Navascués *et al*, 2000**)**. To enable migration and expansion of their population, embryonic microglia also release matrix metalloproteinase 8 (MMP8) and MMP9, which remodel the extracellular matrix **(**Kierdorf *et al.*, 2013**)**.

Throughout the course of embryonic and postnatal development, the CNS goes through significant waves of cell death, known as programmed cell death (PCD). This apoptotic process is responsible for eliminating cells and it is essential for maintaining tissue balance and proper formation of neuronal circuits **(**Mosser *et al.*, 2017**;** Nguyen *et al*, 2021**)**. During the early stage of apoptosis, the dying neurons release soluble chemoattractants which function as "find-me" signals, attracting microglia towards them **(**Marín-Teva *et al*, 2011**)**. Some classical "find-me" signals include adenosine triphosphate (ATP), uridine diphosphate (UDP) and CX3C motif chemokine ligand 1 (CX3CL1, also known as fractalkine). They attract microglia to the apoptotic neurons by binding to the specific receptors on microglial surface, respectively $P2Y_{12}$, $P2Y_6$, and CX3CR1 receptors **(**Haynes *et al*, 2006**;** Honda *et al*, 2001**;** Inoue, 2007**;** Koizumi *et al*, 2007**;** Sokolowski *et al*, 2014**;** Yu *et al*, 2022**)**. When microglia are attracted to the vicinity of the apoptotic neuron, phagocytosis is initiated through the binding of "eat-me" signals, such as phosphatidylserine, complement component 1q (C1q), and complement component 3 (C3), which are present on the plasma membrane of apoptotic neurons, to the corresponding receptors on the microglial surface. These receptors include the TAM (TYRO3, AXL, MMER) receptor tyrosine kinases, CD93, and complement receptor type 3 (CR3) **(**Elliott & Ravichandran, 2010**;** Färber *et al*, 2009**;** Schafer & Stevens, 2015**;** Smolders *et al*, 2019**)**. The binding of "eat-me" signals to microglial receptors facilitates the engulfment and clearance of the dying neurons by microglia during brain development.

Following the embryonic colonization of the brain parenchyma and subsequent postnatal proliferation, microglia undergo specific phases of differentiation, which are dependent on the signals derived from the maturing CNS. Among all the signals, transforming growth factor beta (TGFβ) is crucial for the postnatal maturation and development of microglia **(**Spittau *et al*, 2020**;** Thion *et al*, 2018**;** Wurm *et al*, 2021**;** Zöller *et al*, 2018**)**. Attaai et al. demonstrated that during the mouse early postnatal stage (P0 – P14), microglia possess an amoeboid-like morphology and exhibit high levels of phagocytic activity. However, at a later postnatal stage (P14 – P28), microglia transform into a typical ramified morphology, indicating a shift from activated microglia to homeostatic microglia. This transformation is mediated by the TGFβ1

signaling pathway between neurons and microglia **(**Attaai *et al*, 2018**)**. The proper development of postnatal microglia into mature microglia, characterized by ramified and dynamic processes, has been shown to be associated with their role in surveying the synaptic microenvironment and refining neural circuits (Miyamoto *et al*, 2013; Paolicelli & Ferretti, 2017).

1.1.2.1. Microglia and synapse interactions

Neuronal synapses are specialized junctions enabling communication between two neurons interconverting electrical signals (action potentials) into chemical signals (neurotransmitter release) and back into electrical signals (opening of ion channel). They are composed of a presynaptic and a postsynaptic terminal and establish neural circuits. Neuronal synapses are dynamic and can be modified by the neurons themselves or by glial cells in response to changes in neuronal activity. While previous research on synapses has focused on the tripartite synapse model, which includes neuronal pre- and post-synapsis and astrocytic processes, recent findings have shown that the initial wave of synaptogenesis in mice happens around E14, when microglia are the only glial cells present in the brain **(**Kettenmann *et al*, 2013**;** Reemst *et al*, 2016**)**. This suggests a contribution of microglia in synapse formation during embryonic development. Furthermore, microglia have been proposed to continue to contribute to synapse sculpting during postnatal development and early adulthood through various mechanisms, including contacting synapses with their motile processes, secretion of soluble molecules and remodeling of extracellular matrix (ECM) (Figure 1.3) **(**Andoh & Koyama, 2021**)**.

In a study conducted by Miyamoto et al., it was shown that during the early postnatal period (P8 – P10), in the mouse somatosensory cortex, microglia make contact with neuronal dendrites through their processes, causing a transient local increase in Ca^{2+} influx. This led to an accumulation of actin, which ultimately resulted in the formation of dendritic spines (Figure 1.3 A) **(**Miyamoto *et al*, 2016**)**. Another study from Weinhard et al. also showed that microglia in the hippocampal CA1 region briefly but repeatedly contacted the same dendritic spine, inducing the formation of filopodia on the spine head. These microglia-induced spine head filopodia were more likely to develop the spine into forming stable synapses **(**Weinhard *et al*, 2018**)**. In addition to physical contact using their processes, microglia can also stimulate the formation of dendritic spines by releasing soluble factors such as brain-derived neurotrophic factor (BDNF) and interleukin 10 (IL10) (Figure 1.3 B). The absence of microglial BDNF was reported to reduce learning-dependent spine formation in the motor cortex of juvenile mice

(P30 and P60), suggesting that microglia secrete BDNF to promote spine formation **(**Parkhurst *et al*, 2013**)**.

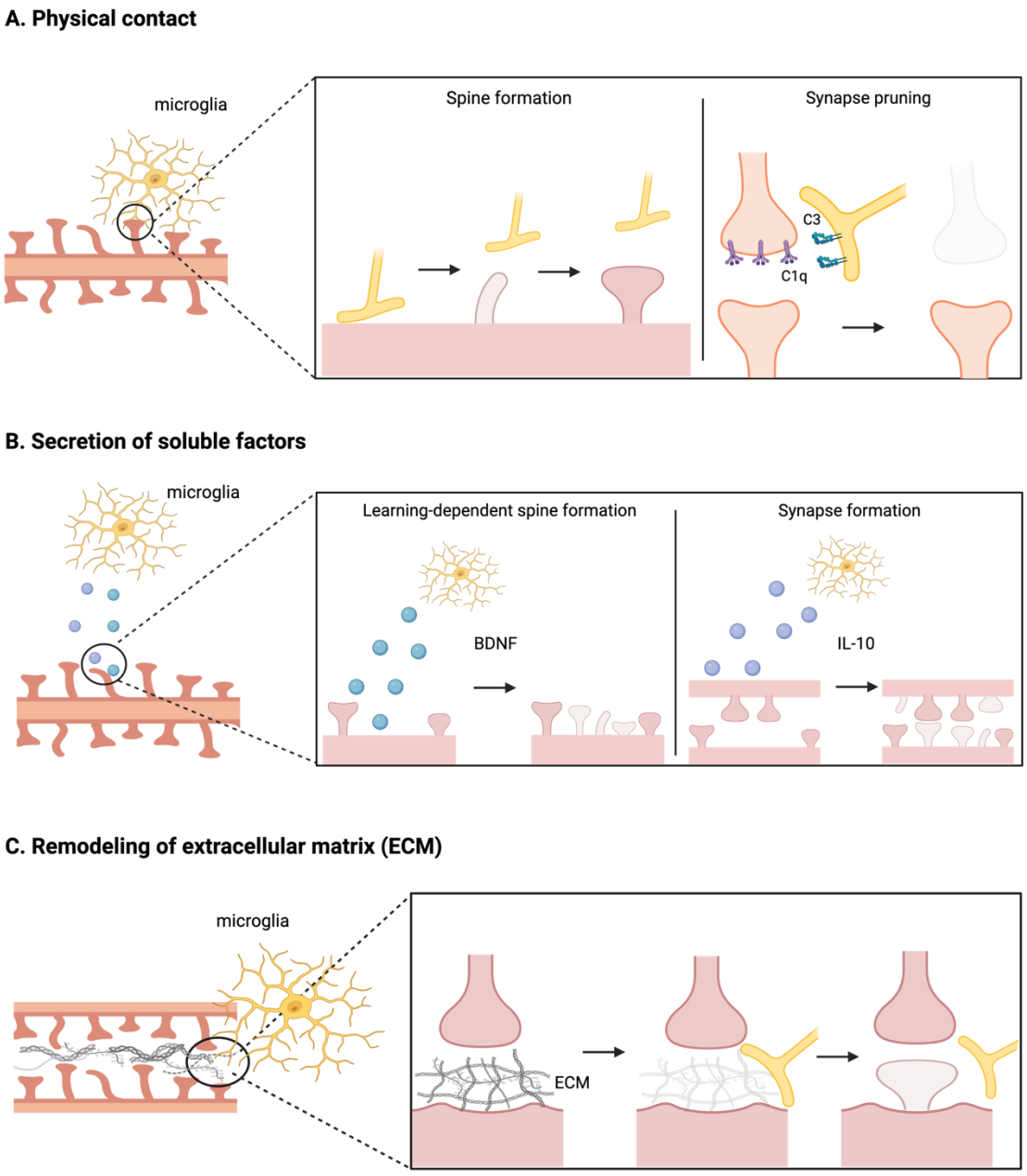

Figure 1.3: Mechanisms of microglia and synapse interaction
(A) Physical contact of microglial processes with dendritic shafts and spines can induce actin accumulation at the contact point, which further leads to the formation of filopodia with the high potential to mature into spines. Microglia also prune less active synapses via recognizing complement factor signals through complement receptors (CR3) on their processes. **(B)** Microglia secrete soluble factors that can stimulate the development of spines and synapses. Microglial BDNF promotes learning-associated spine formation, and microglial IL10 promotes synapse formation. **(C)** Microglia can digest the extracellular matrix (ECM) surrounding synapses in response to neuronal signals, creating space for spine formation.

Microglial IL10 has also been found to be a key factor in the development of both excitatory and inhibitory synapses in primary cortical and hippocampal neurons from rats **(**Lim *et al*, 2013**)**. In recent years, there has been a growing recognition that the extracellular matrix (ECM) surrounding synapses play a significant role in synaptic plasticity (Figure 1.3 C). Nguyen et al. showed that microglia in the dentate gyrus can facilitate experience-dependent spine formation by degrading the ECM around the synapse through neuronal IL33 signaling **(**Nguyen *et al*, 2020**)**.

Microglia might play a dual role in shaping neural circuits, as they are not only responsible for inducing spine formation, but have been suggested to also participate in pruning synaptic marterial during brain development. Schafer et al. proposed that microglia eliminate synapses through activity- and complement-dependent mechanisms. They observed that in the dorsal lateral geniculate nucleus (dLGN) microglia engulfed less presynaptic materials from the more active retinal ganglion cells (RGC). Also, in P5 mice lacking complement 3 (C3) or complement receptor 3 (CR3), microglia were found to engulf significantly reduced amount of RGC presynaptic material when compared to their WT littermates **(**Schafer *et al*, 2012**)**. In addition to complement pathways, local externalization of phosphatidylserine (PS) on the surface of pre-synapses, which serves as another "eat-me" signal of neurons, was also shown to play a role in regulating synapse pruning by microglia in the dLGN of P5 mice and hippocampal CA1 of P10 mice **(**Scott-Hewitt *et al*, 2020**)**. On the other hand, in the dLGN of P5 mice, the membrane expression of CD47, which functions as "don't-eat-me" signal, on the active synapses can protect the functional synapses from being excessively eliminated by microglia. This is mediated by CD47 binding to its corresponding receptor, signal regulatory protein α (SIRPα), on microglia **(**Lehrman *et al*, 2018**)**. It is possible that in the postnatal period, complement signaling and CD47 act in a coordinated manner to regulate the development of neural circuits.

1.1.2.2. Microglia and neurodevelopmental disorders

Synapses serve as communication sites between neurons in the brain and they are fundamental for the formation and function of neural circuits. Disturbance in synapse formation and elimination have been linked to various neurodevelopmental disorders. Growing evidence suggests that disturbed synapse pruning by microglia during development is associated with autism spectrum disorders (ASD) and schizophrenia (SCZ).

Autism spectrum disorders (ASD)

ASD is a group of neurodevelopmental disorders, such as Asperger syndrome, childhood disintegrative disorder, and certain monogenic syndromes like Rett syndrome, fragile X syndrome, and Prader-Willi syndrome **(**Grafodatskaya *et al*, 2010**;** Hosseini & Molla, 2023**)**. The global prevalence of ASD is approximately 1 % among children, with a 4:1 male-to-female ratio **(**Zeidan *et al*, 2022**)**. The manifestations of ASD are heterogenous and include repetitive behaviors, impaired social interaction, and communication deficits. Although the exact cause of ASD is still unclear, human and animal studies have shown that both genetic and environmental factors contribute to the development of ASD by altering neuronal circuit development and disrupting synapse maturation during critical periods of brain development **(**Sauer *et al*, 2021**)**.

ASD is characterized by neuropathological features, such as increased brain volume, higher spine density and abnormal morphology of microglial cells during development **(**Elder *et al*, 2008**;** Hardan *et al*, 2006**;** Hutsler & Zhang, 2010**;** Morgan *et al*, 2010**)**. Considering that many of the risk genes for ASD are related to synapses, and given that microglia are thought to play a crucial role in synapse remodeling during development, various animal studies have been carried out to explore whether dysfunctional pruning of synapses by microglia could be responsible for causing ASD **(**Koyama & Ikegaya, 2015**)**. The *Fmr1* KO mouse has been proposed as a model for studying ASD. *Fmr1* KO mice exhibit some aspects of ASD-like behavior, including altered social and persistent behaviors **(**Bernardet & Crusio, 2006**)**. Recent research has shown that in adult mice, the deletion of *Fmr1* results in an increase in spine density in CA1 pyramidal neurons. This increase was proposed to be associated with reduced engulfment of post-synapses by microglia **(**Jawaid *et al*, 2018**)**. A different study, employing an ASD mouse model induced by maternal immune activation, showed reduced social interaction and increased repetitive behavior, and impaired pruning of excitatory synapses by microglia **(**Andoh *et al*, 2019**)**.

Schizophrenia

Schizophrenia is a psychiatric disorder characterized by a variety of psychotic symptoms. The positive symptoms include hallucinations, delusions and thought and movement disorder, whereas negative symptoms include inappropriate emotional responses, speech reduction or muteness, and extreme apathy **(**Correll & Schooler, 2020**)**. Schizophrenia can be accompanied by cognitive dysfunction, including attention, concentration and memory loss. It is estimated

that schizophrenia affects about 1 % of the population globally, with a slightly higher male-to-female ratio of 1.4:1 **(**Li *et al*, 2022**)**. Numerous genetic factors have been linked to schizophrenia, with many of them being associated with synaptic function and microglial pruning of synapses. For instance, *disrupted-in-schizophrenia 1* (*DISC1*), *neuregulin 1* (*NRG1*) and *complement component 4* (*C4*) have been found to play a role in the development of schizophrenia **(**Sachs *et al*, 2005**;** Sekar *et al*, 2016**;** Stefansson *et al*, 2004**)**. Postmortem brains of schizophrenic patients exhibit distinctive features, including reduced grey matter and decreased density of dendritic spines in the cortex **(**Parker & Sweet, 2017**;** Wong & Van Tol, 2003**)**. These abnormalities have been proposed to be a consequence of excessive pruning by microglia (Sellgren *et al*, 2019). Overactive microglia in the brain might result in the destruction of healthy synaptic connections, leading to the anatomical phenotype and the cognitive and behavioral symptoms associated with schizophrenia.

According to a study conducted in postmortem human brains, individuals with schizophrenia demonstrated increased *C4* mRNA levels in various brain regions such as cortex, cerebellum and corpus callosum. In addition, a substantial portion of the C4 colocalized with pre- and postsynaptic markers (VGLUT1/2 and PSD95), indicating that C4 is mainly produced by neurons and localized in the synapses **(**Sekar *et al.*, 2016**)**. Another recent study utilizing a coculturing system of neuronal and microglial cells derived from schizophrenic patients and healthy controls revealed that microglia derived from the schizophrenic patients engulf a significantly higher amount of postsynaptic material, PSD95. The increased engulfment of microglia derived from schizophrenic patients was partially attributed to increased C3 expression in dendritic spines (Sellgren *et al.*, 2019). In conclusion, disruption in synapse remodeling by microglia might affect proper refinement of neural circuits. Briefly, insufficient synaptic pruning might be associated with ASD, whereas excessive pruning might be linked to schizophrenia.

1.1.3. Microglia as the primary innate immune cells in the CNS

Besides contributing to the establishment of neuronal connectivity during CNS development, microglia as the primary innate immune cells in the CNS, also serve as the first line of defense in the brain. They express several types of receptors on their dynamic processes, which allow them to continually scan the brain parenchyma for signs of damage and infection. When encountering insults, microglia respond in two ways. Firstly, they release cytokines to initiate

an immune response. Secondly, they migrate to the damaged sites and clear up the foreign invaders or the damaged cells, ensuring the homeostasis in the brain.

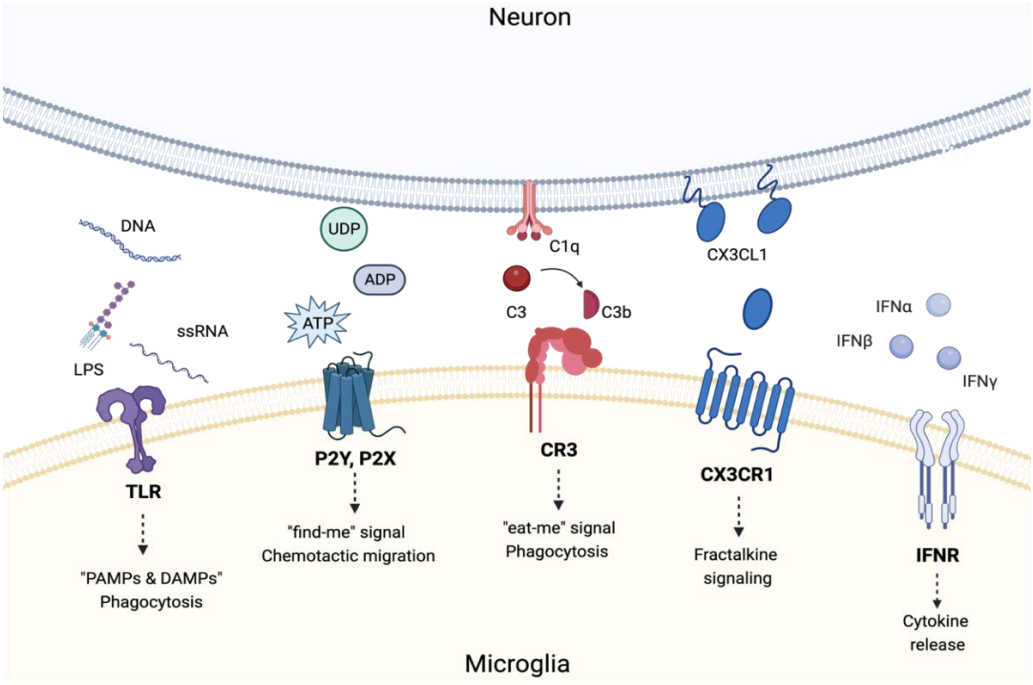

Figure 1.4: Key microglial receptors and their corresponding ligands, as well as the downstream functions

Microglia possess a wide range of receptors that enable them to perform their innate immune functions. Toll-like receptors (TLRs) allow microglia to detect pathogen-associated molecular patterns (PAMPs) and damage-associated molecular patterns (DAMP), such as viral ssRNA, nucleic acids, and LPS, triggering downstream phagocytic signaling. Purinergic receptors (P2Y, P2X) are capable of recognizing extracellular nucleotides such as ATP, UTP and UDP. These nucleotides are released from damaged cells and act as "find-me" signals mediating microglial chemotactic movements. Complement receptor 3 (CR3) identifies C3b, which serves as "eat-me" signal on inactive synapses or dying cells, triggering the process of phagocytosis to eliminate the targets. Fractalkine receptors (CX3CR1) mediate microglial chemotactic movements via binding of fractalkine released from neurons. Interferon receptors (IFNARs and IFNGRs) recognize interferon cytokines (IFNα, IFNβ and IFNγ), leading to the activation of anti-viral responses and the release of inflammatory cytokines.

For example, microglia can recognize various pathogen-associated molecular patterns (PAMPs) such as lipopolysaccharide (LPS) from bacteria, single-stranded RNA (ssRNA) from viruses, and protozoal products, like proteins, lipids, nucleic acids, via toll-like receptors (TLRs) **(**Facci *et al*, 2014**;** Lehnardt, 2010**)**. TLRs are a group of pattern recognition receptors (PRR) located on the plasma membrane or the membrane of intracellular organelles (Figure 1.4). They can detect invading pathogens or endogenous damage signals which trigger innate immune responses. Human microglia possess 10 TLRs (TLR1 – TLR10), whereas rodent microglia possess 12 TLRs (TLR1 – TLR9, TLR11 and TLR13) **(**Kawasaki & Kawai, 2014**)**. Activation of TLRs triggers the downstream NF-kB signaling cascade, and eventually results in the release

of pro-inflammatory cytokines **(**Newton & Dixit, 2012**)**. TLRs can also detect damage-associated molecular patterns (DAMPs), such as RNA or heat shock proteins (HSP) released by damaged cells **(**Piccinini & Midwood, 2010**)**.

Besides TLRs, microglia also possess groups of purinergic receptors, including G-protein-coupled metabotropic P1 adenosine receptors, G-protein-coupled metabotropic P2Y purinoreceptors, and ionotropic P2X purinoreceptors. Extracellular nucleotides, such as ATP and the pyrimidine derivative UDP, are released from damaged cells, binding to and activating the purinoreceptors (Figure 1.4). Acting as DAMPs, they serve as "find-me" signals for microglia, initiating signaling cascades which mediate microglial chemotaxis, phagocytic functions and cytokine release **(**Hu & Gao, 2021**;** Jiang & Roger, 2020**;** Kettenmann *et al.*, 2011**)**. Complement type 3 receptor (CR3), also known as integrin $\alpha_M\beta_2$ or CD11b/CD18, and Fc receptors are also major mediators of microglial phagocytosis (Figure 1.4). CR3 on microglia can recognize the C1q-dependent localization of C3b on the apoptotic cells or inactive neuronal synapses, whereas the Fc receptors on microglia can recognize targets that are tagged with immunoglobulin G (IgG) antibodies **(**Abd-el-Basset & Fedoroff, 1994**;** Fraser *et al*, 2010**;** Schafer *et al.*, 2012**)**. The activation of CR3 and Fc receptors initiates downstream signaling cascades, which ultimately lead to the engulfment of the targets. The engulfment involves the reorganization of the actin cytoskeleton, which is typically achieved through the signaling of the RHO-family of small GTPases **(**Aloisi, 2001**;** Brown & Neher, 2014**)**.

Besides the receptors mentioned above, microglia also possess a wide range of receptors which shape the innate immune functions of microglia by recognizing various types of cytokines and chemokines. To name a few, microglial fractalkine receptors (CX3CR1) mediate microglial chemotactic movement through the binding of the fractalkine (CX3CL1) released from neurons (Figure 1.4). Microglia express both types of interferon receptors: type I interferon receptor (IFNAR) which recognize IFNα and IFNβ (Figure 1.4), and type II interferon receptor (IFNGR) which recognizes IFN γ **(**McDonough *et al*, 2017**)**. Activation of IFNRs leads to phosphorylation of the transcription factor STAT1, which then enters the cell nucleus and activates genes related to anti-viral response and inflammation **(**Platanias, 2005**)**.

1.1.3.1. Microglial morphology

In the adult mouse and human brain, microglia possess a ramified morphology under homeostatic conditions (Figure 1.5 A). This allows microglia to maintain brain homeostasis by

constantly surveying the brain parenchyma with their dynamic processes. When microglia detect signals in the surveyed extracellular environment, they are capable of changing their morphology (summarized in Figure 1.5).

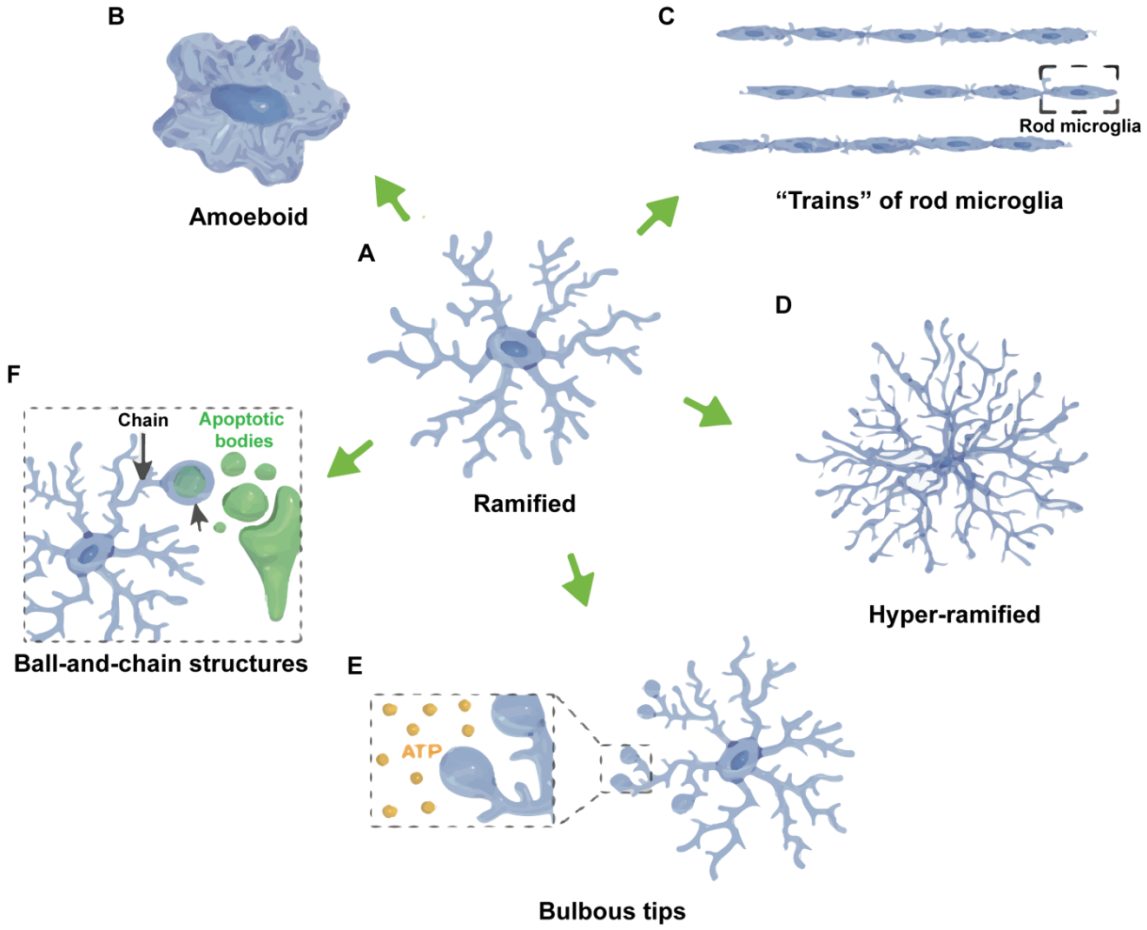

Figure 1.5: Microglial morphology
(A) Under homeostatic condition, microglia exhibit a ramified morphology with dynamic processes which enable them to continuously survey their microenvironment. Upon detection of extracellular stimuli, microglia change their morphology in accordance with their functional activities. **(B)** Upon activation, microglia transform into an amoeboid shape, characterized by the loss of processes and an enlarged cell body. Microglia with amoeboid morphology are associated with high phagocytic capabilities. **(C)** In the vicinity of damaged neurons, microglia adopt a rod-shape morphology, forming a protective barrier around neighboring healthy neurons. **(D)** In case of chronic inflammation, microglia display a hyper-ramified morphology characterized by an increased number of branches. **(E)** When sensing extracellular ATP released from damaged cells, microglia extend their processes and form bulbous structures at the tip of their processes in response to the ATP gradients. **(F)** Microglia can engulf apoptotic materials by forming a spherical phagocytic cup around them, creating a ball-and-chain structure. The phagocytic cup (ball) is located at the end of the microglial process (chain). Figure adapted from (Vidal-Itriago et al, 2022).

Microglial morphology, therefore, changes in accordance with their functional activities and their activation status. When activated, they shift from a ramified to an amoeboid shape by

losing processes and enlarging the cell body (Figure 1.5 B). This morphological transformation is usually associated with higher proliferative and phagocytic capacities **(**Giulian & Baker, 1986**)**. In addition to the amoeboid morphology, activated microglia can assume a rod-like shape. These microglia have narrow cell soma, with polarized thin processes at the ends of the cells **(**Taylor *et al*, 2014**)**. They have been linked to several neurological disorders and are often found in close proximity to injured neurons, forming a barrier to protect the neighboring healthy neurons (Figure 1.5 C) **(**Ziebell *et al*, 2012**)**. In case of chronic stress without pathological condition or inflammation, microglia exhibit a hyper-ramified morphology (Figure 1.5 D) with an increased number of branching points **(**Hinwood *et al*, 2012**)**. The increased ramification is linked to elevated levels of β1-integrin **(**Hinwood *et al*, 2013**)**.

In the adult mouse brain, microglia extend their processes along ATP gradients released from neurons, forming bulbous structures at the tip of the processes (Figure 1.5 E). These structures are transient and serve the purpose of monitoring neuronal activity **(**Bernier *et al*, 2019**;** Dissing-Olesen *et al*, 2014**)**. Microglia can also phagocytose small amounts of apoptotic material using ball-and-chain structures, without undergoing a transformation into an amoeboid shape (Figure 1.5 F). Instead, they form a spherical pouch (ball), which is typically considered as a phagocytic cup, at the terminal of their processes (chain) **(**Cunningham *et al*, 2013**;** Frost & Schafer, 2016**)**.

1.1.3.2. Microglial activation

For a long time, microglial activation was defined using the classic M1/M2 model which is derived from the polarized phenotype of T helper (Th) cells (classical Th1 and alternative Th2) **(**Biswas & Mantovani, 2010**)**. M1 microglia are typically activated in response to pathogens like viruses and bacteria, as well as pro-inflammatory signals such as LPS, IFNγ and TNFα. This type of activation usually occurs in the acute phase of inflammation, during which the M1 microglia secrete pro-inflammatory cytokines including IL6, IL1β and TNFα, or chemokines such as CXCL10 and CCL5 **(**Atri *et al*, 2018**)**. M1 activation is typically seen as cytotoxic and has the potential to cause tissue damage. This type of activation can be detected by the elevated expression of specific surface markers, including CD32, CD86 and major histocompatibility complex II (MHCII) **(**Kigerl *et al*, 2009**)**.

The alternative activation of M2 microglia typically occurs in response to persistent inflammation and is triggered by the presence of anti-inflammatory factors such as IL4 **(**Guo

et al, 2022**)**. The M2 activation serves the function of suppressing inflammation via secreting anti-inflammatory cytokines like IL4 and IL10, and restoring tissue homeostasis by releasing trophic factors such as BDNF, insulin-like growth factor 1 (IGF1) and TGFβ. M2 activation is typically characterized by the presence of surface markers CD206 and CD163 **(**Xiong *et al*, 2016**)**. In addition to the specific M1 and M2 activation markers, there are several other common markers whose levels usually increase when microglia become activated, irrespective of the type of activation. These markers include CD68 and CD45 **(**Jurga *et al.*, 2020**;** Rice *et al*, 2017**)**.

Interestingly, recent transcriptomic studies have uncovered intriguing evidence that challenges the traditional view of microglial activation states as either M1 or M2. These studies have revealed that microglial activation is more nuanced and multifaceted than previously thought **(**Ransohoff, 2016**)**. Notably, the expression profile of microglia differs significantly from that of other tissue macrophages, even when both types of cells are found in close proximity in an inflamed brain tissue **(**Ajami *et al*, 2011**;** Yamasaki *et al*, 2014**)**. The new findings highlight the unique characteristics of microglia and indicate the need for more comprehensive understanding of the functional implications of their activation states.

Taken together, microglia play multifunctional roles in the CNS and are essential for maintaining brain homeostasis. They likely participate in shaping neural circuits during development, and function as vigilant soldiers to survey and eliminate exogenous pathogens and endogenous cell debris throughout life. To carry out their diverse functions, microglia rely on motility, which is driven by the intracellular force generated by the actin cytoskeleton.

1.2. The actin cytoskeleton

The cytoskeleton, as the name indicates, functions as the skeleton to support the structure of a eukaryotic cell. Aside from regulating cell morphology, the highly motile cell cytoskeleton is essential for a variety of cell functions such as migration, division, intracellular transport and mechanical interaction with its surroundings. The cytoskeleton is composed of 3 filament systems: microtubules, intermediate filaments and actin filaments. Microtubules are hollow and stiff cylinders with a diameter of 25 nm that are made up of tubulin. Microtubules participate in cell mitosis and are in charge of intracellular transport and maintenance of cell structure. Intermediate filaments are 10 nm-diameter cable-like fibers composed of a broad array of intermediate filament proteins. Intermediate filaments safeguard DNA by lining beneath the inner nuclear membrane and provide mechanical strength to cells by stretching throughout the cytoplasm. Actin filaments, also known as microfilaments, are dynamic linear polymers with a diameter of 7 nm, which are composed of actin monomers. Actin networks are spread across the cell and are particularly abundant underneath the plasma membrane, where they provide the support for cell shape, membrane dynamics, and adhesion, thus generating the force necessary for cell movement **(**Alberts *et al*, 2008**)**. The actin cytoskeleton is pivotal for cell morphology, cell motility and particle engulfment, all of which are important immune cell properties. This study focuses on the role of the actin cytoskeleton in microglia.

1.2.1. Actin filaments

The basic unit of filamentous actin (F-actin) is a 42 kDa globular actin (G-actin) monomer. Actin filaments are generated from an actin nucleus consisting of 3 actin monomers, and polymerize into double helical actin filaments. The filaments can also depolymerize back to actin monomers. An actin filament has a polarity due to structural differences at both ends. The addition and removal of actin monomers occur at different rates at either end of the filament, resulting in preferential elongation at one end (barbed (+) end) and favored shortening at the other (pointed (-) end). Under physiological conditions, actin monomers binding ATP and Mg^{2+}, which stabilizes ATP-protein interaction **(**Kabsch *et al*, 1990**)**, are added to the barbed end of an actin filament. When the actin filament lengthens, the ATP that is loaded on the incorporated G-actin is hydrolyzed to ADP and inorganic phosphate (P_i) via actin's ATPase activity. This favors G-actin disassociation from the pointed end of the actin filament **(**Korn *et al*, 1987**;** Wegner, 1976**)**. The addition of actin monomers to the filament is dependent on the concentration of free monomers. The pointed end and the barbed end of the actin filament have different critical concentrations (C_c) for the addition of actin monomers. In the presence of

ATP, the C_c is lower at the barbed end (0.1 µM) of the filament than at the pointed end (0.6 µM) **(**Pollard, 2016**)**. When the local monomer concentration falls between the C_cs of the barbed and pointed end of the filament, net addition of monomers will occur at the barbed end, while net loss of monomers will happen at the pointed end without further filament elongation. This process of the filament dynamically moving towards the barbed end is called actin treadmilling (Figure 1.6) **(**Dominguez & Holmes, 2011**;** Uzman, 2001**)**. Actin treadmilling is essential for several functions of immune cells such as cell migration, phagocytosis and exocytosis **(**Jaumouillé & Waterman, 2020**;** Novak *et al*, 2008**)**.

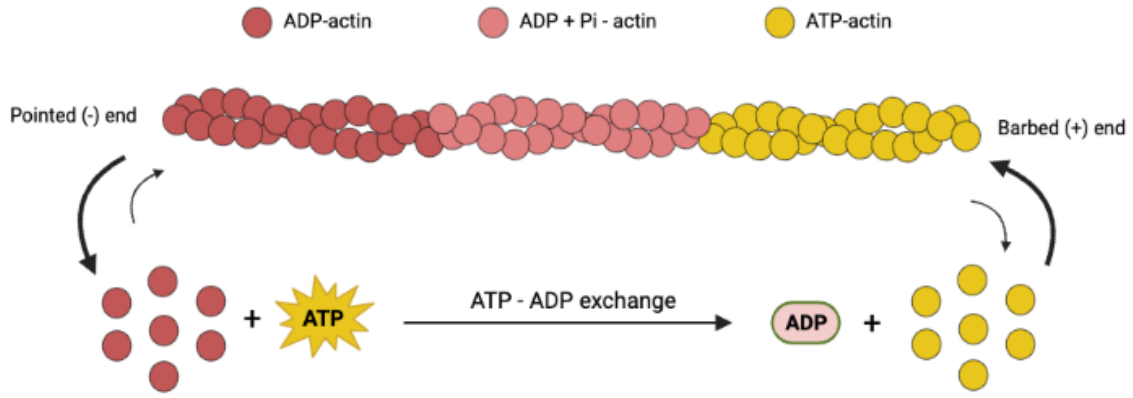

Figure 1.6: The actin treadmilling process
ATP-actin monomers (yellow) are added to the barbed (+) end of an actin filament. As the filament elongates, the ATP on the incorporated G-actin is hydrolyzed to ADP and inorganic phosphate (Pi) (light pink). Following the release of Pi, the ADP-actin (dark pink) dissociates from the pointed end of the filament. Disassociated ADP-actins exchange their ADP for ATP, which facilitates the addition of the actin monomers to the barded end. The thickness of the arrows is proportional to the rates of actin addition or disassociation. Figure adapted from **(**Reinke, 2021**)**.

1.2.2. Actin binding proteins and actin nucleation factors

The actin cytoskeleton is essential for several cellular processes that are critical to immune functions, including chemotactic migration, phagocytosis, cytokinesis and regulation of cell morphology **(**Tur-Gracia & Martinez-Quiles, 2021**)**. All of these dynamic cell functions require continual and accurate arrangement of actin filaments into higher-level F-actin networks. This is achieved by a large collection of actin binding proteins (ABPs), including actin nucleation factors. Actin binding proteins can be grouped based on their roles in actin dynamics. In brief, profilins are monomeric actin binding proteins, which facilitate actin polymerization while cofilins regulate severing and depolymerization of actin filaments **(**Bamburg, 1999**;** Bernstein & Bamburg, 2010**;** Witke, 2004**)**. CAPG, gelsolin, and tropomodulin are capping proteins that bind to the barbed or pointed ends of actin filaments to restrict the addition and removal of

monomers **(**Harris & Weeds, 1984**;** Remedios *et al*, 2003**;** Sun *et al*, 1994**)**. Filamin, fascin and spectrin are cross-linking proteins which connect filaments into bundles and networks **(**Matsudaira, 1994**;** Pollard, 2016**;** Winder & Ayscough, 2005**)**. As previously stated, actin polymerization begins with an actin nucleus, which is made up of three actin monomers. Because this process is slow and energetically-inefficient, cells utilize actin nucleators such as formins, spire and the ARP2/3 complex to promote the formation of the actin nucleus from actin monomers and to nucleate filaments on an existing filament **(**Chesarone & Goode, 2009**;** Weston *et al*, 2012**)**.

Actin nucleators are divided into 3 classes: the actin-related protein 2/3 (ARP2/3) complex with its nucleation promoting factors (NPFs), formins, and WH2 domain-containing nucleators (e.g. SPIRE, COBL and LMOD) (Figure 1.7). This study is focused on the ARP2/3 complex because one of its NPFs, the WAVE regulatory complex (WRC), plays a crucial role in controlling cell motility and other dynamic cell functions. Thus, it will be described in greater depth in this section.

The ARP2/3 complex is a 220 kDa, seven-subunit protein structure composed of actin-related protein 2 (ARP2), ARP3, actin-related protein complex 1 (ARPC1), ARPC2, ARPC3, ARPC4 and ARPC5 **(**Goley & Welch, 2006**)**. The ARP2/3 complex initiates actin nucleation via simulating an actin trimer to form a new (daughter) actin filament on an existing (mother) filament at a 70° angle (Figure 1.7) **(**Campellone & Welch, 2010**)**. The ARP2/3 remains bound to both the mother filament and the pointed end of the daughter filament. This allows both the mother and daughter filaments to polymerize freely at the barbed end, and generate a branched actin network **(**Mullins *et al*, 1998**)**. The nucleation and branching activity of the ARP2/3 complex plays a crucial role in various cell functions, such as cell adhesion, cell migration, lamellipodia formation and phagocytosis **(**Goley & Welch, 2006**;** Pollard & Borisy, 2003**;** Svitkina & Borisy, 1999**;** Welch *et al*, 1997**)**. The ARP2/3 complex is by default inactive and is activated by a group of nucleation promoting factors (NPFs) to initiate the actin nucleation, as will be described in the next section.

Formins function as both actin nucleation and elongation factors in cells. They are multidomain proteins containing formin homology domain 1 (FH1) and formin homology domain 2 (FH2) **(**Faix & Grosse, 2006**)**. Formins nucleate actin filaments by stabilizing freshly formed actin dimers/trimers with their FH2 domain (Figure 1.7). The FH1 domain of formins aids actin filament elongation by directing profilin-bound actin monomers to the filament's barbed end

(Kovar, 2006**;** Romero *et al*, 2004**)**. Contrary to the ARP2/3 complex, formins remain bound to the barbed end of the filament, enhancing filament elongation and preventing capping proteins from ending the polymerization **(**Firat-Karalar & Welch, 2011**)**.

SPIRE, cordon bleu (COBL) and leiomodin (LMOD) are WH2 domain-containing nucleators. Their WH2 domains occur in four, three and one tandem repeats respectively (Figure 1.7) **(**Dominguez, 2016**)**. The central repeats of SPIRE's WH2 domains bind to four G-actin monomers, stabilizing the monomers to form a single linear actin filament string **(**Qualmann & Kessels, 2009**)**. COBL and LMOD nucleate actin filaments in a similar fashion. Their WH2 domains bind to three actin monomers to assemble a polymerization seed.

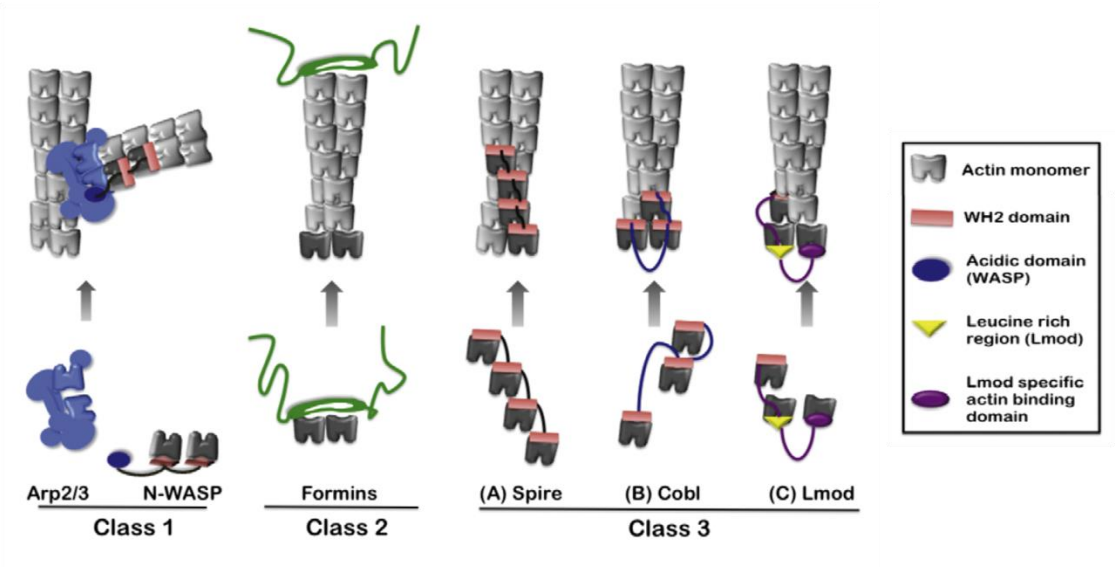

Figure 1.7: Actin nucleation factors
The ARP2/3 complex and its nucleation promoting factors (NPFs) such as WAVE regulatory complex and N-WASP belong to class 1 actin nucleators. The ARP2/3 complex initiates actin nucleation by forming new actin branches on an existing actin filament at a 70° angle. Formins, categorized as class 2 actin nucleators, promote actin nucleation by stabilizing a dimeric actin nucleus and actively directing actin monomers to the barbed end of the filament. WH2 domain-containing nucleators, such as SPIRE, COBL and LMOD, are categorized as class 3 actin nucleators. They promote actin nucleation by stabilizing an actin nucleus of different sizes and remaining bound to the pointed end of the filament. Figure reprinted from **(**Chesarone & Goode, 2009**)**.

1.2.3. Nucleation promoting factors (NPFs)

In the inactive ARP2/3 complex, the actin-like subunits ARP2 and ARP3 are held apart by the other five subunits of the complex, preventing them from nucleating the daughter actin filament **(**Espinoza-Sanchez *et al*, 2018**)**. NPFs engagement can alter this conformation of the ARP2/3

complex, resulting in its activation **(**Espinoza-Sanchez *et al.*, 2018**)**. Based on the mechanisms by which NPFs activate ARP2/3 complex, NPFs can be categorized into two classes.

Class I NPFs have a distinct VCA domain (veprolin-homology domain (WH2 domain), cofilin-homology/central domain and acidic domain) **(**Rotty *et al*, 2013**)**. Class I NPFs activate the ARP2/3 complex by coupling their CA domain to the ARP2 and ARP3 subunits of the ARP2/3 complex, bringing them together. The V domain of class I NPFs binds to one G-actin monomer, which is brought in contact with the ARP2 and ARP3 subunits to form the trimeric nucleus allowing polymerization of the nascent daughter filament **(**Boczkowska *et al*, 2008**;** Chereau *et al*, 2005**;** Marchand *et al*, 2001**;** Rotty *et al.*, 2013**)**. Class I NPFs include Wiskott-Aldrich syndrome protein (WASP), neural WASP (N-WASP), WASP veprolin homologus protein regulatory complex (WAVE regulatory complex), WASP and WAVE homologue (WASH) and junction-mediating and regulatory complex (JMY) **(**Eden *et al*, 2002**;** Kabrawala *et al*, 2020**;** Rottner *et al*, 2010**)**.

Class II NPFs bind to the ARP2/3 complex with their acidic domain. Unlike class I NPFs, class II NPFs bind to F-actin instead of a G-actin monomer to activate the ARP2/3 complex **(**Goode *et al*, 2001**;** Uruno *et al*, 2001**)**. Class II NPFs include cortactin, PAN1 and actin-binding protein 1 (ABP1) **(**Goley & Welch, 2006**)**. Class II NPFs have a relatively weak capacity to promote ARP2/3-mediated nucleation. They can, however, bind to the ARP2/3 complex simultaneously with class I NPFs. While class I NPFs are released from the complex after the nucleation, class II NPFs remain associated with the complex at the Y-branch point, stabilizing the branched actin network and inhibiting the branch dissociation **(**Weaver *et al*, 2001**)**.

1.2.4. The WAVE regulatory complex (WRC)

Class I NPFs are the primary ARP2/3 complex activators. Among the class I NPFs, the WRC is of particular interest for this work due to its essential component, CYFIP1, which is the protein targeted for depletion in microglia in this study. Besides, the WRC plays a significant role in ARP2/3-mediated cell motility and pathogen engulfment, which are crucial functions of immune cells **(**Kage *et al*, 2022b**;** Litschko *et al*, 2017**;** Pils *et al*, 2012**;** Stahnke *et al*, 2021**;** Takenawa & Suetsugu, 2007**)**. The WRC is a ～400 kDa pentameric heterocomplex, consisting of WAVE, ABI (Abelson-interacting protein), NAP (NCK-associated protein), CYFIP (cytoplasmic FMRP-interacting protein), HSPC300 (heat-shock protein C300) (Figure 1.8) **(**Eden *et al.*, 2002**)**. Most of the WRC members have several isoforms, specifically WAVE1/

WAVE2/ WAVE3, ABI1/ ABI2/ ABI3, NAP1/ NAP1L (also known as HEM1) and CYFIP1/ CYFIP2 **(**Rottner *et al*, 2021**)** are known in mouse and human. Single-cell RNA-Seq data have suggested that in the mouse brain, *Wave2*, *Abi1* and *Cyfip1* are ubiquitously expressed, while *Wave1*, *Wave3*, *Abi2*, *Nap1* and *Cyfip2* are enriched in non-myeloid cells. *Abi3* and *Hem1* are exclusively expressed in microglia (Zhang *et al*, 2014b). *Wave2*, *Abi1*, *Nap1*, and *Cyfip1*-null mice are embryonically lethal (*Wave2*: E12.5, *Abi1*: E11.5, *Nap1*: E8.5, *Cyfip1*: E8.5), while the *Cyfip2*-null mouse is perinatally lethal (P0) **(**Dubielecka *et al*, 2011**;** Pathania *et al*, 2014**;** Stöcker, 2015**;** Yan *et al*, 2003**;** Zhang *et al*, 2018**)**. Although *Wave2* and *Cyfip1* are ubiquitously expressed in the brain, they are enriched in microglia (Zhang *et al.*, 2014b). Especially *CYFIP1* is highly expressed almost exclusively in microglia in the human brain **(**Zhang *et al*, 2016**)**.

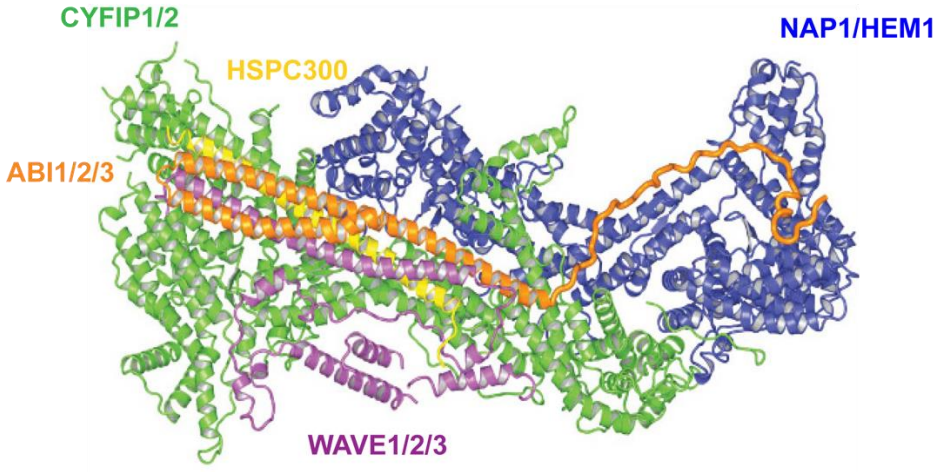

Figure 1.8: Structure and components of the WRC
The WRC is a pentameric heterocomplex composed of WAVE1/2/3 (purple), ABI1/2/3 (orange), HSPC300 (yellow), CYFIP1/2 (green) and NAP1/HEM1 (blue). It can be divided into two subcomplexes: a CYFIP-NAP dimer and a WAVE-ABI-HSPC300 trimer. The VCA domain of WAVE protein is intrinsically hindered by CYFIP, resulting in the autoinhibition of WRC. Figure reprinted and adapted from **(**Chen *et al*, 2010**)**.

The WRC can be structurally divided into two subcomplexes, a CYFIP – NAP scaffolding dimer and a WAVE – ABI – HSPC trimer (Figure 1.8) **(**Chen *et al.*, 2010**;** Gautreau *et al*, 2004**)**. Different isoforms of WRC subunits can form different WRCs, but different subunit isoforms do not co-exist in the same WRC **(**Gautreau *et al.*, 2004**;** Hauck, 2021**)**. For instance, the CYFIP2-dependent WRCs are composed of CYFIP2, WAVE1 or WAVE3, ABI1 or ABI2, NAP1 and HSPC300 **(**Hauck, 2021**)**.

The WRC is intrinsically autoinhibited. The VCA domain of WAVE is sequestered by CYFIP, preventing it from accessing the ARP2/3 complex **(**Chen *et al.*, 2010**)**. The CYFIP1-WRC has been shown to be activated by the RHO-family GTPase RAC1 **(**Chen *et al*, 2017**;** Koronakis *et al*, 2011**;** Schaks *et al*, 2018**)**. RAC1-binding sites of the WRC are located on the surface of CYFIP1. When RAC1 interacts with CYFIP, it changes the WRC's conformation resulting in WRC activation **(**Schaks *et al.*, 2018**)**. The conformational change liberates the VCA domain for ARP2/3 complex activation (Figure 1.9) **(**Chen *et al.*, 2010**;** Ding *et al*, 2022**)**.

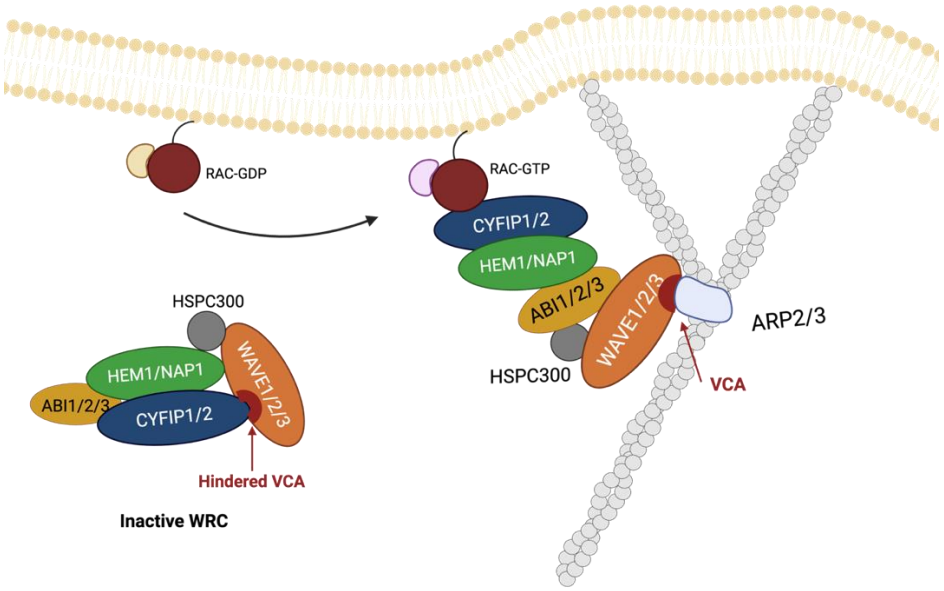

Figure 1.9: WRC activation leading to ARP2/3-mediated actin nucleation
The WRC is intrinsically inactive as the VCA domain of WAVE is hindered by CYFIP, preventing its interaction with the ARP2/3 complex. The WRC can be activated by the RHO family GTPase RAC1. Binding of GTP-bound RAC1 to CYFIP induces conformational changes of the WRC, leading to the release of the VCA domain. The liberated VCA domain can then bind to the ARP2/3 complex and initiate actin branching.

1.2.5. CYFIP1

In eukaryotic cells, CYFIP has several interacting partners, which have determined its different names. CYFIP was first identified as a 140 kDa specifically RAC1-associated protein (SRA) and the interacting partner of profilin (POP) in 1998 **(**Kobayashi *et al*, 1998**;** Witke *et al*, 1998**)**. Later, researchers found CYFIP as a novel mediator of p53 mutant, 121F-dependent apoptosis in cell lines, and termed it p53-inducible RNA, 121F-specific (PIR121) **(**Saller *et al*, 1999**)**. CYFIP was finally given the name cytoplasmic FMR1-interacting protein in 2001 owing to its interaction with the fragile X messenger ribonucleoprotein (FMRP) **(**Schenck *et al*, 2001**)**. It

was in the same study that the two isoforms of CYFIP, CYFIP1 and CYFIP2, were identified. Both CYFIP1 and CYFIP2 belong to a highly conserved protein family that is widely expressed. Human CYFIP1 and CYFIP2 share an amino sequence identity of 98.7 % and 99.9 % with their mouse orthologues. Besides, CYFIP1 and CYFIP2 have 87.7 % sequence identity and 94.5 % sequence similarity with each other **(**Schenck *et al.*, 2001**)**. The gene encoded for CYFIP1 is situated on chromosome 15 in human and on chromosome 7 in mouse, whereas the gene encoded for CYFIP2 is located on chromosome 5 in human and on chromosome 11 in mouse. Interestingly, CYFIP1 and CYFIP2 exhibit distinct binding preference for FMRP and its related proteins, even though they possess high sequence identity. CYFIP1 was found to interact exclusively with FMRP, while CYFIP2 was observed to interact with both FMRP and its related proteins, FXR1P and FXR2P, in vitro **(**Schenck *et al.*, 2001**)**. This discovery suggests that while the CYFIP isoforms may share similar functions, they likely have distinct and separate roles in cell processes.

In 2004, Steffen et al. identified CYFIP1's crucial role in WAVE-mediated actin assembly as part of the WRC. In this study, it was demonstrated that CYFIP1 serves as an essential component within the WRC by linking activated RAC1 to WAVE and thereby regulating downstream lamellipodia and membrane ruffling formation in the cell **(**Steffen *et al*, 2004**)**. In 2008, Napoli and colleagues made a significant discovery concerning the function of CYFIP1 in FMRP-associated mRNA translation. They found that in neurons, and particularly in spines, CYFIP1 is recruited by FMRP, a known local repressor of mRNA translation, to bind to eukaryotic translation initiation factor 4E (eIF4E). By binding directly to eIF4E, CYFIP1 blocks the formation of the translation initiation complex eIF4F, which results in the translational repression of FMRP-targeted mRNAs **(**Napoli *et al*, 2008**)**. Subsequent studies suggested that CYFIP1 is present in both the WRC and translational inhibitory complexes (FMRP-CYFIP1), although not simultaneously: CYFIP1 can transition between these two complexes via a conformational change mediated by activated RAC1 **(**De Rubeis *et al*, 2013**;** Di Marino *et al*, 2015**)**. In conclusion, CYFIP1 is a critical regulator of WRC-mediated actin polymerization and FMRP-mediated mRNA translation inhibition in synaptic spines.

Studies have shown that the level of CYFIP1 can influence dendritic complexity and spine morphology of neurons **(**De Rubeis *et al.*, 2013**;** Oguro-Ando *et al*, 2015**;** Pathania *et al.*, 2014**)**. Both CYFIP1 and CYFIP2 are enriched at the excitatory synapses but also present at inhibitory synapses **(**Davenport *et al*, 2019**;** Pathania *et al.*, 2014**)**. Elevated CYFIP1 enhances neuronal

arborization *in vitro* and increases spine density *in vivo*, while decreased CYFIP1 level, on the other hand, results in reduced neuronal arborization and higher proportion of immature spines both *in vitro* and *in vivo* **(**Oguro-Ando *et al.*, 2015**;** Pathania *et al.*, 2014**)**. Changes in *Cyfip1* gene dosage also affects F-actin dynamics in dendritic spines and disrupts the excitatory/inhibitory balance **(**Davenport *et al.*, 2019**;** Pathania *et al.*, 2014**)**.

1.2.6. CYFIP1 in autism and schizophrenia

CYFIP1 is found in region 15q11.2 of the human chromosome. Copy number variation of this regions is associated with autism spectrum disorder and schizophrenia **(**Burbach & van der Zwaag, 2009**;** Crespi *et al*, 2010**)**. Microdeletion of this region has been linked with schizophrenia and certain cases of autism **(**Doornbos *et al*, 2009**;** Kirov *et al*, 2008**;** Stefansson *et al*, 2008**;** Wassink *et al*, 2001**)**, while duplications of region 15q11.2-q13 is associated with elevated risk of autism **(**Veenstra-Vanderweele *et al*, 2004**)**. Region 15q11.2 of human chromosome comprises four genes, *TUBGCP5*, *CYFIP1*, *NIPA2* and *NIPA1*. Among these genes, *CYFIP1* is believed to be the disease-causing gene due to its role in dendritic protein synthesis **(**Burbach & van der Zwaag, 2009**;** Napoli *et al.*, 2008**)**.

The recent study conducted by Norrozi et al. revealed a significant over-expression of *CYFIP1* mRNA in the blood of young ASD patients when compared to the age-matched control group **(**Noroozi *et al*, 2018**)**. On the other hand, in a separate proteomic study conducted on the prefrontal cortex of schizophrenia patients, the level of CYFIP1 was found reduced when compared to the age-matched control individuals **(**Hirayama-Kurogi *et al*, 2017**)**. Among the limited number of studies investigating synaptopathy in the human brain of autism patients, it has been reported that autistic patients had greater spine density but immature spine morphology in layer II, III and V pyramidal neurons in the temporal cortex when compared to the control group **(**Hutsler & Zhang, 2010**;** Irwin *et al*, 2001**;** Martinez-Cerdeno, 2017**)**. Research on schizophrenia patients has shown a decrease in the spine density of pyramidal neurons located in the layer III Brodmann area within the cerebral cortex or the prefrontal cortex, compared to control individuals **(**Garey *et al*, 1998**;** Glantz & Lewis, 2000**;** Konopaske *et al*, 2014**)**.

In summary, the expression level of CYFIP1 is closely linked with the pathophysiology of autism and schizophrenia. Increased CYFIP1 level is associated with elevated spine density and immature spines observed in autism, while decreased CYFIP1 level is related to reduced

spine density seen in schizophrenia. These findings emphasize the vital role of CYFIP1 in dendritic spine development, and suggest that CYFIP1 may be a critical player in the etiology of these disorders.

1.2.7. *CYFIP1/2* expression pattern in the brain

CYFIP1 is widely expressed across most human tissues, while its paralog *CYFIP2*, is primarily expressed in the CNS (Gene ID *CYFIP1*: 23191; Gene ID *CYFIP2*: 26999). Previous transcriptomic studies by Zhang et al. have provided a more detailed understanding of the distinct CNS cell-specific expression patterns of the two *CYFIP* paralogs in human and mouse brain tissues. In human, *CYFIP1* shows exclusively high expression in microglia, while *CYFIP2* is predominantly expressed in neural cells such as neurons, astrocytes and oligodendrocytes. In mice, *Cyfip1* is ubiquitously expressed, but with particularly high expression in microglia, whereas *Cyfip2* is primarily found in neurons (Zhang *et al*, 2014a; Zhang *et al.*, 2016). Subsequent investigation using immunofluorescence staining in mice has validated that CYFIP2 is primarily present in neurons **(**Özer, 2020**)**. However, the expression pattern of CYFIP1 at the protein level in the mouse brain still remains to be determined.

1.2.8. The actin cytoskeleton in innate immune cells functions

Innate immune cells such as macrophages, dendritic cells and granulocytes represent the first line of defense against infections in living organisms. These cells are highly mobile and continuously monitor their surroundings. When they detect signals from either pathogens or damaged tissues, they undergo morphological changes and migrate towards the site of infection or damage, where they carry out phagocytosis and other critical immune functions. The actin cytoskeleton provides the mechanical force required for these responses, making it a crucial component of the innate immune cells. Therefore, understanding the mechanisms by which the actin cytoskeleton influences the functions of innate immune cells is vital for our understanding of the innate immune response. The following sections will describe how the actin cytoskeleton contributes to major immune functions such as phagocytosis and cell migration.

1.2.8.1. The actin cytoskeleton in membrane ruffling and phagocytosis

Macrophages maintain tissue homeostasis by actively surveying their environment for potential targets. This surveillance is achieved by generating membrane protrusions, also known as ruffles **(**Freeman *et al*, 2020**)**. The membrane ruffles, on one hand, act as contact points between the cell and the targets that need to be cleared via phagocytosis; on the other hand, they also

uptake extracellular molecules and nutrients to support the health and functions of the macrophage **(**Flannagan *et al*, 2012**)**. To overcome the contractile tension of the membrane, the ruffles rely on the force generated by actin polymerization. This process involves the reorganization of local cortical F-actin, which is partly mediated by the ARP2/3 complex. The ARP2/3 complex-regulated actin polymerization is responsible for generating large ruffles, such as planar and circular dorsal ruffles **(**Mylvaganam *et al*, 2021**;** Suetsugu *et al*, 2003**)**. The dorsal ruffles play a critical role in the process of phagocytosis **(**Rotty *et al*, 2017**)**. Moreover, the actin structures mediated by the ARP2/3 complex are essential for organizing the complement receptors 3 (CR3) on the macrophage membrane, optimizing the efficiency of phagocytosis **(**Rotty *et al.*, 2017**)**.

The process of phagocytosis can be broadly divided into four major steps, including cortical actin disruption, generating the base of phagocytic cups, extension of phagocytic cups, closure of phagocytic cups (Figure 1.10) **(**Freeman & Grinstein, 2014**)**. To initiate phagocytosis, the F-actin networks underneath the macrophage membrane have to be disrupted to increase the receptor mobility and provide free G-actin monomers for the following actin polymerization. This process can be facilitated by actin severing and debranching proteins, such as coronins and cofilins **(**Cai *et al*, 2007**;** Kueh *et al*, 2008**;** Yan *et al*, 2005**)**. Following that, macrophages begin to construct the foundation of phagocytic cups. This step involves the clustering of phagocytic receptors in order for them to bind to the ligands on the targets. The downstream signaling cascades activate many NPFs, including WASP and the WRC, resulting in ARP2/3 complex-dependent actin polymerization for phagocytic cup extension **(**Kheir *et al*, 2005**)**. The extension of phagocytic cups requires adhesive structures to maintain the physical contact between the macrophage and the targets. The adhesions generate traction forces, which facilitate the protrusion while simultaneously limiting the retrograde actin flow. As the polymerization process advances at the tip of the phagocytic cup, there is also a dynamic depolymerization occurring at the base. This provides both the necessary elasticity and a steady supply of G-actin monomers for the ongoing process **(**Jaumouillé *et al*, 2019**)**. The final step of phagocytosis is the closure of the phagocytic cup, in which the edges of the cup come into contact and merge to form a phagosome. Proteins such as dynamin and myosin-X modulate the constrictive force required to merge the edges of the phagocytic cup. The phagosome in the end separates from the membrane and moves into the cytoplasm **(**Gold *et al*, 1999**;** Marie-Anaïs *et al*, 2016**;** Swanson *et al*, 1999**)** (Figure 1.10).

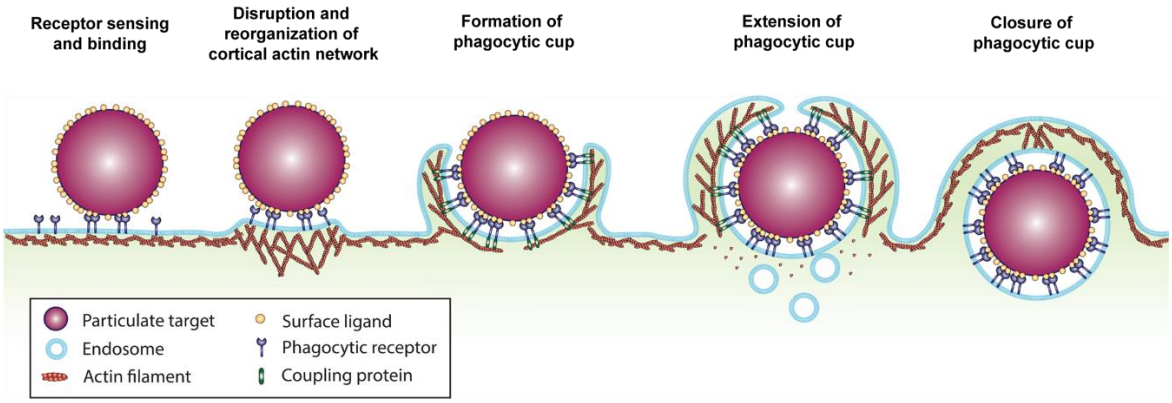

Figure 1.10: Major steps of phagocytic cup formation
Upon detecting phagocytic cues, macrophages initiate signaling pathways through interactions between their phagocytic receptors and surface ligands on the targets. These pathways trigger actin network rearrangement, facilitating the formation of phagocytic cups. As phagocytic receptors couple with target ligands, actin filaments polymerize towards the edge of the phagocytic cup, extending the cup until its edges meet and fully envelop the targeted particle. Subsequently, the phagosome detaches from the plasma membrane and moves into the cytoplasm. Figure reprinted and adapted from **(**Jaumouillé & Waterman, 2020**)**.

1.2.8.2. The actin cytoskeleton in cell migration

The migration of immune cells is critical for ensuring an effective immune response, facilitating wound healing and maintaining tissue homeostasis **(**Trepat *et al*, 2012**)**. When macrophages sense the presence of a chemoattractant, they respond by migrating along the external gradient of the signaling molecule **(**Iijima *et al*, 2002**)**. During embryonic development, microglia progenitors migrate via CSF1-induced chemotaxis from the yolk sac to the brain parenchyma, where they eventually mature into microglia **(**Chitu & Stanley, 2017**;** Wu *et al*, 2018**)**. In the course of infection or apoptosis in the CNS, microglia detect signals released by damaged cells, such as UDP or CX3CL1, and migrate along the molecular gradient towards the affected area **(**Koizumi *et al.*, 2007**;** Truman *et al*, 2008**)**. There, they engulf and remove the damaged cells to restore tissue homeostasis **(**Sierra *et al*, 2013**)**. To migrate successfully, immune cells must undergo dynamic cytoskeletal remodeling which provides them the necessary mechanical forces to move across tissues with different physical properties.

Cell migration can be broadly divided into four major steps, consisting of membrane protrusion, formation and stabilization of adhesion to the extracellular substrate, actomyosin-based contraction of the cell body, and the detachment at the rear end (Figure 1.11) **(**Lauffenburger & Horwitz, 1996**)**. Immune cells, to efficiently migrate towards a chemoattractant source in a 2D environment, need to form protrusions and stabilize them through adhesion at the leading edge of the cell. The primary mechanism of protrusion on a flat surface for immune cells is

through the formation of lamellipodia **(**Ridley, 2011**)**. Lamellipodia are thin, sheet-like protrusions made up of branched actin filaments that are controlled by the ARP2/3 complex **(**Chhabra & Higgs, 2007**;** Goley & Welch, 2006**)**. They create the pushing force at the leading edge, which is crucial for directed migration **(**Insall & Machesky, 2009**;** Suraneni *et al*, 2012**)**.

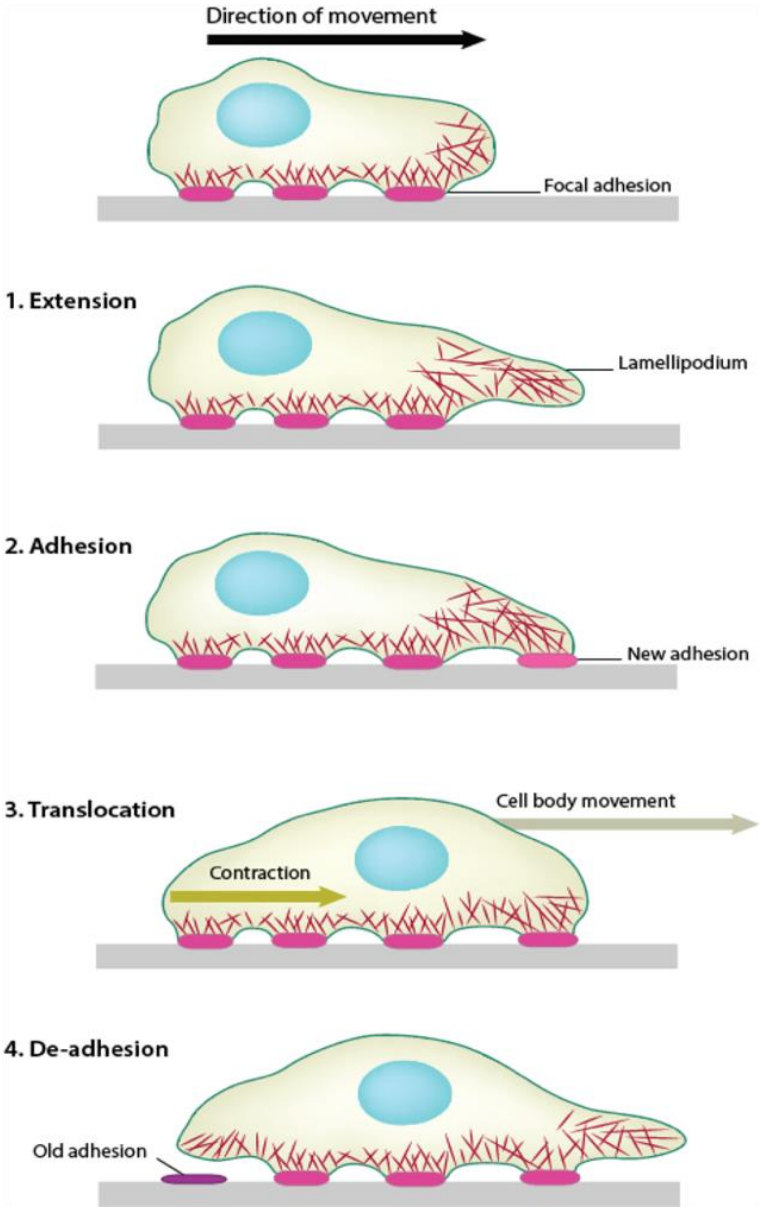

Figure 1.11: Major steps of cell migration
A lamellipodium at the leading edge of a cell generates protrusive force for migration, but it adheres weakly to the substrate. Focal adhesions, formed underneath the lamella between the lamellipodium and cell body, create strong adhesions to the substrate. As the cell stabilizes new adhesions, inner tension is generated via stress fibers, propelling the cell forward. This tension triggers disassembly of focal adhesion at the trailing edge, releasing them from the rear end of the cell. (Figure reprinted from Mechanobiology institute, University of Singapore (MBInfo), https://reurl.cc/01zZzl).

Lamellipodia exhibit weak attachment to the extracellular substrate. The lamellipodia which fail to attach strongly enough frequently retract towards the cell body. This continual and dynamic process is commonly referred to as membrane ruffling **(**Borm *et al*, 2005**;** DeMali & Burridge, 2003**)**. Attachment formation and stabilization occur at the lamella, which are thick adhesion sites between lamellipodia and the cell body. Lamella possess unique actin networks, which differ from those found in lamellipodia. The focal adhesion complexes are formed underneath the lamella, with a ring of adhesion proteins including integrins, focal adhesion kinase (FAK), vinculin, talin, paxillin, and actin networks formed by the ARP2/3 complex **(**Block *et al*, 2008**)**. It is noteworthy that both WASP and WAVE proteins play unique roles in regulating the ARP2/3 complex-mediated actin polymerization in macrophages. WAVE2 is responsible for providing branched actin networks at the front protrusions, whereas WASP is critical for the stabilization of these protrusions **(**Ishihara *et al*, 2012**;** Kheir *et al.*, 2005**)**.

In order to create the traction force and facilitate the translocation of the cell body, cells require a degree of external adhesiveness and inner tension **(**Rougerie *et al*, 2013**)**. The regulation of myosin activity by RHOA plays a crucial role in controlling cell contractility during macrophage migration **(**Sellers, 2000**;** Wheeler & Ridley, 2007**)**. Actin filaments combine with myosin II to form stress fibers, which generate actomyosin tension. This tension is produced by myosin II moving along the actin filaments, generating a sliding process and ultimately leading to the translocation of the cell body **(**Chi *et al*, 2014**)**. During migration, the tension created by stress fibers also causes the destabilization of focal adhesions at the trailing edge, ultimately disassembling and releasing them at the rear end of the cell **(**Ridley *et al*, 2003**;** Shutova *et al*, 2012**)**. The entire process involving the formation of protrusions, stabilization of adhesion, translocation of the cell body and retraction at the rear end, enables the cell to migrate forward (Figure 1.11).

1.3. Aim of this study

CYFIP1, a crucial component of the WAVE regulatory complex, plays a key role in regulating the actin cytoskeleton in eukaryotic cells. It is expressed in all cell types in the brain. Copy number variations of *CYFIP1* have been associated with schizophrenia and autism spectrum disorders. However, most studies on CYFIP1 have mainly focused on the role of CYFIP1 in neurons, with limited information regarding changes in glial cells and their influence on neuronal phenotypes. Unraveling the precise molecular function of CYFIP1 has been challenging owing to the predominant expression of CYFIP2, the other CYFIP isoform, in neurons. Interestingly, *CYFIP1/Cyfip1* shows particularly high expression in microglia, the innate immune cells in the brain, where it is the sole expressed CYFIP isoform. Despite growing evidence showing a significant role of microglia in neuronal synapse development, very few studies have explored the function of CYFIP1 in microglia and the impact of microglial CYFIP1 depletion on neurons.

In this study, we aimed to address the functions of CYFIP1 in microglia by evaluating the impact of its deletion on the adult mouse brain. This work focused on four key aspects. First, we aimed at identifying the microglia-specific CYFIP1-WRC using freshly isolated microglia from the adult mouse brain, and evaluated changes in microglial morphology and homeostatic status in the adult mouse brain in a microglia-specific *Cyfip1* KO mouse model. Second, we investigated the impact of CYFIP1 depletion on microglial motility and phagocytic function using *in vitro* primary microglial cultures. Third, by using the same *in vitro* primary microglia culture system, we explored the relevance of the CYFIP1-WRC in regulating microglial actin dynamics. And forth, we investigated the effect of microglia-specific CYFIP1 depletion on neuronal number and on synapse density and maturation in the adult mouse brain.

Chapter 2. Results

2.1. CYFIP1 expression in the mouse brain and microglial WAVE regulatory complex

Cytoplasmic FMRP interacting protein 1 (CYFIP1), also known as specifically RAC1 activated protein 1 (SRA1), is evolutionarily conserved in eukaryotic cells. CYFIP1 is globally expressed in all mammalian cells. Previous single-cell transcriptomic studies indicated that *Cyfip1* is expressed in all cell types in the CNS. However, highest expression was found in microglia, both in mouse and human (Uhlen *et al*, 2015; Zhang *et al.*, 2014a; Zhang *et al.*, 2016). At present, the expression pattern of CYFIP1 across CNS cells at the protein level has not been investigated yet. Therefore, in this chapter, we aimed to investigate and compare CYFIP1 protein expression levels in microglia, neurons and astrocytes. Due to difficulties in isolating fresh and intact oligodendrocytes, CYFIP1 levels in oligodendrocytes were not included for comparison with other major CNS cells in this study. Additionally, we sought to characterize the microglia-specific WAVE regulatory complexes (WRC), studying the expression of the diverse isoforms of its members, which can give rise to distinct WRC compositions within cells. This could help us understand the possible roles of the CYFIP1-WRC in functions.

2.1.1. CYFIP1 is the only CYFIP isoform expressed in microglia and is highly expressed

In order to investigate CYFIP1 protein level in major CNS cells, microglia, astrocytes and neuronal synaptosomes were freshly isolated from 2-month-old CTRL mouse brains (see chapter 4.2.2.1 and 4.2.2.2). Since isolating fresh and undamaged whole neurons is challenging and previous studies have shown considerable CYFIP1 protein levels in neuronal synapses (Pathania *et al.*, 2014), synaptosomal samples were used as neuronal counterparts in this study.

Western blotting of protein extracts from the isolated cell types followed by relative quantification analysis showed that CYFIP1 protein level in microglia (6.8±1.1) was seven times higher compared to synaptosomes (1±0.13) and four times higher compared to astrocytes (1.7±0.13) (Figure 2.1 A and B). Besides CYFIP1, we also investigated the expression of the other CYFIP isoform, CYFIP2, in the same cell types. Our data showed that CYFIP2 is expressed only in neurons, but not in microglia and astrocytes (Figure 2.1 A and B). In conclusion, CYFIP1 and CYFIP2 co-exist in neurons, while CYFIP1 is the only CYFIP isoform found in microglia and astrocytes.

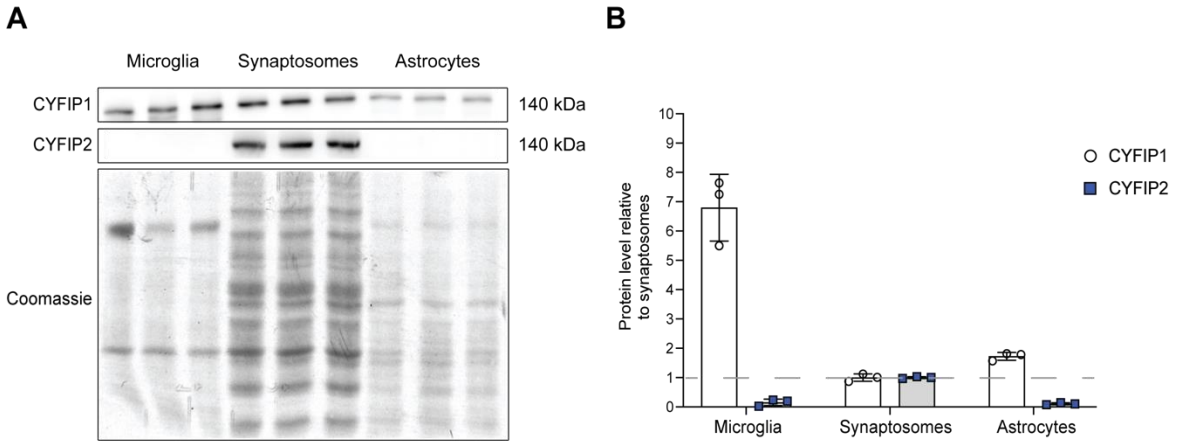

Figure 2.1: CYFIP1 is the only CYFIP isoform in microglia and is highly expressed. CYFIP1 and CYFIP2 levels in freshly-isolated microglia, neuronal synaptosomes and astrocytes from 2-month-old CTRL mice were determined using semi-quantitative western blotting. **(A)** Western blotting images show that CYFIP1 is found in microglia, synaptosomes and astrocytes, while CYFIP2 is only detected in synaptosomes. Total protein on the membrane was quantified using Coomassie staining. **(B)** Calibrated quantification of protein signals and normalization to synaptosomes of both CYFIP isoforms demonstrate that CYFIP1 is the only CYFIP isoform in microglia and astrocytes, whereas CYFIP1 and CYFIP2 co-exist in neurons. All nine samples for each CYFIP isoform were loaded on the same blot. Data are presented as mean ± SD. The empty circles and blue squares represent the values of the individual samples. N = 3 mice per group.

2.1.2. Microglia possess a unique CYFIP1-WRC

The WRC is composed of five members – CYFIP, NAP, WAVE, ABI and HSPC300. All WRC members have 2-3 isoforms except for HSPC300. There are CYFIP1 and CYFIP2; NAP1 and HEM1 (also named NAP1-like); WAVE1, WAVE2 and WAVE3; ABI1, ABI2 and ABI3. Different isoforms can assemble to form different WRCs. A previous study has shown that CYFIP2, the dominant CYFIP isoform in neurons, forms complexes with NAP1, WAVE1 or 3, and ABI1 in the embryonic mouse brain (Hauck, 2021). In addition, CYFIP1 and CYFIP2 does not co-exist in the same complex (Hauck, 2021). The CYFIP1-dependent WRC in the brain has not yet been fully characterized due to technical reasons. Since CYFIP1 is the only CYFIP isoform in microglia, we hypothesized that it might be possible to identify the specific CYFIP1-WRCs in these cells.

To identify the components of microglial WRC, western blotting was performed using lysates from microglia isolated from 2-month-old CTRL mice. All the isoforms listed above were tested. Western blotting images show that microglia have a unique WRC consisting of CYFIP1, HEM1, WAVE2 and ABI3 (Figure 2.2 A and B). Our findings, for the first time, identify the

microglia-specific WRC and support previous research indicating that CYFIP1 and CYFIP2 take part in distinct WRCs composed of unique subunits isoforms.

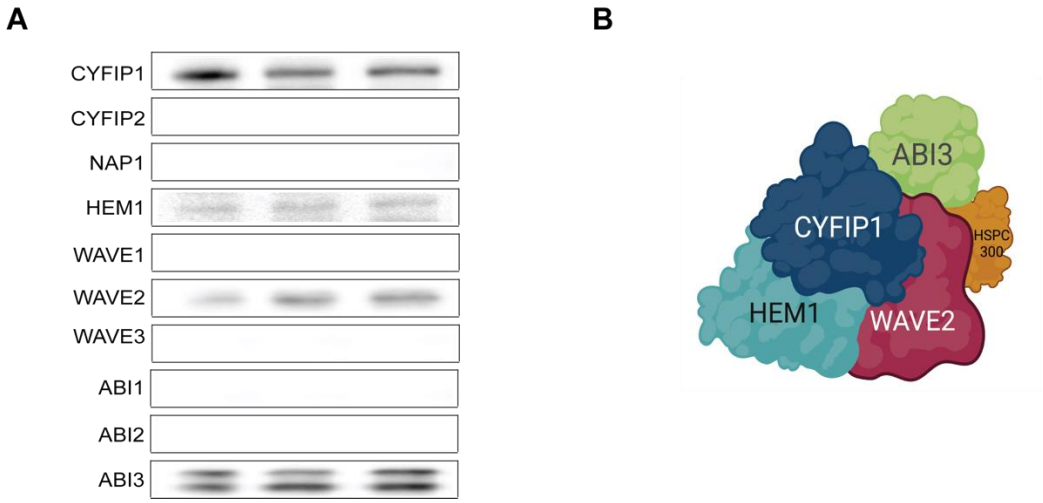

Figure 2.2: Microglia have a unique CYFIP1-dependent WRC.
Components of microglial WRC complex were identified using western blot on microglia isolated from 2-month-old CTRL mice. **(A)** Western blotting signals from membranes probed with specific antibodies for all known isoforms of the WRC components. Microglial WRC is constituted of CYFIP1, HEM1, WAVE2 and ABI3. **(B)** Graphic representation of the microglial WRC.

2.1.3. *Cyfip1* is successfully deleted in microglia in *Cyfip1*$^{flx/flx}$;*Cx3cr1*$^{cre/+}$ mice

Cyfip1 homozygous mutant mice are embryonically lethal (Pathania *et al.*, 2014). *Cyfip1*$^{-/-}$ embryos die around embryonic day 8.5 (Chung *et al*, 2015; Stöcker, 2015), after failing to properly gastrulate, which indicates the importance of CYFIP1 during embryonic development. For this reason, in order to study the function of CYFIP1 in microglia, we created a *Cyfip1* conditional knockout (cKO) mouse model using a cell-specific Cre/loxP system. *Cyfip1* was deleted specifically in myeloid cells, including microglia by cross breeding *Cyfip1*$^{flx/flx}$ mice (Massimi, 2008)with mice expressing the Cre recombinase driven by the endogenous *Cx3cr1* promoter (Yona *et al*, 2013) (*Cx3cr1*-Cre knock-in mice, see chapter 4.1). CX3CR1 is a fractalkine receptor expressed in myeloid cells. In the CNS, *Cx3cr1* is expressed in microglia and border-associated macrophages (Harrison Jeffrey K *et al*, 1998), so the *Cx3cr1* locus is frequently used to delete genes in microglia. However, some studies have reported a transient *Cx3cr1* expression in neurons during development using rodent models (Haimon *et al*, 2018; Hughes *et al*, 2002; Meucci *et al*, 2000). In order to verify the cKO specificity of the *Cyfip1*$^{flx/flx}$;*Cx3cr1*$^{cre/+}$ mouse model, we examined CYFIP1 protein levels in microglia,

neuronal synaptosome, astrocytes and oligodendrocytes isolated from 2-month-old CTRL and *Cyfip1* cKO mice.

Our western blotting results showed the efficient depletion of CYFIP1 in microglia from *Cyfip1* cKO mice when compared to CTRL mice, while CYFIP1 protein levels remained unaffected in neuronal synaptosomes and astrocytes from the *Cyfip1* cKO mice when compared to CTRL mice (Figure 2.3 A and B). However, we noticed a 50 % reduction of CYFIP1 in oligodendrocytes isolated from *Cyfip1* cKO mice when compared to CTRL (Figure 2.3 B). It may be a cell-autonomous effect caused by the partial deletion of *Cyfip1* in oligodendrocytes, since *Cx3cr1* mRNA was detected in oligodendrocyte precursor cells (OPCs) in mouse brains, albeit the expression was low compared to microglia (Watson *et al*, 2021; Zhang *et al.*, 2014b). On the other hand, the level of microglial contamination in the isolation process of oligodendrocytes could be a contributing factor to the observed reduction of CYFIP1 level in oligodendrocytes from *Cyfip1* cKO mice.

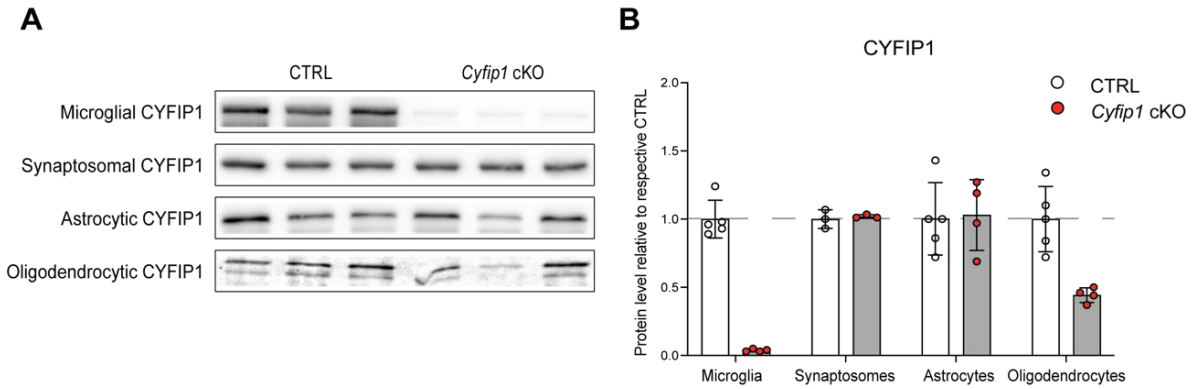

Figure 2.3: Efficient *Cyfip1* deletion in microglia in *Cyfip1*$^{flx/flx}$;*Cx3cr1*$^{cre/+}$
The specificity of CYFIP1 depletion in *Cyfip1* cKO animals was investigated in microglia, neuronal synaptosomes and astrocytes from 2-month-old CTRL and *Cyfip1* cKO mice using western blotting. **(A)** Membranes probed with anti-CYFIP1 antibodies. Three representative samples from each genotype per cell type are shown. **(B)** Quantification and normalization to CTRL levels of CYFIP1 show that CYFIP1 is efficiently depleted in microglia from *Cyfip1* cKO mice, whereas CYFIP1 levels in neuronal synaptosomes and astrocytes from *Cyfip1* cKO mice remain unaltered when compared to CTRL mice. CYFIP1 level in oligodendrocytes from *Cyfip1* cKO mice shows a reduction compared to the CTRL mice. Data are presented as mean ± SD. Empty and red circles represent the values from individual animals. N = 5 for CTRL and n = 4 for *Cyfip1* cKO animals used to isolate microglia, astrocytes and oligodendrocytes. N =3 for each genotype used to isolate neuronal synaptosomes.

2.1.4. *Cyfip1* deletion in microglia leads to loss of microglial WRC

To investigate the impact of CYFIP1 loss on the other members of microglial WRC, we examined the protein levels of HEM1, WAVE2 and ABI3 in microglia isolated from 2-month-old CTRL and *Cyfip1* cKO mice. Our western blotting analysis revealed that the protein levels of the CYFIP1-dependent WRC members - HEM1, WAVE2 and ABI3, are all significantly reduced to almost undetectable levels in *Cyfip1* cKO microglia when compared to CTRL microglia (Figure 2.4 A and B).

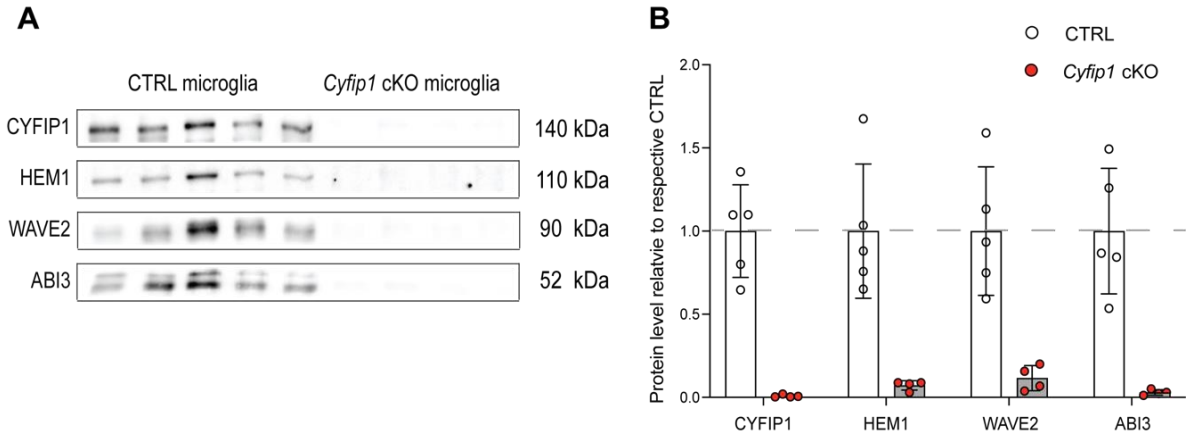

Figure 2.4: *Cyfip1* deletion results in complete loss of the WRC in microglia.
The effect of CYFIP1 loss on the levels of the other CYFIP1-dependent WRC members was investigated in microglia isolated from 2-month-old CTRL and *Cyfip1* cKO animals using western blotting. **(A)** Membranes probed with anti-CYFIP1, anti-HEM1, anti-WAVE2 and anti-ABI3 antibodies show the levels of each CYFIP1-dependent WRC member in CTRL and *Cyfip1* cKO microglia. **(B)** Relative quantification of protein levels of each CYFIP1-dependent WRC member (HEM1, WAVE2 and ABI3 normalized to the corresponding CTRL) shows that they are virtually lost in *Cyfip1* cKO microglia when compared to the CTRL microglia. Data are presented as mean ± SD. Empty and red circles represent the values from individual animals. N = 5 mice in the CTRL group, n = 4 for *Cyfip1* cKO group.

Our result is consistent with other studies on CYFIP1, which showed a decreased level of CYFIP1-dependent WRC components (NAP1-WAVE2) when *Cyfip1* was knocked out or knocked down (Litschko *et al.*, 2017; Steffen *et al.*, 2004). Our findings are the first to identify a microglia-specific WRC and to reveal that the depletion of CYFIP1 leads to the loss of the microglial CYFIP1-dependent WRC (CYFIP1-HEM1-WAVE2-ABI3).

2.2. *Cyfip1* cKO mice show slight reduction in the corpus callosum size, with no other brain morphological changes

To investigate if the loss of CYFIP1 in microglia impacts gross brain morphology in *Cyfip1* cKO mice, sagittal brain sections from 2-month-old CTRL and *Cyfip1* cKO mice were stained with hematoxylin and eosin (H&E) (see chapter 4.2.4.3.). The brain anatomy of *Cyfip1* cKO mice did not show obvious differences from the CTRL mice, except for the corpus callosum that appeared thinner (Figure 2.5 A). In order to quantify these observations, we measured the area of each brain region and normalized it to the total brain area to determine the relative size of corpus callosum, cerebral cortex, hippocampus and cerebellum in anatomically matching sections from CTRL and *Cyfip1* cKO mice.

The size of cortex, hippocampus and cerebellum did not differ between the CTRL and *Cyfip1* cKO mice (Figure 2.5 C-E), but the corpus callosum in *Cyfip1* cKO mice was approximately 25 % smaller than in CTRL mice (Figure 2.5 B). Interestingly, another study in our lab also found reduced myelin basic protein (MBP) levels in the corpus callosum of *Cyfip1* cKO mice (Letmathe, unpublished data). Previous studies reported reduced myelin thickness and MBP intensity in the corpus callosum of *Cyfip1*$^{+/-}$ rodents (Domínguez-Iturza *et al*, 2019; Silva *et al*, 2019). In our system there are two possible explanations for these findings, which would also be in agreement with the previous studies. An ectopic partial deletion of *Cyfip1* in oligodendrocytes of our *Cyfip1* cKO mice (Figure 2.3) might have affected their actin cytoskeleton, which plays a vital role in the formation of myelin structures. It is also possible that corpus callosum thickness was indirectly affected by the loss of CYFIP1 in microglia. Future studies should explore this possibility.

2.3. Microglial cell number is higher across different brain regions in *Cyfip1* cKO mice

A previous study on CYFIP1 in neural stem cells (NSCs) using a *nestin*-Cre driver line revealed that CYFIP1 loss in NSCs during embryonic development increases NSC cell number in the subventricular zone (Habela *et al*, 2020). In order to investigate the impact of CYFIP1 loss on the number of microglial cells, we immunolabeled microglia using anti-IBA1 antibodies in sagittal brain sections obtained from 2-month-old CTRL and *Cyfip1* cKO mice. Microglia cell numbers were counted across different brain regions, including cortex, hippocampus, amygdala, thalamus and cerebellum. Confocal images showed slightly elevated microglial cell

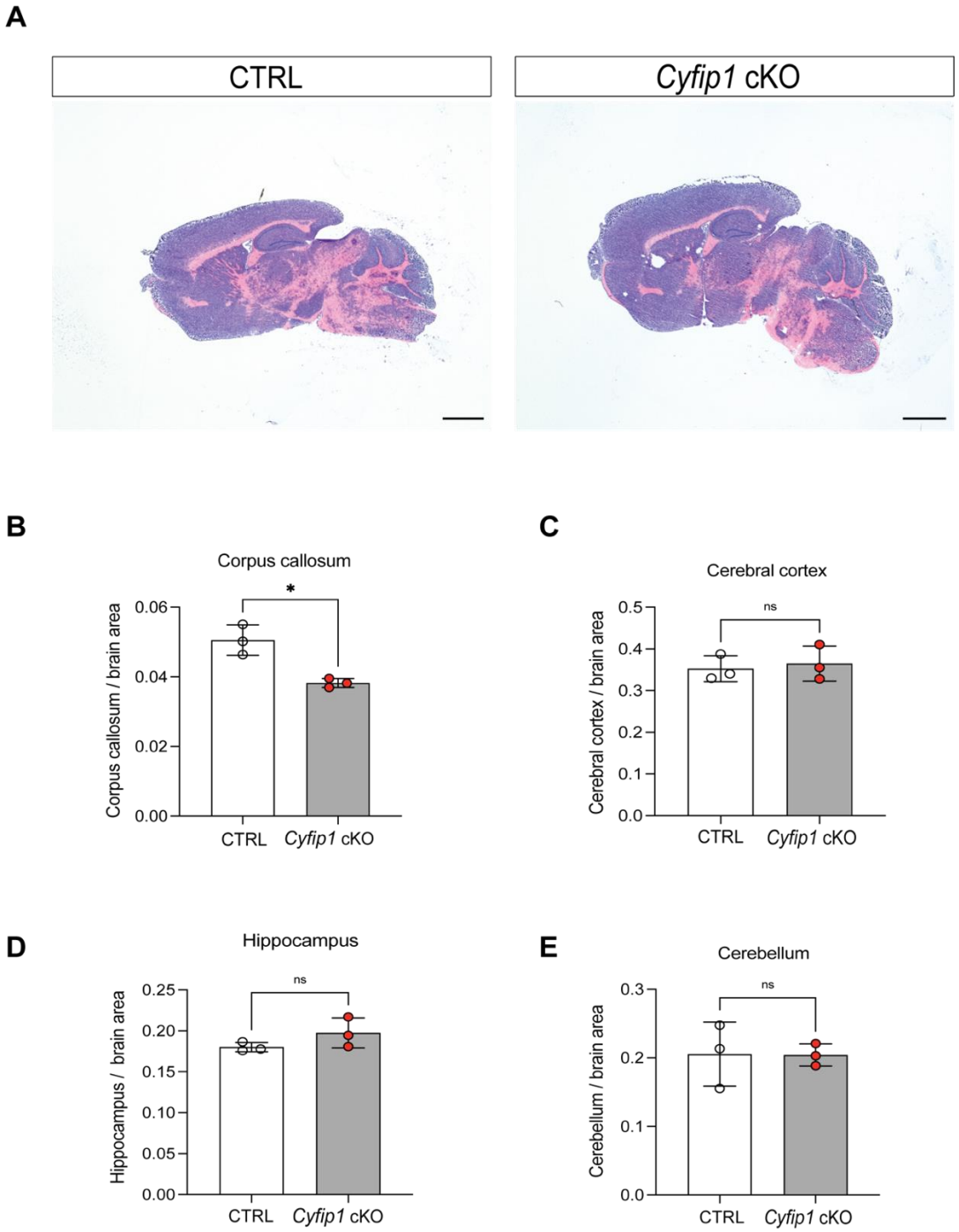

Figure 2.5: Loss of microglial CYFIP1 results in a thinner corpus callosum, with no other major brain morphological changes.
Gross brain morphology was assessed by H&E-staining of sagittal brain sections from 2-month-old CTRL and *Cyfip1* cKO mice. **(A)** Representative images of H&E-stained sagittal brain sections from CTRL and *Cyfip1* cKO mice show comparable brain morphology. **(B)** The corpus callosum of *Cyfip1* cKO mice is reduced by approximately 25 % when compared to the CTRL mice. The size of **(C)** cortex, **(D)** hippocampus and **(E)** cerebellum in *Cyfip1* cKO mice is unchanged in comparison to the CTRL mice. Brain area = area of the brain section. Scale bar = 2 mm. Data are presented as mean ± SD. Empty and red circles represent the values from individual animals. N = 3 animals per genotype. Unpaired two-tailed t-test. $^{*}p < 0.05$ compared to CTRL, ns = not significant.

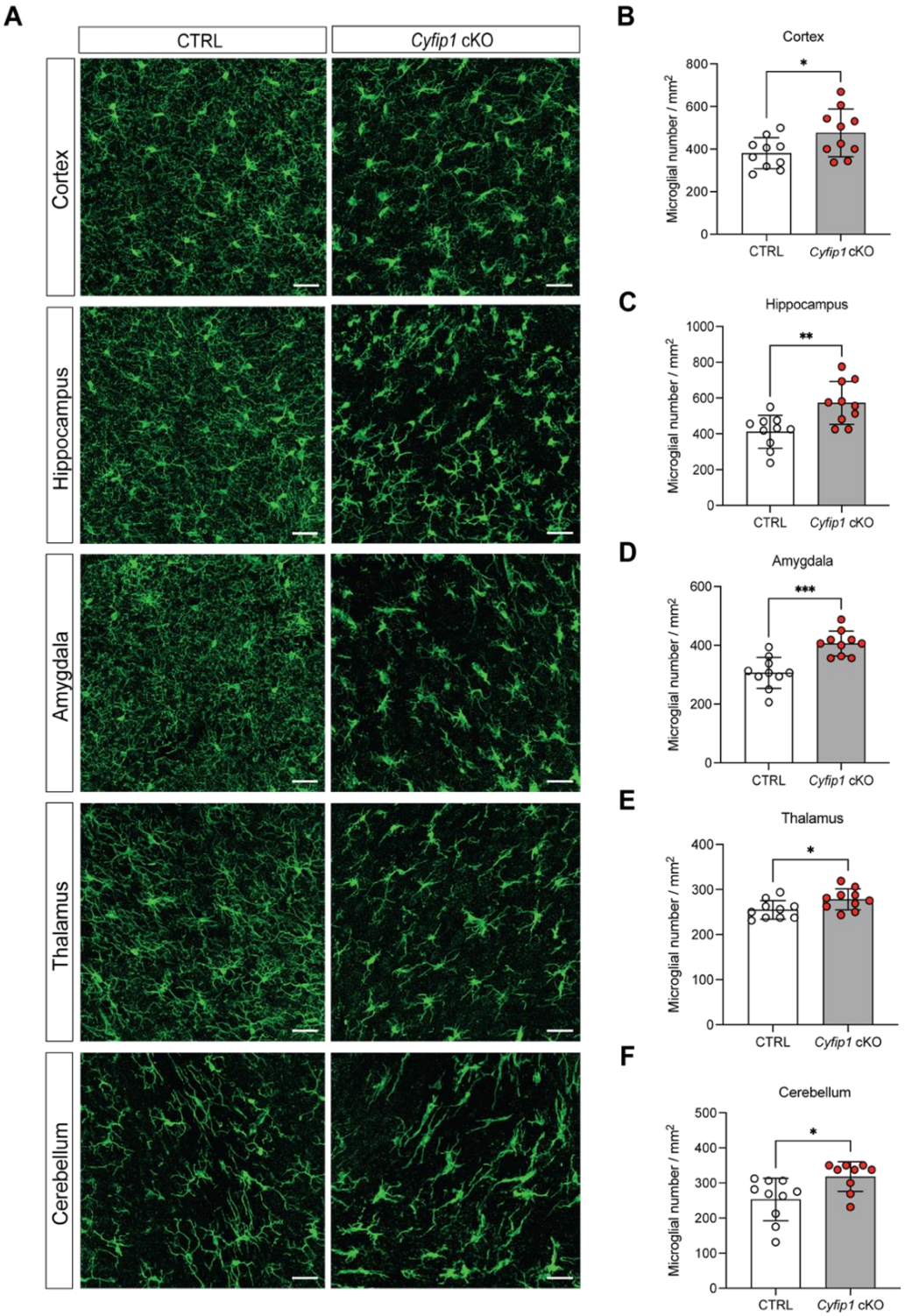

Figure 2.6: *Cyfip1* cKO mice have increased numbers of microglia across various brain regions. Microglial cell numbers across different brain regions were evaluated in brain sections from 2-month-old CTRL and *Cyfip1* cKO mice by immunolabeling microglia with anti-IBA1 antibodies (green). **(A)** Representative confocal images of microglial cells in the cortex, hippocampus, amygdala, thalamus and cerebellum. **(B - F)** Quantification of microglial cells per mm^2 show that *Cyfip1* cKO mice have higher microglial density than the CTRL mice in all the brain regions investigated. Scale bar = 30 µm. Data are presented as mean ± SD. Empty and red circles represent the values from individual animals. N = 10 animals (5 males and 5 females) per genotype. Two regions of interest (ROI) are imaged per brain region per animal. Two-tailed unpaired t test. $^{*}p < 0.05$, $^{**}p < 0.01$, $^{***}p < 0.001$.

density and reduced coverage of microglial fine processes in the assessed brain regions of *Cyfip1* cKO mice when compared to the CTRL mice (Figure 2.6 A).

Quantification of IBA1+ microglial cells revealed that *Cyfip1* cKO mice have approximately 1.1 – 1.4 times more microglial cells per mm^2 than CTRL mice across all brain regions investigated. In both CTRL and *Cyfip1* cKO mice, microglial cell number was slightly higher in the cortex and hippocampus compared to amygdala, thalamus and cerebellum (Figure 2.6 B - F).

2.4. *Cyfip1* deletion reduces microglial morphological complexity and surveying volume

Changes in *Cyfip1* gene dosage have been shown to affect cell morphology. For example, it has been shown that haploinsufficiency of *Cyfip1* is associated with reduced dendritic complexity (Pathania *et al.*, 2014), whereas *Cyfip1* overexpression leads to aberrant neurite outgrowth and spine density (Oguro-Ando *et al.*, 2015).

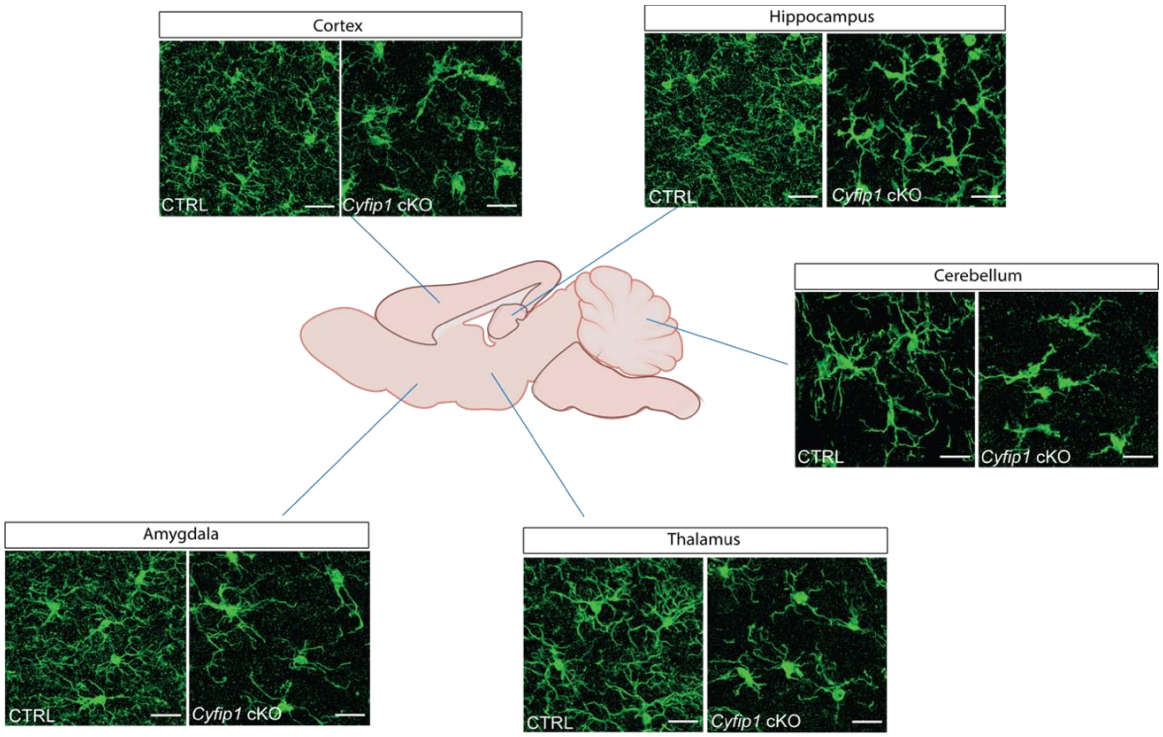

Figure 2.7: Microglial *Cyfip1* deletion results in global alteration of microglial morphology in the mouse brain.
Brain tissue obtained from 2-month-old CTRL and *Cyfip1* cKO mice was immunolabeled with anti-IBA1 antibodies for the visualization of microglial morphology. Representative confocal images show a heterogenous microglial morphology across different regions, independent of the genotype. Loss of CYFIP1 in microglia has a global effect reducing microglial morphological complexity across various brain regions (cortex, hippocampus, amygdala, thalamus and cerebellum). Scale bar = 20 µm.

Given the close association between the morphology of microglia and their functions and homeostatic status, we aimed to investigate the effect of CYFIP1 loss on microglial morphology. To analyze microglial morphology, brain sections obtained from 2-month-old CTRL and *Cyfip1* cKO mice were immunolabeled with anti-IBA1 antibodies and imaged with confocal microscopy. Microglial morphology in various brain regions was then evaluated. Figure 2.7 shows an overview of microglial morphology in the cortex, hippocampus, amygdala, thalamus and cerebellum of CTRL and *Cyfip1* cKO mice. Microglial morphology varies across different brain regions, regardless of the genotype. For instance, cortical and hippocampal microglia exhibit more fine processes than microglia in amygdala, thalamus and cerebellum. *Cyfip1* cKO microglia invariably showed a reduced morphological complexity when compared to the CTRL microglia from the same brain region, indicating a consistent impact of CYFIP1 loss on microglial morphology.

To delve deeper into microglial morphological alterations, we analyzed microglial morphology using MotiQ, an ImageJ-based open source plugin developed in our lab (Hansen *et al*, 2022) to perform automated cell morphology analysis. This analysis approach is based on a thresholding function to separate cells from the background and then creates binary images for 3D reconstruction from confocal imaging Z-stacks. The microglial cell, its convex hull and the cell's cytoskeleton are reconstructed (Figure 2.8 A), and several morphological parameters are automatically calculated.

From the 3D reconstruction of microglial cells, we were able to obtain the volume and ramification index of microglia. The cell volume reflects the size of microglial cells, and the ramification characterizes the overall complexity of microglial cell shape. The ramification index represents the ratio of the cell surface area to the surface area of a perfect sphere with the same volume as the cell. It is a unit-free parameter. The convex hull depicts the volume surveyed by each microglial cell (spanned volume), providing information about the size of the cell's territory. The parameters of the cell skeleton include the number of branches, the number of junctions and the average branch length. These parameters provide additional information on the subcomponents of microglial processes.

Only the analysis of microglia in the cortex is shown here, since the morphological changes observed in the cortex of *Cyfip1* cKO mice were found to be conserved across all brain regions investigated. 3D reconstruction revealed that *Cyfip1* cKO microglia had a 25 % reduction in cell volume and 23 % decrease in ramification when compared to CTRL microglia (Figure 2.8

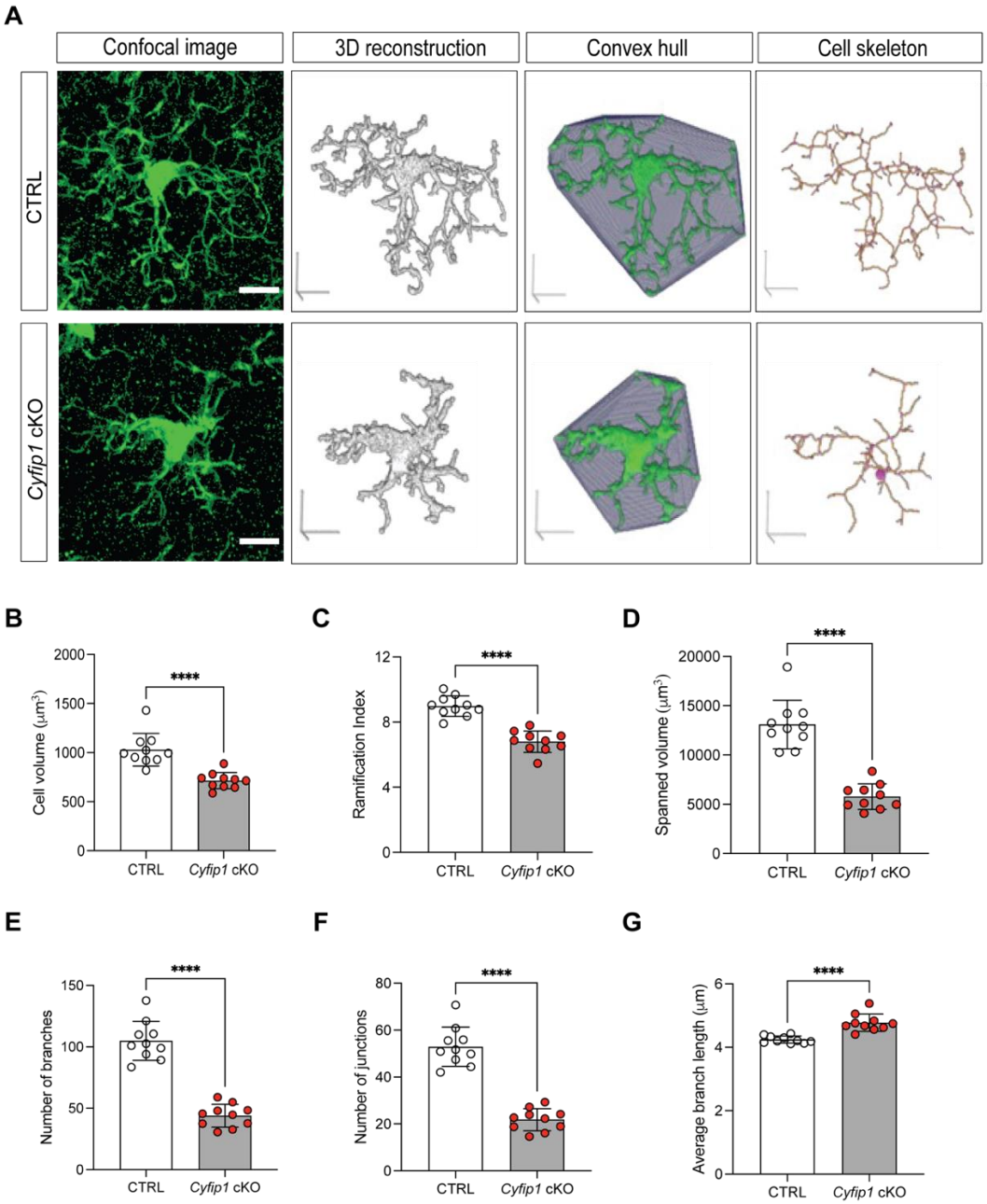

Figure 2.8: *Cyfip1* cKO microglia have reduced morphological complexity and surveying volume.

The morphology of microglia in 2-month-old CTRL and *Cyfip1* cKO mice was analyzed using immunostaining with anti-IBA1 antibodies. **(A)** Representative confocal images of a cortical microglial cell from CTRL and *Cyfip1* cKO mice, its 3D reconstruction, convex hull representing microglial spanned volume, and the cell cytoskeleton showing the branches and junctions. **(B, C)** Quantified cell volume and ramification index of *Cyfip1* cKO microglia are reduced by approximately 25 % when compared to the CTRL microglia. **(D)** Spanned volume of *Cyfip1* cKO microglia is significantly decreased by 55 % compared to CTRL microglia. **(E, F)** The number of branches and junctions in *Cyfip1* cKO microglia is reduced by 50 % in comparison to CTRL microglia. **(G)** *Cyfip1* cKO microglia show a 13 % increase in their average primary branch length in comparison to the CTRL microglia. Scale bar = 10 µm. Data are presented as mean ± SD. Empty and red circles represent the values from individual animals. N = 10 animals per genotype (5 males and 5 females). Two regions of interest (ROI) are imaged per brain region per animal. Unpaired two-tailed t-test. $^{****}p < 0.0001$.

B, C). *Cyfip1* cKO microglia also exhibited a 55 % decrease in the spanned volume when compared to the CTRL microglia (Figure 2.8 D). Alterations of cell skeleton were also observed in *Cyfip1* cKO microglia, in particular a 50 % reduction in the number of branches and junctions (Figure 2.8 E and F), accompanied by a greater length of the primary branch (Figure 2.9 G) than in the CTRL microglia.

Since it was reported that microglia exhibit sex-dependent morphology during development (Gildawie *et al*, 2020), we further divided each genotype group into male and female subgroups to determine whether the morphological alterations observed in *Cyfip1* cKO microglia in our study are sex-dependent. Our results revealed that in both *Cyfip1* cKO and CTRL mice, microglia morphology in males and females was comparable (Figure 2.9). However, microglia in the cortex of male mice exhibited greater ramification than those in female mice. This phenotype was observed in both *Cyfip1* cKO and CTRL mice, indicating that the impact of CYFIP1 on microglial morphology was not sex-dependent. Overall, our findings reveal a fundamental role of CYFIP1 in microglial morphogenesis that is sex-independent.

2.5. *Cyfip1* cKO microglia show a non-homeostatic phenotype

Microglia are characterized by their ramified morphology, which consists of highly branched and motile processes, which continually survey the microenvironment in the brain. Upon sensing an imbalance in the brain environment, they gradually transform their morphology to respond to the perturbation. These morphological transformations usually involve soma enlargement and thickened, shortened processes, which indicate an “activated state” of microglia (Fernandez-Arjona *et al*, 2017). Following our discovery of morphological alterations in *Cyfip1* cKO microglia, we noticed that the morphological changes in *Cyfip1* cKO microglia aligned with the characteristics of activated microglia. To explore whether the absence of CYFIP1 disrupts microglial homeostasis, we immunolabeled microglia with anti-IBA1 and anti-CD68 antibodies. CD68 is a commonly used marker for activated microglia, and its upregulation has been used to detect microglial activation (Hong *et al*, 2016; Matsui *et al*, 2013).

Z-stack confocal images of IBA1 and CD68 immunolabeled cortical and hippocampal microglia from 2-month-old *Cyfip1* cKO and CTRL mice were used for 3D reconstruction. Microglial cell volume and CD68 volume were reconstructed (see chapter 4.2.7.2), and the percentage of CD68 volume to microglial cell volume was calculated to determine the average proportion of CD68 expression in the cell.

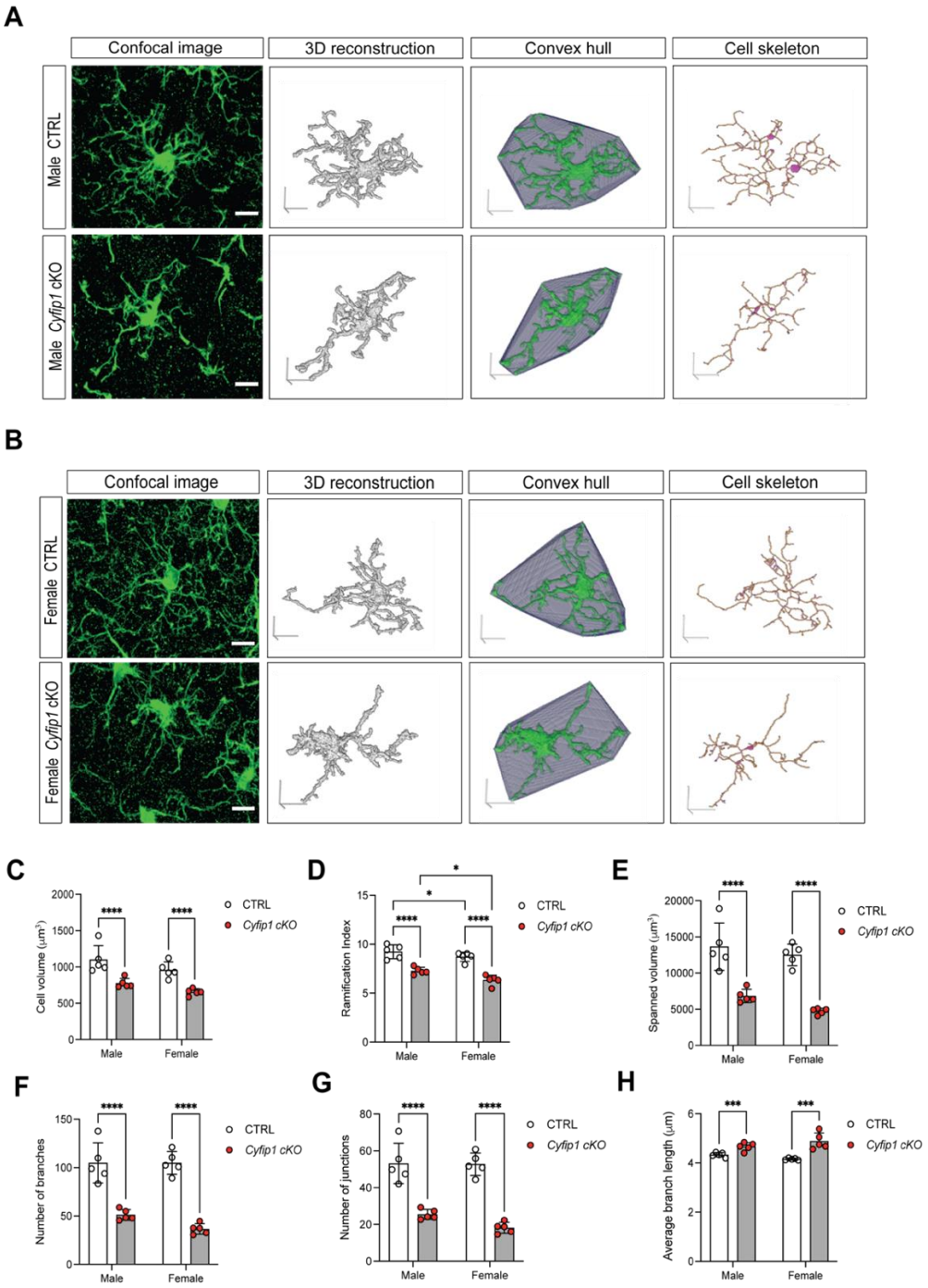

Figure 2.9: Morphological changes of microglia in *Cyfip1* cKO mice are sex-independent. The morphology of microglia was compared in 2-month-old CTRL and *Cyfip1* cKO male and female mice. Cortical microglia from male and female mice are shown as an example. **(A)** Representative confocal images of cortical microglia, MotiQ-reconstruction, convex hull calculation and their cytoskeleton from male and **(B)** female mice. No sex-dependence can be detected in **(C)** cell volume, **(E)** spanned volume, **(F)** numbers of branches and **(G)** junctions, and **(H)** average branch length. **(D)** In both CTRL and *Cyfip1* cKO mice, the ramification index of microglia is higher in males than in females. Scale bar = 10 µm. Data are presented as mean ± SD. Empty and red circles represent the values from individual animals. N = 5 animals per genotype in each sex. Two regions of interest (ROI) are imaged per brain region per animal. Two-way ANOVA with Tukey's post-hoc test. $^{*}p < 0.05$, $^{***}p < 0.001$ $^{****}p < 0.0001$.

Figure 2.10 A and C shows that, in both the cortex and hippocampus, *Cyfip1* cKO microglia express significantly higher levels of CD68 compared to CTRL microglia. Through quantitative analysis, we found that in the cortex of the CTRL mice, CD68 volume represents approximately 13 % of microglia volume, while the percentage increased to 20 % in the cortical microglia of *Cyfip1* cKO mice (Figure 2.10 B).

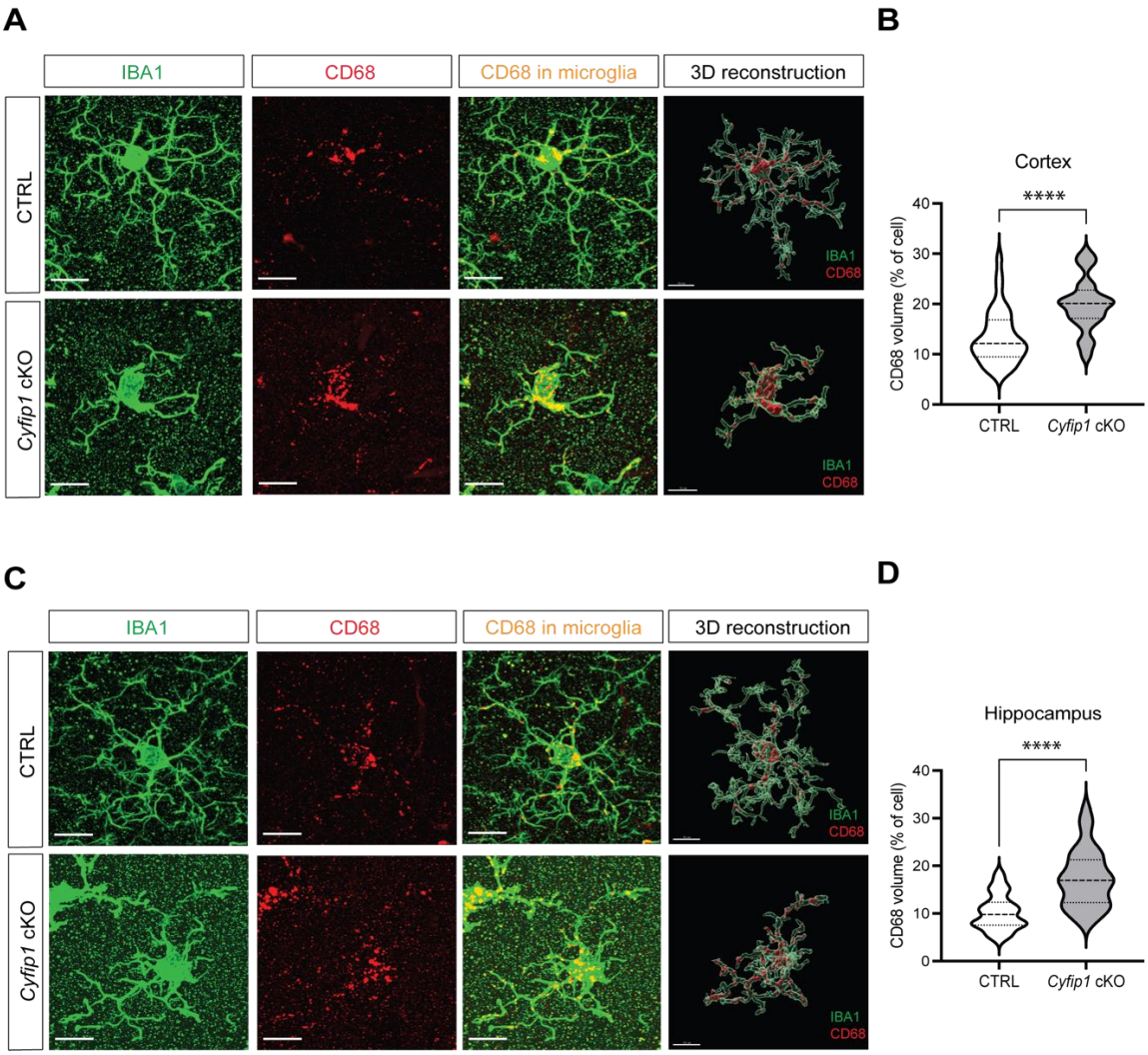

Figure 2.10: The level of CD68, a microglial activation marker, is increased in *Cyfip1* cKO microglia.
Microglia from 2-month-old *Cyfip1* cKO and CTRL mice were immunolabeled with anti-IBA1 (green) and anti-CD68 (red) antibodies. The proportion of CD68 level within the cell was determined by calculating the ratio of CD68 volume to the microglial cell volume. Representative images of a **(A)** cortical and **(C)** hippocampal CTRL and *Cyfip1* cKO microglial cell labelled with the described antibodies and its 3D reconstruction. The CD68 expression in *Cyfip1* cKO microglia is significantly increased when compared to the CTRL microglia in both **(B)** the cortex and **(D)** the hippocampus. Scale bar = 10 µm. Data are presented as median (thick black dash line) with 25th to 75th percentile (thin grey dash lines). CTRL: n = 36 cells from 10 animals (5 males, 5 females), *Cyfip1* cKO: n = 40 cells from 10 animals (5 males, 5 females). Two regions of interest (ROI) are imaged per brain region per animal. Mann-Whitney test. $^{****}p < 0.0001$.

In the hippocampus, the CD68 occupancy in the CTRL microglia was 10 %, whereas it was increased to 20 % in the *Cyfip1* cKO microglia (Figure 2.10 D). The increased proportion of CD68 volume indicates an activated state of *Cyfip1* cKO microglia.

2.6. CYFIP1 is essential for microglial phagocytic function

To better study the mechanistic implications of CYFIP1-dependent WRC in microglial functions and motility, we established an *in vitro* culture system using primary microglia harvested from postnatal day 0 – 3 (P0 – P3) mice (see chapter 4.2.1). Primary cells are regarded as a better model for studying cellular processes in comparison to cell lines, since they are directly isolated from the tissue of interest without induced genetic modifications that lead to immortalization.

As the major phagocytes in the brain, phagocytic function of microglia is critical for clearing pathogens and apoptotic cells. In recent years, microglia were also proposed to be involved in the formation of neural circuits during development by phagocytosing synaptic components (Paolicelli *et al.*, 2011; Schafer *et al.*, 2012) . To investigate if loss of CYFIP1 affects microglial phagocytosis of synaptic material, we established an *in vitro* synaptosome phagocytosis assay (see chapter 4.2.2.4). Primary microglia from *Cyfip1* cKO and CTRL mice were given pHrodo-labeled synaptosomes. pHrodo is a pH-sensitive fluorescent dye which exhibits increased fluorescence in response to acidic environments. Thus, when the pHrodo-labeled synaptosomes are engulfed by primary microglia and internalized into lysosomes, an increased fluorescent signal is emitted due to the decrease of pH value. Live-cell imaging was performed for 24 hours to investigate microglial phagocytic activity. Immunofluorescence staining of microglia was also performed at the end of live-cell imaging to assess synaptosome engulfment at the single-cell level.

In Figure 2.11 A, representative images of microglial phagocytic status at the end time point (24 h) are shown. The images show that *Cyfip1* cKO microglia had significantly reduced engulfment of synaptosomes in comparison to the CTRL microglia. The time-lapse analysis of synaptosome engulfment over a period of 24 hours (Figure 2.11 B) revealed that the total pHrodo intensity (corresponding to engulfed synaptosomes) in *Cyfip1* cKO microglia was significantly lower than in CTRL microglia starting from 14 h. Moreover, the pHrodo intensity in *Cyfip1* cKO microglia did not increase from 13 h onwards, whereas the pHrodo intensity in CTRL microglia continued to increase steadily until 18 h (Figure 2.11 B). At the end of live-

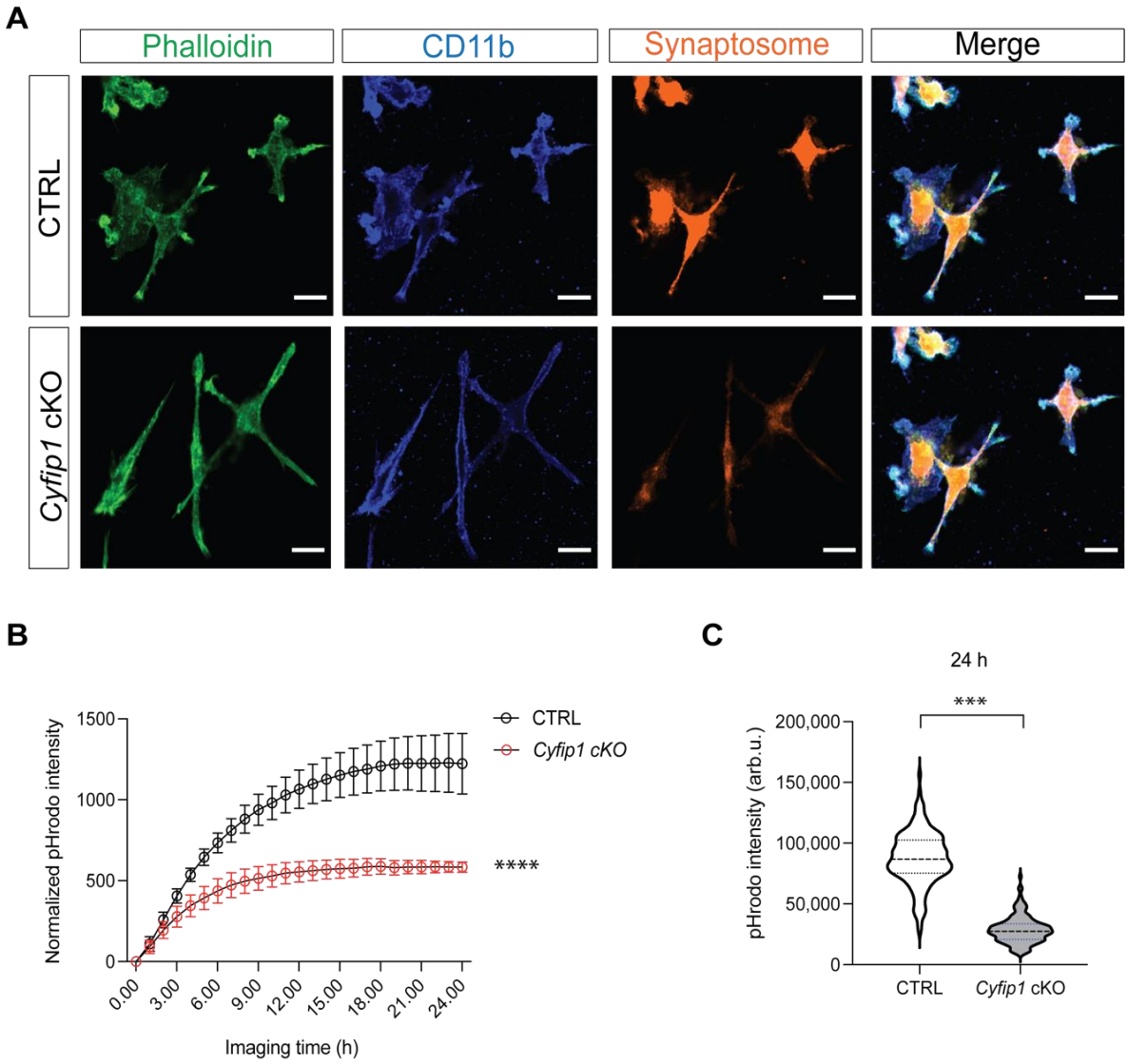

Figure 2.11: Loss of CYFIP1 impairs microglial phagocytosis.
An *in vitro* synaptosome phagocytosis assay was developed to investigate the role of CYFIP1 in microglial phagocytic function. Primary microglia were given pHrodo-labeled synaptosomes, and their phagocytic behavior was monitored through live-cell imaging with one-hour intervals for a period of 24 hours. **(A)** Representative confocal images of primary CTRL and *Cyfip1* cKO microglia identified by CD11b (blue) labeling with their actin cytoskeleton visualized using phalloidin (green) staining and the engulfed synaptosomes (orange) at the end of the phagocytosis assay (24 h). Scale bar = 20 µm. **(B)** Time-lapse analysis reveals that the intensity of engulfed synaptosomes (pHrodo intensity) is significantly lower in the *Cyfip1* cKO microglia when compared to the CTRL microglia. Data are presented as mean ± SD. N =3 independent phagocytosis assays. Repeated measures ANOVA with Šídák's multiple comparisons test of *Cyfip1* cKO versus CTRL within each time point: $p<0.05$ from 3 h, $p<0.01$ from 5 h, $p<0.001$ from 7 h, $p<0.0001$ from 9 h. Genotype x time interaction, $p < 0.0001$, $F(24, 96) = 12.90$. **(C)** The average pHrodo intensity within each individual cell at the end of the phagocytosis assay is 70 % lower in *Cyfip1* cKO microglia than that in the CTRL. Data are presented as median (thick black dash line) with 25th to 75th percentile (thin grey dash lines). N = 150 cells per genotype. Z test. $^{***}p < 0.001$, $^{****}p < 0.0001$.

cell imaging, microglia were fixed and subjected to staining with phalloidin and anti-CD11b antibodies. Phalloidin was used to stain actin filaments, allowing a good visualization of cell structure, while CD11b labeling was used to mark microglia. The pHrodo intensity in each microglial cell was measured, and a total of 150 cells per genotype were analyzed. It was observed that at the end of the phagocytosis assay, the average pHrodo intensity of synaptosomes in *Cyfip1* cKO microglia was approximately 70 % less than the average pHrodo intensity in the CTRL microglia (Figure 2.11 C). Our results indicate that loss of CYFIP1 significantly reduces the phagocytic ability of microglia.

2.7. CYFIP1 is necessary for microglial motility

Microglia are highly dynamic cells, which constantly monitor the brain parenchyma using their motile processes (Nimmerjahn *et al.*, 2005). They possess two types of motility: baseline motility, which involves the continuous extension and retraction of processes for the interactions with the environment, such as physically contacting neuronal synapses (Paolicelli *et al.*, 2011; Parkhurst *et al.*, 2013; Schafer *et al.*, 2012) , as well as clearing extracellular matrix (Crapser *et al*, 2021; Nguyen *et al.*, 2020) and cell debris; and directional motility, which is triggered by signals of tissue damage and involves chemotactic movement of processes followed by cell migration towards the site of injury (Franco-Bocanegra *et al*, 2019). Both baseline motility and directional motility of microglia are largely dependent on the constant remodeling of the actin cytoskeleton. To investigate the role of the CYFIP1-WRC in microglial motility, we established an *in vitro* wound healing assay (see chapter 4.2.2.3) to explore the directed movement of microglia. We also utilized immunocytofluorescence (see chapter 4.2.6.2) to quantify microglial lamellipodia, and conducted live-cell imaging to observe microglial membrane ruffling (see chapter 4.2.6.1).

2.7.1. *Cyfip1* deletion impairs directed migration of microglia

In order to investigate the directed migration of microglia, an in vitro wound healing assay was performed using primary microglia from *Cyfip1* cKO and CTRL mice. A scratch was introduced in a dense microglia culture and the closure of the wound by microglia was monitored for a duration of 72 hours through bright-field live-cell imaging. Representative bright-field images at the end time-point (72 h) showed that the wound was thoroughly covered by CTRL microglia, while the wound in the *Cyfip1* cKO cultures remained largely uncovered, indicating that *Cyfip1* cKO microglia were unable to efficiently migrate and close the wound (Figure 2.12 A). We further conducted a time-lapse analysis on the closure of the wound

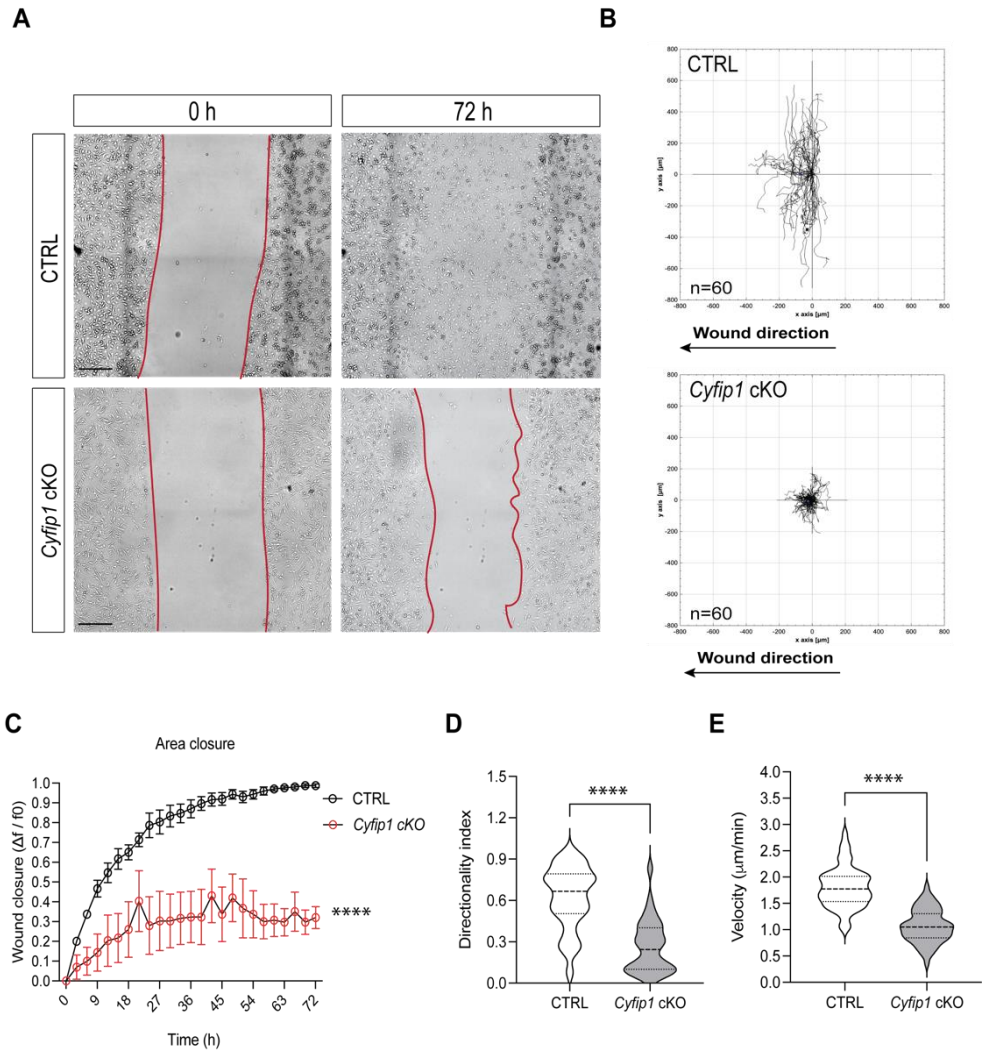

Figure 2.12: Loss of CYFIP1 impairs directed migration and speed of microglia.
An *in vitro* wound healing assay was used to study the role of CYFIP1-dependent WRC in the directed migration of microglia. **(A)** Representative bright-field images of the wound healing assay at the start (0 h) and end time-point (72 h) from one CTRL and one *Cyfip1* cKO microglia culture, scale bar = 1 mm. **(B)** Trajectory plots of CTRL and *Cyfip1* cKO microglial cells show that *Cyfip1* cKO microglia exhibit erratic and undirected movement. Both CTRL and *Cyfip1* cKO microglial cells are tracked from the right side of the wound. N = 60 cells per genotype from 3 independent wound healing assays. **(C)** Time-lapse analysis of the wound healing assay reveals that CTRL microglia completely cover the wound in around 60 h, while *Cyfip1* cKO microglia only cover approximately 40 % of the wound in 72 h. The wound closure ($\Delta f/f_0$) is calculated by normalizing at any time-point the wound area covered by microglia ($\Delta f = f_0 - f_t$) to the initial wound area (f_0). Data are presented as mean ± SD. N = 3 independent wound healing assays. Repeated measures ANOVA with Šídák's multiple comparisons test of *Cyfip1* cKO versus CTRL within each time point: *p-value* significant from 15 h. Genotype x time interaction, $p < 0.0001$, F (24, 96) = 11.16. **(D)** Violin plots of the directionality index (straight line distance between start and end position/total distance) of CTRL and *Cyfip1* cKO microglia show a significant three-fold reduction in *Cyfip1* cKO microglia compared to the CTRL. **(E)** The velocity of *Cyfip1* cKO microglia is 40 % less than CTRL microglia. In **(D)** and **(E)** data are presented as median (thick black dash line) with 25th to 75th percentile (thin grey dash lines). N = 60 cells per genotype from 3 independent wound healing assays. Mann-Whitney test. $^{****}p < 0.0001$.

throughout the 72-hour period. The closure of the wound was evaluated by normalizing the wound area covered by microglia to the initial wound area, thereby indicating the ratio of wound coverage by microglia. If the wound is covered completely, the ratio of wound closure is 1. Time-lapse analysis revealed that CTRL microglia efficiently covered 80 % of the wound within the initial 36 hours, and the wound was completely closed by approximately 60 hours. In contrast, *Cyfip1* cKO microglia were only able to close 30 – 40 % of the wound area throughout the 72-hour observation period (Figure 2.12 C). Moreover, the wound area covered by *Cyfip1* cKO microglia increased and decreased during the observation time, suggesting that *Cyfip1* cKO microglia did not migrate in a steady and directional manner.

To investigate whether the inefficient closure of the wound by *Cyfip1* cKO microglia was caused by decreased migration velocity or impaired directional movement, we tracked the migratory behavior of individual CTRL and *Cyfip1* cKO microglia cells located on the border of the wound. Figure 2.12 B shows the superimposition of the migratory paths of 60 CTRL and 60 *Cyfip1* cKO microglia from the same side (right side) of the wound. Based on the trajectory plots in Figure 2.12 B, we observed that most CTRL microglia initially migrated horizontally towards the wound and then turn vertically to fill the available space. In contrast, *Cyfip1* cKO microglia exhibited no directional movement, they appeared to circle around their original position instead of migrating towards the wound. We quantified the directionality of migrating microglia by normalizing the linear distance between the start and end points of the migration to the total distance covered by microglial cells during their migration: the closer the directionality ratio to 1 the more linear and directional microglial movement (Figure 2.12 D). The result revealed that *Cyfip1* cKO microglia had significantly more erratic and undirected movement compared to the CTRL microglia, with less than three-fold directionality ratio than CTRL microglia. Finally, the velocity of migrating microglia was determined by normalizing the total distance covered by the microglia to the duration of migration. The analysis revealed that the velocity of migrating *Cyfip1* cKO microglia was decreased by 40 % compared to the velocity of the migrating CTRL microglia (Figure 2.12 E). In summary, our findings indicate that loss of CYFIP1 leads to impaired microglial migration, with loss of both speed and directionality, and severely reduces the ability to effectively close a wound.

2.7.2. The proportion of cells with lamellipodia is reduced in *Cyfip1* cKO primary microglia

It is well-known that cell migration in 2D cultures is primarily driven by the formation of lamellipodia (Raftopoulou & Hall, 2004), which is regulated by the WRC via activating the ARP2/3 complex (Chen *et al.*, 2010; Innocenti, 2018; Kage *et al*, 2022a). In order to better understand the mechanistic role of the actin cytoskeleton in the observed migratory defects in *Cyfip1* cKO microglia, we labeled the actin filaments with fluorescent phalloidin and examined the proportion of cells containing lamellipodia in both *Cyfip1* cKO and CTRL microglia in standard culture condition.

Confocal images showed that *Cyfip1* cKO microglia exhibited distinct morphological differences from the CTRL microglia (Figure 2.13 A). A lamellipodium is formed by the accumulation of branched cortical F-actin, which pushes the membrane outward and indicates the direction of cell migration.

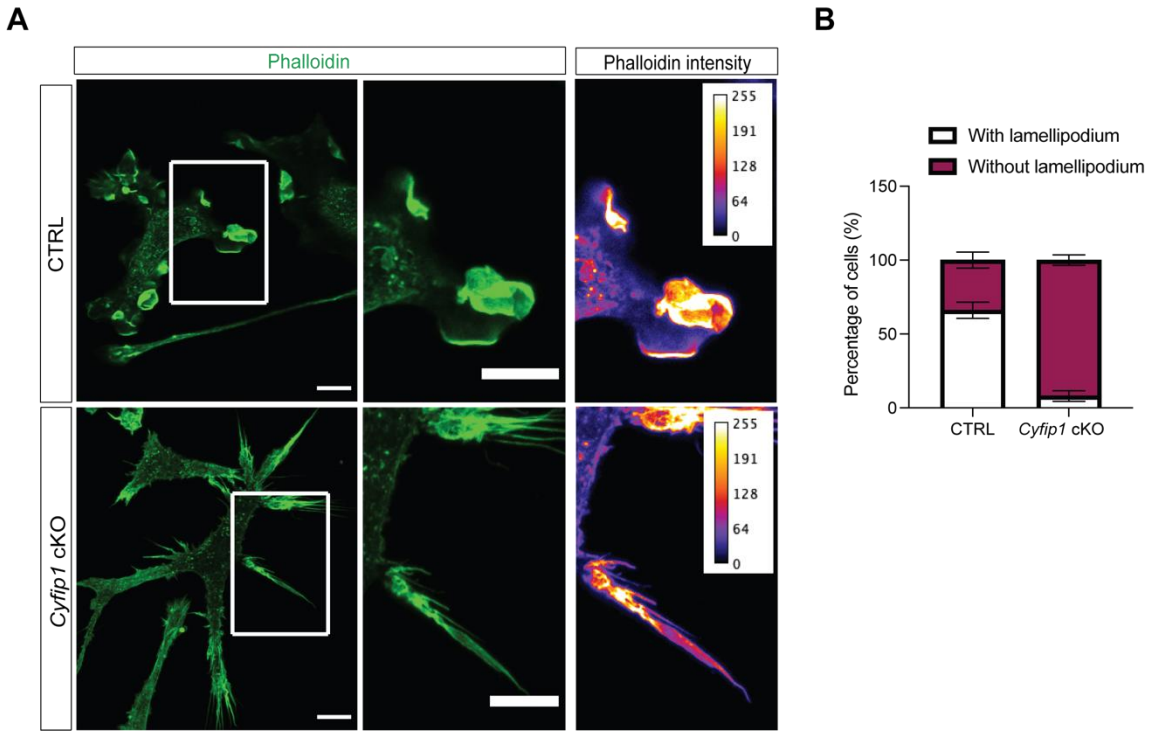

Figure 2.13: *Cyfip1* cKO microglia show a reduced proportion of cells with lamellipodia. Actin filaments in both the CTRL and *Cyfip1* cKO primary microglia were labeled with phalloidin (green). **(A)** Representative confocal images show the morphology of primary CTRL and *Cyfip1* cKO microglia. White squares regions are magnified to show the peripheral F-actin structures found in CTRL and *Cyfip1* cKO microglia and the F-actin levels. Scale bar = 10 µm **(B)** More than 60 % of the CTRL microglia possess lamellipodia, whereas lamellipodia are only observed in less than 10 % of the *Cyfip1* cKO microglia. Data are presented as mean ± SD. CTRL: n = 622, *Cyfip1* cKO: n = 322 from 3 independent primary cultures.

In CTRL microglia, lamellipodia were found in approximately 60 % of the cells. However, lamellipodia were only observed in less than 10 % of the *Cyfip1* cKO microglia and the morphology of *Cyfip1* cKO microglia appeared to be more spiky. It is likely that loss of the WRC in cells causes imbalance among actin nucleators, leading to formin-dependent actin polymerization. This indicates that the majority of *Cyfip1* cKO microglia may utilize different mechanisms for migration, which do not involve the force of lamellipodium formation (Figure 2.13 B). Our findings provide insights into the mechanism underlying CYFIP1-related microglial migratory deficits.

2.7.3. Membrane ruffles are lost in *Cyfip1* cKO microglia

In order to further characterize membrane dynamics of *Cyfip1* cKO compared to CTRL primary microglia, we set up phase contrast live-cell imaging and focused on membrane ruffling (see chapter 4.2.6.1). Membrane ruffles are non-adhesive lamellipodia that fail to attach to or are dynamically released from the substrate and retract towards the cell body (Borm *et al.*, 2005). These dynamic structures absorb extracellular molecules and occasionally serve as contact points between the phagocyte and the phagocytic targets (Flannagan *et al.*, 2012). Figure 2.14 A shows multiple membrane ruffles (red arrows) at the cell periphery of the CTRL microglia. These ruffles were highly dynamic. They underwent constant turnover, with each ruffle lasting for one to two seconds throughout the course of imaging. However, membrane ruffling was absent at the cell periphery of *Cyfip1* cKO microglia, which is in agreement with our findings in chapter 2.7.2, that *Cyfip1* cKO microglia are deficient in developing lamellipodia. Videos of *Cyfip1* cKO and CTRL microglial membrane ruffling can be accessed via scanning the QR codes in Figure 2.14 B. Overall, our findings demonstrate that loss of CYFIP1 in microglia impairs 2D microglial motility, affecting both migration velocity and directionality. This effect is likely caused by defective or abolished formation of lamellipodia and membrane ruffles.

2.8. Loss of CYFIP1 in microglia impairs the dynamics of actin filaments

As indicated earlier in this study, CYFIP1 is the only CYFIP isoform found in microglia, and *Cyfip1* deletion results in loss of the WRC, which plays a critical role in forming branched actin networks. Consequently, we found that loss of CYFIP1 disrupts the formation of microglial lamellipodia and membrane ruffles, which are driven by the dynamic reorganization of actin filaments at the cell periphery coordinated by the downstream effector of the WRC, the ARP2/3 complex.

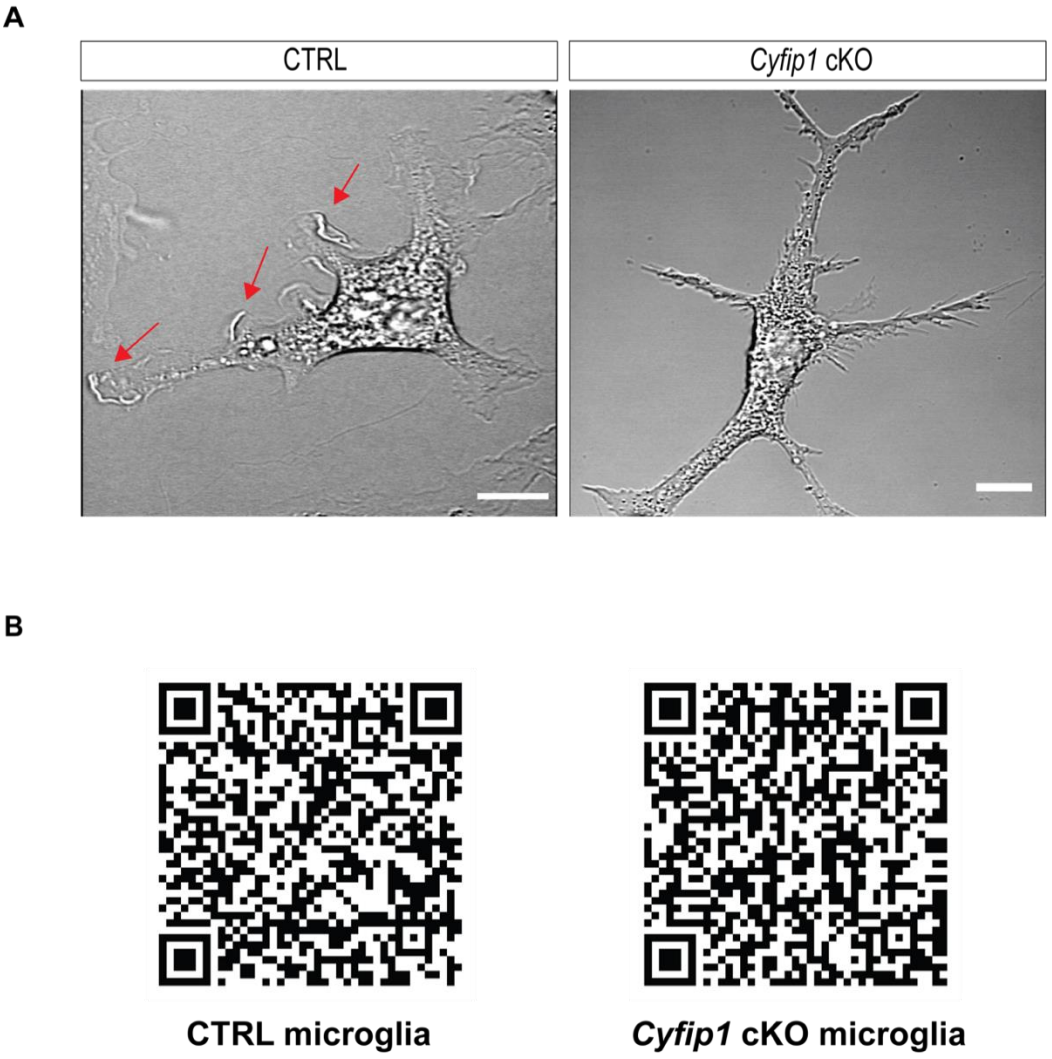

Figure 2.14: Loss of CYFIP1 impairs microglial membrane ruffling.
Membrane ruffling of primary CTRL microglia and *Cyfip1* cKO was monitored using bright-field live-cell imaging. **(A)** Representative phase contrast images of single CTRL and *Cyfip1* cKO microglial cells allow the visualization of multiple membrane ruffles at the periphery of the CTRL microglia, whereas they are virtually absent in *Cyfip1* cKO microglia. **(B)** QR codes for membrane ruffling videos of CTRL and *Cyfip1* cKO microglia. Scale bar = 10 µm.

Previous studies also showed that removing both CYFIPs or NAP1 in B16-F1 murine melanoma cells reduced F-actin intensity in the cell cortex (Kage *et al.*, 2022a). To investigate whether loss of CYFIP1 affects actin dynamics in microglia, we applied a biochemical approach, separating two insoluble F-actin fractions, stable F-actin networks and short dynamic F-actin networks, and a soluble G-actin fraction from CTRL and *Cyfip1* cKO primary microglia cells by differential centrifugation. The level of actin in each fraction was determined by semi-quantitative western blotting analysis. The F/G-actin ratios were calculated and compared between CTRL and *Cyfip1* cKO microglia. Other studies on actin dynamics have only focused on the ratio of total F-actin to G-actin (Koestler *et al*, 2009; Rasmussen *et al*, 2010; Ricotti *et*

al, 2014). However, it is important to note that dynamic F-actin is crucial for the extension of phagocytic cups in phagocytes as well as for lamellipodia extension (Barger *et al*, 2022). Both functions were impaired in *Cyfip1* cKO microglia (Figure 2.11 and 2.13). Therefore, we separated stable F-actin at 300 g and dynamic F-actin at 10,000 g in resting and phagocytosing microglia (see chapter 4.2.5.1).

Western blotting analysis showed that in non-stimulated cells, the ratio of stable F-actin to G-actin was reduced by 55 % in *Cyfip1* cKO microglia in comparison to CTRL microglia (Figure 2.15 A - C), and the dynamic F-actin was undetectable in *Cyfip1* cKO microglia (Figure 2.15 B and D).

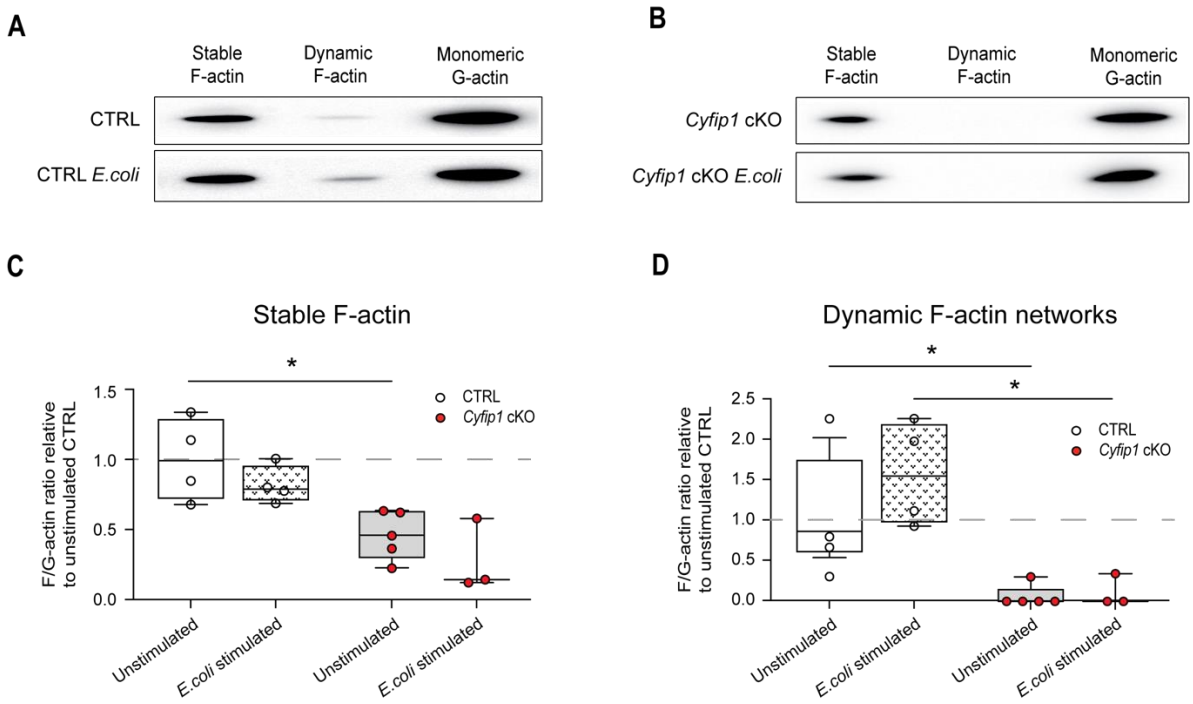

Figure 2.15: *Cyfip1* deletion in microglia results in reduced stable actin filaments and loss of dynamic actin filaments.
An *in vitro* assay was applied to explore the molecular mechanisms by which CYFIP1 regulates actin using differential centrifugation on resting and stimulated microglia cultures. Representative western blots show the levels of stable F-actin, dynamic F-actin and monomeric G-actin in **(A)** CTRL and **(B)** *Cyfip1* cKO primary microglia under unstimulated and *E. coli* stimulated conditions. **(C)** The stable F/G-actin ratio is significantly lower in *Cyfip1* cKO microglia compared to CTRL microglia under unstimulated condition. The stable F/G-actin ratio slightly decreases in both CTRL and *Cyfip1* cKO microglia following *E.coli* stimulation, but not significantly. **(D)** Under unstimulated condition, dynamic F-actin is undetectable in *Cyfip1* cKO microglia. Upon *E.coli* stimulation, the dynamic F/G-actin ratio increases by 60 % in CTRL microglia, while no obvious change is observed in *Cyfip1* cKO microglia. Data are presented as min-max box plot with individual data points (empty and red circles). Middle line represents median. For unstimulated condition, CTRL: n = 4, *Cyfip1* cKO: n = 5. For *E. coli* stimulated condition, CTRL: n = 4, *Cyfip1* cKO: n = 3. Mann-Whitney test. $^{*}p < 0.05$, ns = not significant.

To investigate if disrupted actin dynamics contributes to the poor phagocytic ability of *Cyfip1* cKO microglia, *E. coli* was given to primary microglia as phagocytic prey. *E. coli* was chosen as the phagocytic prey instead of mouse synaptosomes in this assay because synaptosomes contain a significant amount of actin, which would interfere with the actin readout in microglia. Western blotting results revealed no significant difference in stable F-actin levels between CTRL and *Cyfip1* cKO microglia following *E. coli* stimulation (Figure 2.15 A - C). Interestingly, an increase of dynamic F-actin was observed in the CTRL microglia upon *E. coli* stimulation, while no such increase was detected in *Cyfip1* cKO microglia (Figure 2.15 A, B and D). Comparing unstimulated and *E. coli*-stimulated samples within each genotype shows that following *E. coli* stimulation, CTRL microglia exhibited a 20 % decrease in stable F/G-actin ratio, accompanied by a 60 % increase of the dynamic F/G-actin ratio, suggesting a high level of ARP2/3-dependent F-actin networks rearrangements. In contrast, *Cyfip1* cKO microglia showed a 40 % decrease of the stable F/G-actin ratio (Figure 2.15 C) without a detectable concomitant increase of the dynamic F/G-actin ratio (Figure 2.15 D), suggesting that actin dynamics mechanisms might be put in place as compensatory mechanisms.

In summary, our findings reveal that *Cyfip1* cKO primary microglia have a lower stable F/G-actin ratio in comparison to CTRL microglia and undetectable dynamic F-actin already in resting conditions, which agrees with the loss of lamellipodia and membrane ruffles in the *Cyfip1* cKO microglia. Furthermore, the impaired dynamic F-actin response in *Cyfip1* cKO microglia following *E. coli* stimulation also provides an explanation for the compromised phagocytic ability of *Cyfip1* cKO microglia. Our work is the first to show how the different dynamic F-actin and stable F-actin fractions in microglia are regulated, as well as the first to uncover CYFIP1 molecular mechanisms in shaping microglial actin dynamics.

2.9. The number of neurons is unaltered in the cortex and hippocampus of *Cyfip1* cKO mice

Microglia were suggested to play a role in inducing apoptosis of neuronal cells and regulating neuronal precursor cells via phagocytosis during development (Cunningham *et al.*, 2013; Marín-Teva *et al*, 2004; Wakselman *et al*, 2008). A previous study utilizing *Cyfip1*$^{+/-}$ mice also showed a reduction in apoptosis of neuronal progenitors within the hippocampus, leading to an increase in the number of adult-born hippocampal neurons, with potential involvement of microglia in this process (Haan *et al*, 2021). Given the migratory and phagocytic impairment of *Cyfip1* cKO microglia observed in this study, we were interested to investigate the possible

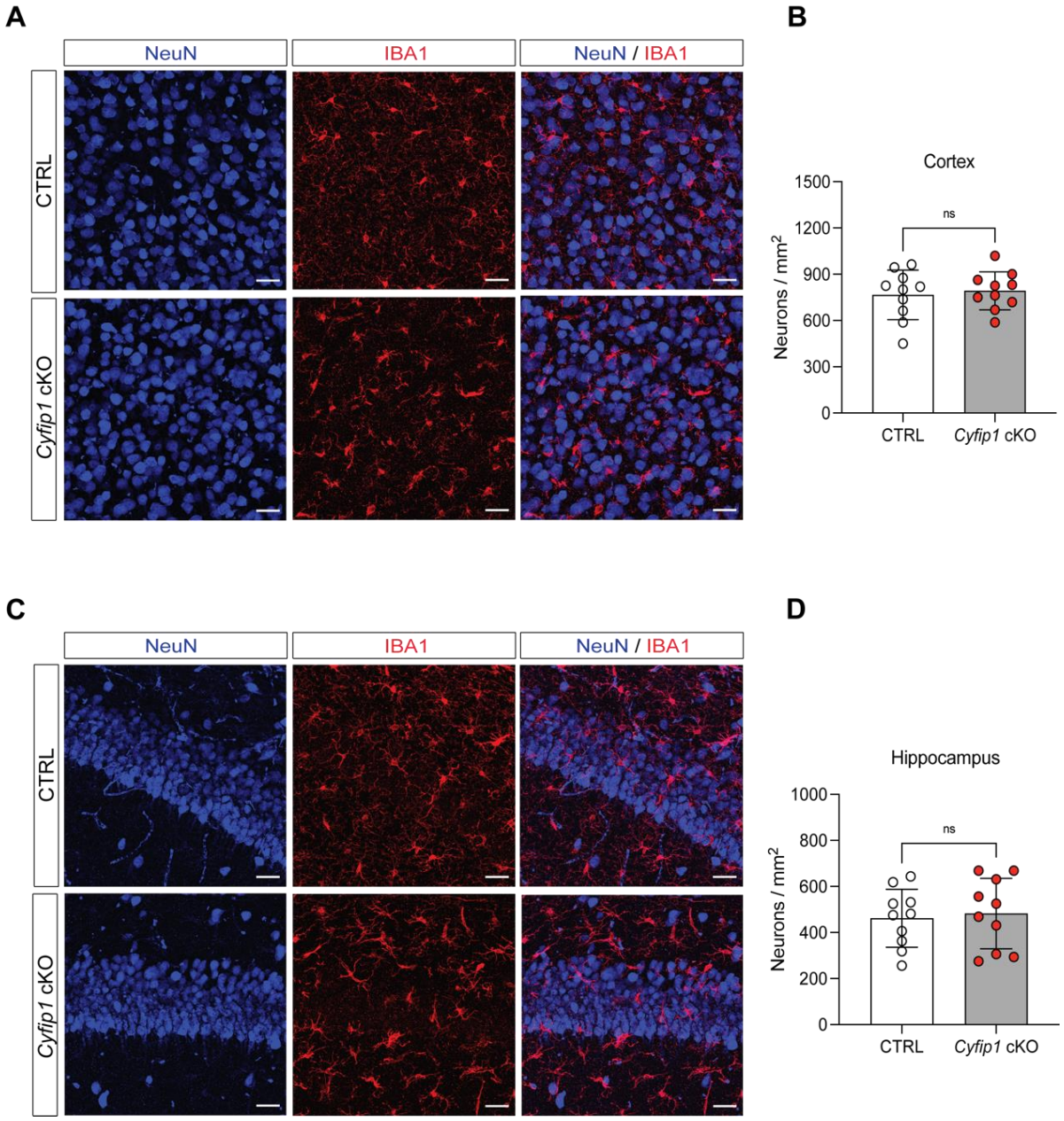

Figure 2.16: *Cyfip1* deletion in microglia does not affect the number of neuronal cells in the cortex and hippocampus.

Neuronal cells in brain slices from 2-month-old CTRL and *Cyfip1* cKO mice were immunolabeled with anti-NeuN antibodies and the numbers of NeuN+ cells per imaging field in the cortex and hippocampus were quantified. Representative confocal images show NeuN+ cells (blue) and microglia (IBA1, red) in the **(A)** cortex and **(C)** hippocampus of CTRL (upper panels) and *Cyfip1* cKO (lower panels) mice. Quantitative analysis reveals no significant difference in the number of neurons between *Cyfip1* cKO and the CTRL mice in either the **(B)** cortex and **(D)** hippocampus. Scale bar = 30 µm. Data are presented as mean ± SD. Empty and red circles represent values from individual animals. N = 10 animals (5 males and 5 females) per genotype. Two regions of interest (ROI) are imaged per brain region per animal. Two-tailed unpaired t test. ns = not significant.

impact on neuronal cell numbers. Therefore, we assessed the number of cortical and hippocampal neurons in 2-month-old CTRL and *Cyfip1* cKO mice.

Confocal images and quantitative analysis of neuronal cells in the cortex (Figure 2.16 A and B) and hippocampus (Figure 2.16 C and D) revealed no significant difference in the number of neurons between *Cyfip1* cKO mice and CTRL mice. This result shows that loss of CYFIP1 in microglia does not affect neuronal cell number.

2.10. *Cyfip1* deletion in microglia affects the maturation of dendritic spines in layer V pyramidal neuron in somatosensory cortex

Previous studies have shown that overexpression of *Cyfip1* leads to increased density of dendritic spines in pyramidal neurons in the mouse cortex (Oguro-Ando *et al.*, 2015). Conversely, *Cyfip1* haploinsufficiency resulted in an elevation of immature dendritic spines in the pyramidal neurons in CA1 region (Pathania *et al.*, 2014). Decreased spine density in cortical pyramidal neurons is a pathological hallmark of schizophrenia (Glantz & Lewis, 2000), while elevated spine density and increased number of immature spines are the characteristics found in autism spectrum disorders and intellectual disability (e.g. fragile X syndrome) (Hinton *et al*, 1991). Given that *CYFIP1* copy number variations and mutations have been associated to autism and schizophrenia and it is highly expressed in microglia, which are believed to be involved in spine remodeling (Weinhard *et al.*, 2018), we aimed to investigate whether the loss of microglial CYFIP1 affects the number and morphology of dendritic spines in the mouse.

Brain sections from 2-month-old CTRL and *Cyfip1* cKO mice were subjected to Golgi staining (see chapter 4.2.4.2 and 4.2.6.3). Golgi staining is an effective approach for randomly and entirely staining a small number of neurons in the brain, enabling the visualization of neuronal and spine morphology. Dendritic spines on the basal primary branches (extending towards the cortical layer VI) of layer V pyramidal neurons (Figure 2.17 A) in the somatosensory cortex were imaged and analyzed. The quantitative analysis showed no significant change of the spine density in *Cyfip1* cKO animals when compared to CTRL mice (Figure 2.17 C). Yet it was striking that the morphology of the spines between the CTRL and *Cyfip1* cKO animals was very different.

In order to quantify the qualitative morphological differences, we divided the spines into mushroom-shape, stubby, branched, thin, and filopodia-like, according to their morphology, and calculated their density (Figure 2.18 A and B). Mushroom-shape, stubby and branched

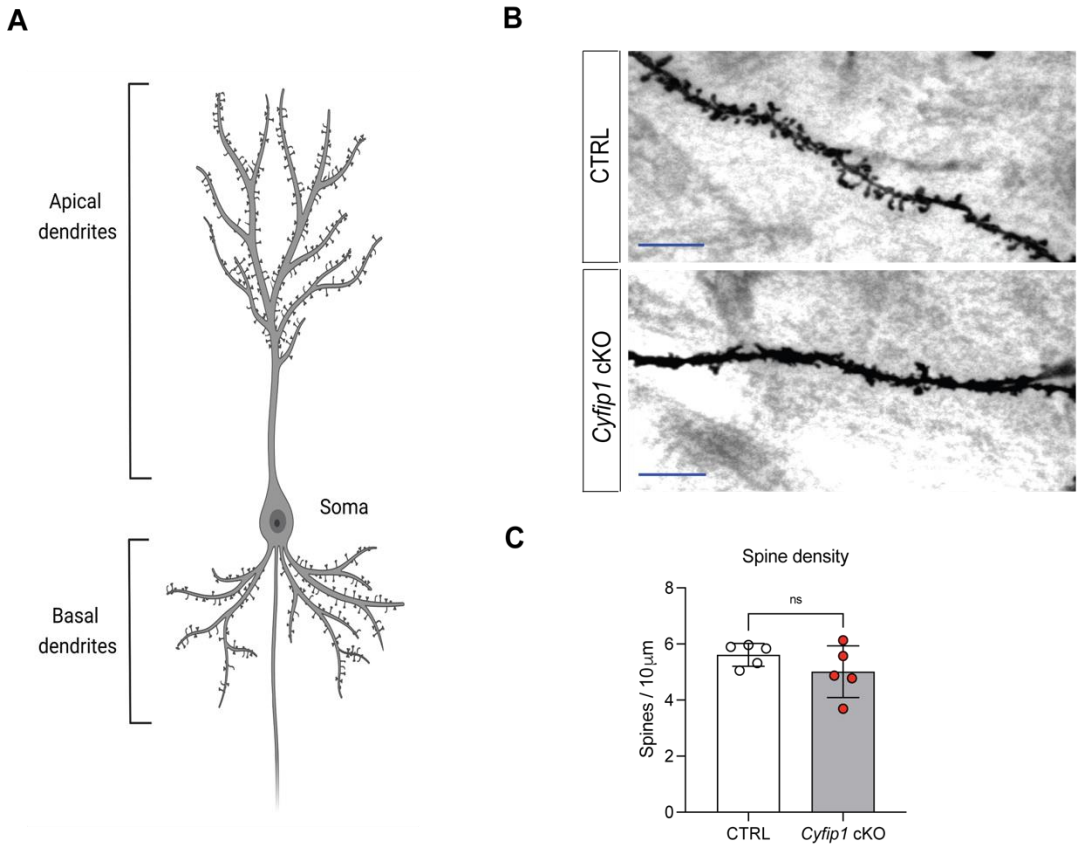

Figure 2.17: CYFIP1 loss in microglia does not alter dendritic spine density on basal primary branches of pyramidal neurons in layer V somatosensory cortex.
Golgi staining was used to investigate the density of dendritic spines. Spines on the basal primary branches of layer V pyramidal neurons in the somatosensory cortex of 2-month-old *Cyfip1* cKO and CTRL mice were quantified. **(A)** Illustration of a pyramidal neuron showing soma, basal and apical dendrites. **(B)** Representative images of primary basal dendric branches from CTRL and *Cyfip1* cKO mice after Golgi staining. Scale bar = 10 µm (**C)** Quantification of spine density on the basal primary dendrites of *Cyfip1* cKO mice shows no difference compared to the CTRL mice. Scale bar = 10 µm. Data are presented as mean ± SD. Empty and red circles represent values from individual animals. CTRL: n = 5 animals (56 cells/5 animals), *Cyfip1* cKO: n = 5 animals (61 cells/5 animals). Two-tailed unpaired t-test on the animal averages. ns = not significant.

spines were further grouped together as mature spines and their density was calculated (Figure 2.18 C). Similarly, thin and filopodia-like spines were grouped together as immature spines to calculate their density (Figure 2.18 D). This approach revealed that the densities of mushroom-shape, stubby and branched spines (number per 10 µm) on the basal primary branches of pyramidal neurons were lower in *Cyfip1* cKO mice when compared to CTRL mice, whereas the densities of thin and filopodia-like spines were significantly higher in *Cyfip1* cKO mice when compared to the CTRL mice (Figure 2.18 B). Grouping the mature and immature spines showed even more clearly that *Cyfip1* cKO mice have significantly fewer mature spines (Figure 2.18 C) and increased immature spines (Figure 2.18 D) in comparison to the CTRL mice. Our

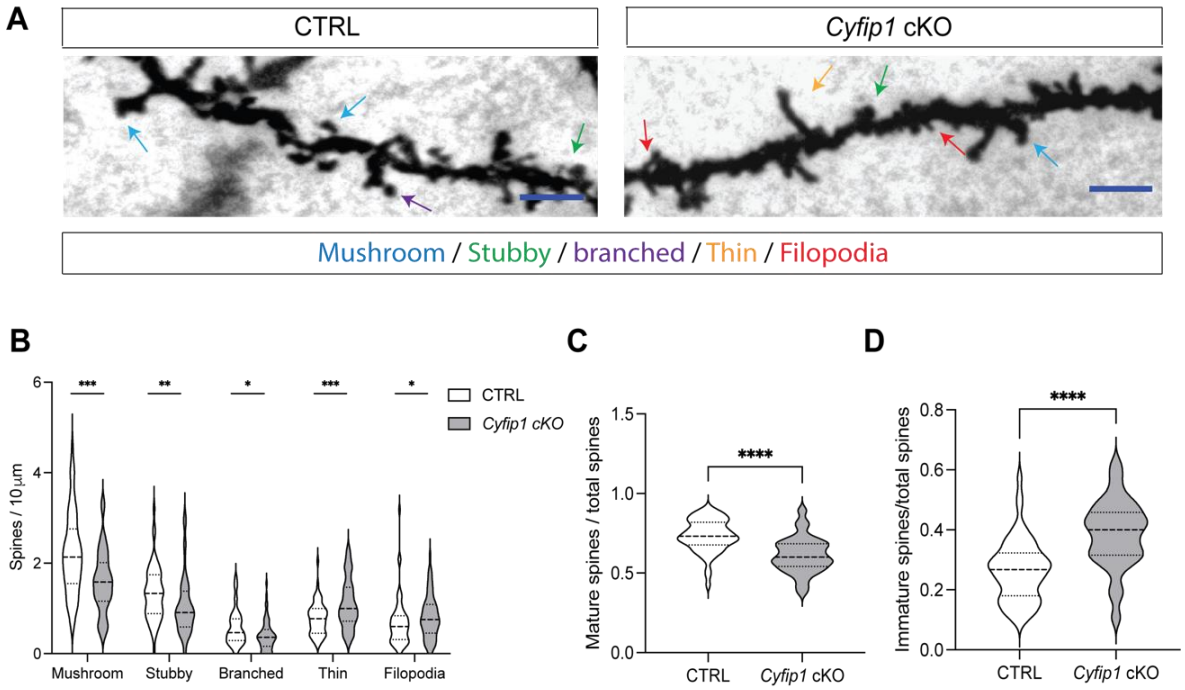

Figure 2.18: Loss of CYFIP1 in microglia affects the maturation of dendritic spines on basal primary branches of pyramidal neurons in layer V somatosensory cortex.
Golgi staining was used to investigate the morphology of dendritic spines. **(A)** Representative high magnification images of dendritic branches with examples of spines classified into distinct morphological types indicated by color-coded arrows: mushroom-shaped (blue arrow), stubby (green arrow), branched (purple arrow), thin (yellow arrow) and filopodia (red arrow). Scale bar = 5 µm. **(B)** Spine density quantification by morphological subtype reveals a reduction in the densities of mushroom-shaped, stubby and branched spines, counterbalanced by an increase in the densities of thin and filopodia-like spines in *Cyfip1* cKO mice compared to CTRL mice. **(C)** *Cyfip1* cKO mice show an overall reduction of mature dendritic spines, and **(D)** global increase of immature spines in comparison to CTRL mice. Data are presented as median (thick black dash line) with 25th to 75th percentile (thin grey dash lines). CTRL: n = 56 cells from 5 animals, *Cyfip1* cKO: n = 61 cells from 5 animals. Mann-Whitney test. $^{*}p < 0.05$, $^{**}p < 0.01$, $^{***}p < 0.001$, $^{****}p < 0.0001$.

findings show that *Cyfip1* deletion in microglia does not affect spine density, but instead maturation of dendritic spines, pointing to a role of microglia in synaptic development through mechanisms that are yet unknown.

2.11. The number of functional excitatory synapses is unaltered in the cortex, but reduced in the hippocampus of *Cyfip1* cKO mice.

The finding of decreased mature and increased immature spines in *Cyfip1* cKO mice raised the question if this would affect the establishment of functional excitatory synaptic contacts in the mutant mice. Therefore, pre- and post-synaptic terminals from brain sections of 2-month-old CTRL and *Cyfip1* cKO mice were immunolabeled with anti-bassoon and anti-HOMER1 antibodies, which target antigens in the pre-synaptic and post-synaptic compartment of

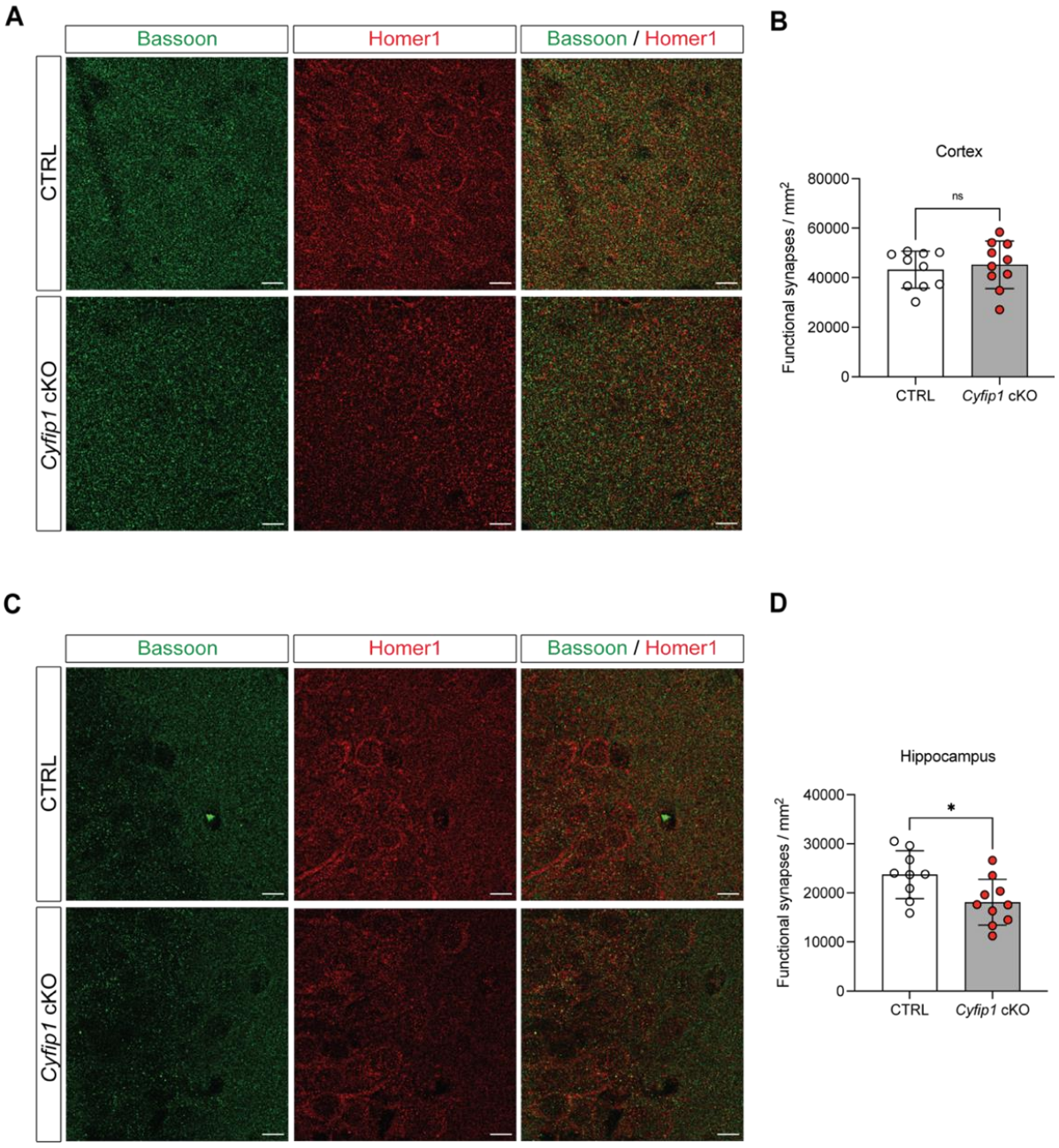

Figure 2.19: Decreased density of excitatory synapses in the hippocampus of *Cyfip1* cKO mice. Brain sections from 2-month-old CTRL and *Cyfip1* cKO mice were immunolabeled with anti-bassoon (pre-synaptic marker) and anti-HOMER1 (post-synaptic marker) antibodies. The colocalization of bassoon (green) and HOMER1 (red) indicates the presence of excitatory synapses. **(A)** Representative images of labeled synapses in the cortex. **(B)** Quantification of colocalization puncta shows no significant difference in the density of excitatory synapses (number of puncta/field) in *Cyfip1* cKO mice in comparison to CTRL mice. **(C)** Representative images of labeled synapses in the hippocampus. **(D)** Quantification of colocalization puncta shows a 20 % decrease of the excitatory synapse density in *Cyfip1* cKO mice compared to CTRL mice. Scale bar = 10 µm. Data are presented as mean ± SD. Empty and red circles represent values from individual animals. N = 10 animals (5 males, 5 females) per genotype. Two regions of interest (ROI) are imaged per brain region per animal. Two-tailed unpaired t test. $^{*}p < 0.05$, ns = not significant.

excitatory synapses, respectively. Colocalization of bassoon and HOMER1 signals is commonly recognized as an indication of functional excitatory synapses (Dani *et al*, 2010; Verstraelen *et al*, 2020). The number of excitatory synapses per imaging field in the cortex of *Cyfip1* cKO mice was not significantly different from that of the CTRL mice (Figure 2.19 A and B). Interestingly, the number of excitatory of synapses in the hippocampus of *Cyfip1* cKO microglia was lower in comparison to the number in CTRL microglia (Figure 2.19 C and D).

Chapter 3. Discussion

3.1. CYFIP1 is the only CYFIP isoform in microglia and is essential for microglial WRC integrity

Changes in *CYFIP1* expression have been linked to schizophrenia and autism spectrum disorders (Hirayama-Kurogi *et al.*, 2017; Noroozi *et al.*, 2018). However, the majority of *Cyfip1* studies have focused on neuronal phenotypes in the heterozygous mouse model, without analyzing *Cyfip1* expression patterns in the brain and the potential impact of *Cyfip1* haploinsufficiency in different CNS cells on the observed phenotype (Oguro-Ando *et al.*, 2015; Pathania *et al.*, 2014). Given the current understanding that not only neurons, but also glial cells contribute significantly to the phenotype of neurodevelopmental disorders, it is crucial to examine the expression pattern of *Cyfip1* across different CNS cells in order to dissect the role of CYFIP1 in the brain.

Previous studies on CYFIP have shown that CYFIP1 is present in almost all mammalian tissues, while CYFIP2 is predominantly expressed in the brain, especially in neurons (Hauck, 2021; Özer, 2020; Uhlen *et al.*, 2015). A recent transcriptomic study showed ubiquitous expression of *CYFIP1*/*Cyfip1* mRNA across different CNS cell types, with particularly high expression in microglia in both human and mice (Zhang *et al.*, 2014b). Since mRNA expression is not always directly correlated to protein expression, we evaluated CYFIP1 protein levels through western blotting analysis in the major cell types of the CNS, including microglia, neurons and astrocytes isolated from the adult mouse brain. Our protein expression analysis of the CYFIP isoforms shows significantly higher levels of CYFIP1 in microglia compared to neurons and astrocytes. Moreover, microglia are entirely devoid of CYFIP2, which is exclusively expressed in neurons (Figure 2.1), as previously reported. With CYFIP1 being the sole CYFIP isoform in microglia, it became clear to us that CYFIP1 might have an irreplaceable function in microglia and that microglia may then significantly contribute to the observed neurological phenotypes if one *CYFIP1* allele is lost in humans, as well as in *Cyfip1*$^{+/-}$ mice.

As CYFIP is a crucial component of the WRC, we further examined the composition of microglial WRC. The WRC can be divided into two subcomplexes, the CYFIP-NAP dimer and the WAVE-ABI-HSPC300 trimer (Chen *et al.*, 2010). CYFIP-NAP dimer functions as a scaffold for the trimer to assemble, but also prevents WAVE from accessing and activating the ARP2/3 complex. Most of the WRC members have multiple isoforms in higher eukaryotes,

except for HSPC300. Different isoforms can theoretically assemble to form different WRCs. HEM1, the only paralog of NAP1, has been identified exclusively in hematopoietic cells, while NAP1 was found in non-hematopoietic cells (Park *et al*, 2008). Considering the hematopoietic origin of microglia, we hypothesized that *Hem1*, rather than *Nap1*, was expressed in mouse microglia. Our hypothesis was confirmed as HEM1 was found to be the sole NAP isoform present in microglia. Together with HEM1, WAVE2 and ABI3, CYFIP1 forms a distinct WRC specific to microglia (Figure 2.2).

Previous studies have shown that removing or reducing one of the WRC members could result in eliminating or downregulating the entire WRC. For example, *Hem1*$^{-/-}$ macrophages showed loss of CYFIP1, WAVE2 and significantly reduced ABI1 (Stahnke *et al.*, 2021). In *Abi1*$^{-/-}$ mouse embryonic fibroblasts (MEFs), protein levels of WAVE2, CYFIP1 and NAP1 were drastically decreased (Dubielecka *et al.*, 2011). Deletion of *Cyfip2* in glutamatergic neurons also significantly reduced protein levels of WAVE1, ABI1, NAP1 and HSPC300 (Özer, 2020). *Cyfip1*-knockdown in cortical neurons showed decreased expression of *Nap1*, *Abi1*, *Wave1* and *Hspc300* mRNA (Abekhoukh *et al*, 2017). In our work, deletion of *Cyfip1* in microglia led to almost complete depletion of HEM1, WAVE2 and ABI3 (Figure 2.4). The extent of WRC loss in *Cyfip1* cKO microglia is more significant compared to the studies mentioned above, most likely because microglia express only one isoform of each WRC component, forming only one WRC. Therefore, loss of any single WRC component would result in almost complete elimination of the WRC in microglia.

3.2. CYFIP1-WRC is important for microglial phagocytosis and cell migration

Having only one WRC (CYFIP1-HEM1-ABI3-WAVE2-HSPC300) makes microglia a great model to study the functions of the CYFIP1-WRC. Our *Cyfip1* cKO primary microglia showed a strong deficiency in phagocytosing synaptosomes (Figure 2.11), as well as complete loss of directional migration and reduced moving speed in a wound healing assay (Figure 2.12). These results are in line with the phenotypes observed in *Hem1*$^{-/-}$ macrophages and *ABI3* knockdown in a human microglia cell line. *Hem1*$^{-/-}$ macrophages presented compromised phagocytic cup formation to enwrap C3bi-coated beads and impaired directional movement together with reduced moving speed in response to complement 5a (C5a) gradient, in both 2D and 3D culture conditions (Stahnke *et al.*, 2021). *ABI3* knockdown microglia also exhibited impaired migration in the wound healing assay, and *Abi3*$^{-/-}$ 5xFAD mice had decreased number of microglia moving towards amyloid-β plaques (Karahan *et al*, 2021).

The formation and extension of the phagocytic cup requires actin polymerization which is mediated, at least in part, by the WRC-dependent ARP2/3 complex. For the phagocytic cup to extend, it is essential for the phagocyte's membrane to establish adhesion with the phagocytic prey to prevent the retrograde fallback of the phagocytic cup. In the same study on *Hem1*$^{-/-}$ macrophages, Stahnke et al. found that focal adhesion dynamics were disrupted. This was evident from the defective activation of focal adhesion kinase (FAK) and its subsequent phosphorylation of paxillin in adhesion assays. *Hem1*$^{-/-}$ macrophages also exhibited loose pockets covering the phagocytic preys, indicating a lack of cell membrane adhesion to the preys (Stahnke *et al.*, 2021). Another study also showed that deletion of *Nap1* decreased the number and area of focal adhesions in the WRC-deficient MEFs (Whitelaw *et al*, 2020). Thus, it is likely that loss of the CYFIP1-WRC also impairs the protrusive and adhesive structures in *Cyfip1* cKO microglia, disrupting the extension and closure of the phagocytic cups, along with the impairment in forming stable adhesions to the substrate during migration. It would be interesting to delve deeper into adhesion dynamics in *Cyfip1* cKO microglia with the aim to understand the impact of CYFIP1-WRC on adhesion in general and whether adhesion underlies the phagocytic and migratory phenotypes reported in this study. Overall, our findings reveal the importance of a fully assembled CYFIP1-WRC for its functionality and shed a light on the mechanistic function of the CYFIP1-WRC in microglial migration and phagocytosis.

Although loss of CYFIP1-WRC hampers the migration of primary microglia, it is noteworthy that *in vivo* microglia still inhabit the brains of *Cyfip1* cKO mice. This indicates that microglial precursor cells in *Cyfip1* cKO mice were capable of successfully migrating into the brain during embryonic development. There are two potential explanations. First, CYFIP1 might have a long half-life *in vivo*. The *Cx3cr1* gene, which provides the endogenous promoter to drive the expression of the Cre recombinase for the conditional deletion of *Cyfip1* in microglia, was shown to be active as early as E8 in mice (Mizutani *et al*, 2012). Around E9.5, when microglial precursor cells migrate into the developing brain, CX3CR1+ cells were observed in both posterior and anterior ends of the neural tube (Mizutani *et al.*, 2012). This suggests that the deletion of *Cyfip1* in the myeloid cells in our *Cyfip1* cKO mice should have occurred concomitant to the migration of microglial precursor cells into the developing brain. However, CYFIP2, the other isoform of CYFIP, was found to have a half-life of approximately 12 days in the mouse brain (Özer, 2020). It is possible that CYFIP1 also has an extended half-life in microglia *in vivo*. Consequently, despite the deletion of *Cyfip1* gene, the undegraded CYFIP1 protein and its WRC members could still allow the migration of microglial precursor cells into

the brain. Second, *Cyfip1* cKO microglia might retain the ability to chemotactically migrate along the CSF1 gradient. CSF1 is the chemoattractant which directs the migration of microglial precursors into the developing brain during the embryonic period (Wu *et al.*, 2018). A previous study revealed that primary macrophages without functional ARP2/3 complex could still efficiently migrate along the CSF1 chemotactic gradient (Rotty *et al.*, 2017). It is possible that despite the impaired WRC-ARP2/3 signaling in the myeloid cells of *Cyfip1* cKO mice, microglial precursor cells can still chemotactically migrate into the developing brain through CSF1 signaling.

3.3. CYFIP1-WRC regulates dynamic F-actin networks, and it is crucial for lamellipodia and membrane ruffles formation

Cell migration on a flat surface requires protrusive force at the leading edge of the moving cell. The protrusions involved in this process are typically the lamellipodia, thin, sheet-like structures supported by branched actin networks (Abercrombie *et al*, 1971). The branched actin network of the lamellipodium is mainly generated by the ARP2/3 complex (Steffen *et al*, 2006; Suraneni *et al.*, 2012). Activation of the ARP2/3 is accomplished by nucleation promoting factors (NPFs) recruited at the plasma membrane and activated by RHO GTPases (Steffen *et al.*, 2004). Among the many NPFs acting on the ARP2/3 complex, the WRC is believed to be the key regulator of lamellipodia and membrane ruffles formation.

In *Cyfip1* cKO primary microglia, we found a loss of lamellipodial structures, while intriguingly, an elevation of long filopodia-like structures was detected (Figure 2.13). This finding is in line with prior studies conducted on cancer cell lines, primary macrophages and fibroblasts, where absence of the WRC, either through knockdown or knockout, resulted in a significant reduction of cells containing lamellipodia and in impaired directional movement. WRC-deficient cells also exhibited a slight increase in filopodia-like structures, similarly to WRC-deficient microglia (Schaks *et al.*, 2018; Stahnke *et al.*, 2021; Steffen *et al.*, 2006; Steffen *et al.*, 2004; Whitelaw *et al.*, 2020) (Figure 2.13). Interestingly, these phenotypes are also consistent with what has been observed in fibroblasts lacking ARP2/3 complex, characterized by the absence of lamellipodia and increased density of filopodia (Suraneni *et al*, 2015; Suraneni *et al.*, 2012; Wu *et al*, 2012). This indicates that the WRC mainly regulates the formation of lamellipodial protrusions by activating the ARP2/3 complex. In the absence of lamellipodia, cell migration relies on formins-dependent filopodial protrusions in combination with myosin II-driven contractility (Suraneni *et al.*, 2015). In this study, loss of WRC in *Cyfip1*

cKO primary microglia likely impaired the activation of the ARP2/3 complex, resulting in the disruption of branched actin networks crucial for lamellipodium formation at the cell periphery. As the compensatory mechanism for the lack of lamellipodium, cells developed filopodia-like protrusions to support directional migration, although with significantly reduced efficiency. Lamellipodial protrusions that fail to adhere to the substrate, retract centripetally, becoming ruffles. This continuous protrusion and retraction of the lamellipodium is known as membrane ruffling (Flannagan *et al.*, 2012). In *Cyfip1* cKO primary microglia, we observed a significant loss of dynamic membrane ruffling (Figure 2.14), consistent with previous studies highlighting the role of WAVE2-dependent WRC in peripheral ruffle formation and directional movement of embryonic fibroblasts (Suetsugu *et al.*, 2003). The loss of membrane ruffling in *Cyfip1* cKO microglia supports the finding of impaired lamellipodia formation, suggesting that CYFIP1-dependent WRC is a key regulator of branched actin-dependent membrane dynamics and, ultimately, immune cell motility.

To delve deeper into the impact of CYFIP1-WRC in actin dynamics, we evaluated the ratio between F- and G-actin of primary microglia (Figure 2.15). The majority of the F-actin is typically found in the center of the cell. It consists of stable and highly interconnected filaments which provide support for cell structure and organelle transport and tethering. The remaining F-actin is localized near the cell periphery and consists of dynamic filaments and networks. Despite constituting a small portion of the cell F-actin, these filaments, due to their high dynamics, play a crucial role in regulating protrusions and the formation of ruffles at the cell membrane. In view of our findings regarding the impaired phagocytic function and reduced cell motility in *Cyfip1* cKO microglia, we separated the fraction of dynamic F-actin from the stable F-actin pool using a differential centrifugation approach in resting and stimulated cells. Under unstimulated conditions, we noticed decreased stable F-actin and, even more interestingly, undetectable levels of dynamic F-actin networks in *Cyfip1* cKO microglia when compared to CTRL microglia. This finding provides a mechanistic explanation for the absence of lamellipodia and membrane ruffles in *Cyfip1* cKO cells: in the absence of dynamic F-actin networks, lamellipodia and consequently membrane ruffles would not be able to form. Upon stimulation of the microglia with a phagocytic prey, both CTRL and *Cyfip1* cKO microglia exhibited a slight reduction in stable F-actin. It is plausible that the cortical actin underneath the plasma membrane was partially disassembled in order to form new networks for phagocytic cup formation. In accordance with this notion, in CTRL microglia, dynamic F-actin networks significantly increased following the stimulation, suggesting successful *de novo* WRC-

ARP2/3-dependent actin polymerization for phagocytic cup formation. However, the dynamic F-actin networks fraction remained undetectable in *Cyfip1* cKO microglia, suggesting a key role of the CYFIP1-WRC for *de novo* dynamic actin polymerization at the cell membrane and providing a mechanistic cue which explains the inability to form phagocytic cups in the absence of the WRC.

In summary, our findings reveal that CYFIP1-WRC plays a crucial role in regulating the formation of dynamic F-actin networks and acts as the primary activator of the ARP2/3 complex in lamellipodia and membrane ruffles formation. This discovery highlights the novel role of CYFIP1-WRC in microglial cytoskeleton dynamics and its significant impact on microglial motility and phagocytic function.

3.4. In *Cyfip1* cKO mice microglia display a non-homeostatic phenotype

Cyfip1 cKO microglia in the mouse brain appeared to be in a non-homeostatic state, with reduced ramification, enlarged cell body and elevated CD68 levels (Figure 2.8 and 2.10). In addition, microglial cell number was higher in *Cyfip1* cKO mice when compared to CTRL mice (Figure 2.6). The cause of the non-homeostatic phenotype of adult microglia in *Cyfip1* cKO mice is unclear. There could be two potential explanations for this phenotype.

First, our finding shows that the absence of CYFIP1-WRC results in the loss of dynamic F-actin networks at the periphery of microglial cells *in vitro* (Figure 2.15). It is possible that the disturbance of F-actin networks underneath microglial cell membrane releases the inflammatory signaling molecules residing in the F-actin, thus initiating downstream inflammatory pathways. When pathogen ligands bind to membrane receptors in immune cells, it disrupts the F-actin networks underneath the plasma membrane are disrupting, releasing signaling molecules to initiate inflammatory responses or phagocytosis. Thus, the disruption of actin networks functions as a link between pathogen detection and the immune response. Interestingly, a recent study reported that disturbance of the actin cytoskeleton in fibroblasts, independent of pathogens, can activate antiviral signaling. This occurs through the release of the protein phosphatase 1-regulatory subunit 12C (PPP1R12C) from F-actin networks into the cytoplasm, which consequently induces an antiviral response (Acharya *et al*, 2022). It is possible that the disruption of F-actin networks caused by the loss of CYFIP1-WRC in microglia, induces a cell-autonomous inflammatory effect that disturbs microglial homeostasis, even in the absence of pathogens.

Secondly, deletion of *Cyfip1* might hamper the maturation process of microglia during development. Depletion of WRC components have been shown to interfere with cell maturation processes. A previous study has indicated the essential role of HEM1 in transitioning the alveolar macrophages from a premature to a mature state during the late embryonic to early postnatal developmental period (Suwankitwat *et al*, 2021). Complete loss of CYFIP1 in embryonic stem cells was shown to downregulate developmental pathways controlled by TGFß signaling with significant reduction in phosphorylated Smad1/5 levels (Stöcker, 2015), and TGFß signaling is essential for microglial maturation during development (Spittau *et al.*, 2020). During the embryonic and early postnatal period, microglia exhibit an immature morphology characterized by reduced branching compared to the mature microglia in the adulthood (Santos *et al*, 2008). During the late embryonic and early postnatal stages, microglia usually exhibit some degree of branching, yet their cell bodies remained enlarged (Santos *et al.*, 2008; Smolders *et al*, 2015). This observation suggests a shift from an ameboid morphology during early embryonic stages to a mature and ramified morphology in adulthood. Microglial cell number usually peaks within the first two postnatal weeks, followed by a decline starting from the third postnatal week, and the cell number remains relatively stable in the early adulthood (Askew *et al*, 2017; Nikodemova *et al*, 2015). Finally, CD68 is upregulated in the embryonic and early postnatal microglia. Its levels begin to diminish after the first postnatal week, coinciding with the microglial transition to a mature and ramified state (Santos *et al.*, 2008). In the 2-month-old *Cyfip1* cKO mice, microglia exhibited a non-homeostatic morphology (Figure 2.8), including elevated CD68 (Figure 2.10), and accompanied by a higher cell number in comparison to age-matched CTRL mice (Figure 2.6). It is possible that, depending on the half-life of CYFIP1, the remaining protein for a certain time continues to contribute to microglial development, which will cease when CYFIP1 is completely depleted. This will likely occur at a specific developmental stage, plausibly during late embryonic development, before microglia have reached their mature and homeostatic state.

Further analysis of microglial morphology at P0 - P14 postnatal stages and investigation of TGFß signaling in *Cyfip1* cKO microglia could provide valuable information for determining whether the non-homeostatic phenotype of microglia observed in *Cyfip1* cKO mice indicates activated or immature microglia.

3.5. Loss of CYFIP1 in microglia impairs the maturation of dendritic spines

For a long time, research has focused on unraveling the cellular functions of CYFIP1 and their possible impact on the etiology of disorders like schizophrenia, autism spectrum disorder, and intellectual disability. Due to the fact that a total deletion of *CYFIP1* is not found in humans and that a complete deletion of *Cyfip1* in mice is early embryonically lethal, studies have utilized heterozygous mice to investigate the alterations produced by *Cyfip1* haploinsufficiency in the brain. In *Cyfip1*$^{+/-}$ mice, hippocampal pyramidal neurons exhibited decreased neuronal branching and increased density of immature spines (Pathania *et al.*, 2014). On the other hand, overexpression of *Cyfip1* in mice was shown to increase spine density and the number of some types of immature spines (Oguro-Ando *et al.*, 2015). While the majority of studies on CYFIP1 have focused on neurons, we show in this work that microglia express the highest levels of CYFIP1 and unlike neurons, microglia do not have any compensatory possibility from the other CYFIP isoform, CYFIP2, which is not expressed in microglia (Figure 2.1). In recent years, there has been a growing belief that microglia also play an important role in synapse remodeling during development (Lehrman *et al.*, 2018; Miyamoto *et al.*, 2016; Paolicelli *et al.*, 2011; Schafer *et al.*, 2012). Surprisingly, no studies have explored the potential contribution of microglia to the spine pathology in *Cyfip1* animal models.

In this study, we first assessed neuronal number in cortex and hippocampus as well as the density of dendritic spines in cortical layer V pyramidal neurons in *Cyfip1* cKO mice, observing no significant differences in both neuronal number and spine density in *Cyfip1* cKO mice when compared to the CTRL mice (Figure 2.16 and 2.17). Our findings present a thought-provoking question to the field of microglia research: do microglia participate in shaping neuronal connectivity by removing excessive synapses and neurons as previously proposed? It is surprising that the number of neurons and dendritic spines did not increase despite the strongly impaired migratory and phagocytic capacity of primary *Cyfip1* cKO microglia (Figure 2.11 and 2.12). However, studying spine morphology, we report an elevated proportion of immature spines and a concomitant loss of mature spines in *Cyfip1* cKO mice (Figure 2.18), which in the context of unaffected spine density, suggests a spine maturation defect. Given the unaltered CYFIP1 levels in synapses of *Cyfip1* cKO mice when compared to CTRL mice (Figure 2.3), we can reasonably exclude the possibility of a cell-autonomous effect due to ectopic *Cyfip1* deletion in the neurons of *Cyfip1* cKO mice. Two other mechanisms might explain the observed phenotype, both involving microglial function.

First, impaired motility and reduced branching of *Cyfip1* cKO microglia might result in a decreased induction of mature spine formation. It has been proposed that microglial contact with dendritic spines or dendrites could have positive effects, inducing local actin accumulation and the formation of filopodia and stable synapses (Miyamoto *et al.*, 2016; Weinhard *et al.*, 2018). The reduced motility and the immature morphology of *Cyfip1* cKO microglia would likely limit their contact with dendritic spines, resulting in fewer occurrences of actin accumulation at the spine heads. Consequently, it could lead to an increased proportion of immature spines in *Cyfip1* cKO mice. Secondly, a higher proportion of GFAP-positive reactive astrocytes and a decrease in the total number of astrocytes were observed in *Cyfip1* cKO mice, without any loss of CYFIP1 in the astrocytes themselves (Letmathe, unpublished data). An increased proportion of reactive astrocytes, coupled with the decrease in total number of astrocytes, could impair the support for spine maturation in *Cyfip1* cKO mice. Under normal conditions, fine astrocytic processes enwrap intimately around dendritic spines, which is believed to stabilize the spines (Clarke & Barres, 2013). The astrocytic contacts, as well as their soluble factors, also promote the maturation of dendritic spines (Allen *et al*, 2012; Bosworth *et al*, 2023; Haber *et al*, 2006; Nishida & Okabe, 2007). However, reactive astrocytes with increased GFAP levels, induced by activated microglia, showed reduced expression of synaptogenic factors. Neurons cultured with GFAP-positive reactive astrocytes had decreased number of excitatory synapses (Liddelow *et al*, 2017). It is possible that in *Cyfip1* cKO mice, the activated microglia induce the transformation of homeostatic astrocytes into reactive astrocytes. This shift towards reactive astrocytes, combined with the reduction in total astrocytic number possibly impairs the support provided by astrocytes for spine maturation.

To further investigate the potential impact of the increased proportion of immature spines on synapse formation, we assessed the number of functional excitatory synapses by quantifying the overlapping signals of pre-synaptic and post-synaptic markers (Figure 2.19). Interestingly, no differences were observed in the number of excitatory synapses in the cortex, whereas a decrease of excitatory synapse number was observed in the hippocampus. This suggests that the formation of excitatory synapses remains mostly unaffected, despite the increased ratio of immature spines in cortical pyramidal neurons. It will be interesting to explore if hippocampal pyramidal neurons undergo more significant changes in dendritic spine density or neuronal branching, given the observed alterations in the number of excitatory synapses in the hippocampus. Finally, to assess the functional implications of the observed dendritic spine

alterations at the neuronal circuit level, future studies should examine postsynaptic currents through electrophysiological recordings.

3.6. Conclusions and outlook

In this study, we investigated the role of CYFIP1 in microglial morphology, motility and functions, and the impact of defective microglia on its interaction with neuronal synapses. We identified for the first time the components of the CYFIP1-WRC in freshly-isolated microglia from the adult mice. Furthermore, with a semi-quantitative biochemical approach, we validated CYFIP1 being the sole CYFIP isoform in microglia with a high level of expression. A *Cyfip1* conditional knockout (cKO) mouse line was generated to study CYFIP1's role in microglial motility and functions. Although no significant changes were observed in gross brain morphology, we found a non-homeostatic microglial phenotype with elevated CD68 levels and reduced ramification in the *Cyfip1* cKO mice. Whether *Cyfip1* cKO microglia exhibit functional activation or represent an immature state is an interesting question worthy of further investigation.

We then explored the role of CYFIP1-dependent WRC in microglial migration and phagocytosis, and most importantly, unraveled the precise role of CYFIP1-WRC in actin dynamics. The absence of CYFIP1-WRC in primary microglia hindered the formation of dynamic F-actin networks, leading to impaired lamellipodia formation and membrane ruffles dynamics and to compromised phagocytosis. Furthermore, *Cyfip1* cKO microglia exhibited impaired directional movement, which can be attributed to their diminished capacity to generate lamellipodia, essential structures where the protrusive force required for cell migration in 2D is generated. Future studies should explore the potential involvement of other mechanisms contributing to the observed impairments, including alterations in adhesion dynamics, signal sensing and RHO GTPase signaling.

Last but not least, we observed an increased proportion of immature dendritic spines in cortical layer V pyramidal neurons, while no significant alterations were detected in spine density or functional synapses within the cortex. These findings indicate that impaired microglial motility, ramification and phagocytosis resulting from the loss of CYFIP1 do not affect neuronal and synapse number, but affect the maturation of dendritic spines during development. To gain further insights into the impact of microglia on synapse development in the brain, as well as its relevance to CYFIP1-related neurodevelopmental disorders, future studies should utilize two-

photon imaging to observe the *in vivo* microglial interaction with synapses in *Cyfip1* cKO mice. Additionally, evaluating changes in neuronal circuitry and animal behavior through electrophysiological recordings and behavioral tests would provide valuable information.

Chapter 4. Material & methods

4.1 Mice

Cyfip1 conditional knock-out mice

Myeloid cell-specific *Cyfip1* knockout mice (*Cyfip1*$^{flx/flx}$; *Cx3cr1*$^{cre/wt}$) were generated by crossing *Cyfip1*-flx/flx animals (provided by Prof. Dr. Walter Witke, bonn University) (Massimi, 2008) with the *Cx3cr1*-cre/cre line (The Jackson Laboratory, Strain # 025524) (Yona *et al.*, 2013). *Cx3cr1*-cre/wt mice were used as control. Mouse breeding and maintenance was performed according to EU regulations and requirements by local administration. Mice were kept in individually-ventilated cages (IVC) under controlled conditions in a 12 h light/dark cycle. 2-month-old animals were used for in vivo experiments. Pups aged from postnatal day 0 to 3 were used for primary mixed glia culture.

4.2 Methods and material

4.2.1. Cell culture Methods

4.2.1.1. Generation of primary mixed glia culture

Primary mixed glia culture was prepared using pups aged between postnatal 0 – 3 days (P0 - P3). Pups were decapitated and the heads were put directly into ice-cold Hank's Buffered Saline Solution (HBSS) (Life Technologies, cat# 14025100). Brains were retrieved on ice and meninges were removed under a binocular microscope. 1 ml of 0.625% trypsin (Life Technologies, cat# 15090046) was used to digest each brain tissue at 37°C for 10 min. 3 ml of DMEM cell culture medium (Life Technologies, cat# 31966047) with 10 % fetal bovine serum (FBS) (Sigma-Aldrich, cat# F7524) and 1 % penicillin-streptomycin (P/S) (Life Technologies, cat# 15140122) was added to stop the trypsin digestion. The brain tissue was centrifuged at 300 g for 10 min to spin it down, and the supernatant was discarded. 1 ml of fresh DMEM culture medium was added to homogenize the brain tissue thoroughly by manually pipetting. Following that, 11 ml of DMEM culture medium was added to each sample, and the samples were filtered through a 70 µm cell strainer to remove larger tissue chunks. At last, the samples were added into 75 cm^2 flasks (Greiner Bio-One, cat# 658175) coated with 0.01% poly-L-lysine Hydrobromide (PLL) (Signa-Aldrich, cat# P1399), and incubated at 37°C with 10% CO_2. The next day, the DMEM culture medium (containing 10 % FBS and 1 % P/S) was replaced with fresh medium to remove cell debris. The primary cell culture was grown for 7 days before astrocyte-conditioned medium (ACM) was harvested.

4.2.1.2. Harvest of primary microglia

After collecting ACM on day 7, fresh DMEM culture medium was added into the flasks and incubated with the cells for 3 more days. On day 10, L929 cell-conditioned medium (LCCM) was added to aid the proliferation of microglia. 3 days following the incubation with LCCM, primary microglia were harvested by gently tapping the flasks. The cell suspension was collected and centrifuged at 300 g for 10 minutes at room temperature. After removing the supernatant, cells were resuspended in 1 ml ACM for further *in vitro* functional assays.

4.2.1.3. Cell plating for *in vitro* assays

Days in vitro (DIV) 13 – 17 primary microglia were harvested from flasks. Cells suspended in ACM were diluted with trypan blue (Life Technologies, cat# 15250061) at a 1:10 ratio and 10 µl of cell suspension was used for cell counting with a cell counter. Once the cell number was determined, additional ACM was added to prepare the cell concentration needed for individual *in vitro* assays. Cells were then seeded onto the µ-Slide 8-well glass-bottom plates (ibidi, cat# 80827) and incubated at 37 °C until live-cell imaging. Timeline and procedure for *in vitro* cell preparation are illustrated in Figure 4.1.

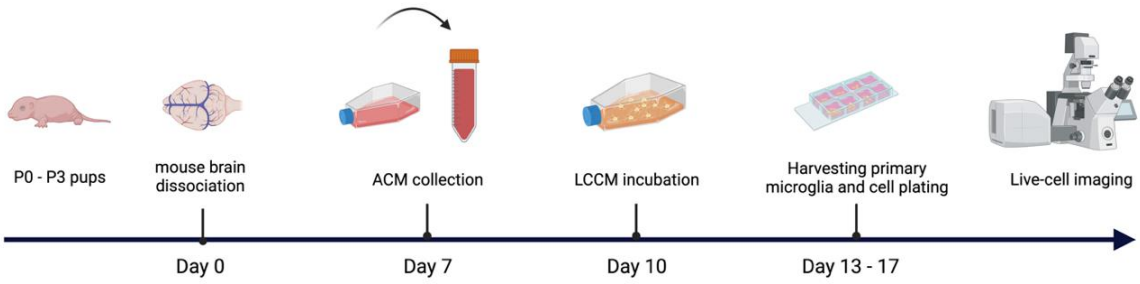

Figure 4.1: Generation of mixed glia cultures and cell plating
Postnatal pups (P0 – P3) were decapitated and their brains were used to generate primary glia cultures. The brain tissue was homogenized and cultured in DMEM medium supplemented with 10 % FBS and 1 % P/S. Astrocyte-conditioned medium (ACM) was collected on day 7 (DIV 7). On DIV 10, L929 cell-conditioned medium (LCCM) was introduced to promote microglia proliferation. On DIV13, primary microglia were harvested by gently tapping the flasks, plated and used in subsequent *in vitro* assay

4.2.2 Cell biology methods

4.2.2.1. Magnetic-activated cell sorting

Magnetic-activated cell sorting (MACS) was invented by Miltenyi Biotec. It is a technique for separating cell populations by labeling cells with antibody-conjugated magnetic beads and then

separating cell fractions using a magnetic field. The procedure consists of 3 major steps: magnetic labeling, magnetic separation and elution of labeled cells (Figure 4.2). MACS MicroBeads, which are 50 nm superparamagnetic particles conjugated with specific antibodies, are used to label target cells. The small size of the beads minimizes cell activation during the separation procedure. It is a fast and gentle method to isolate viable cells with preserved cell integrity and characteristics.

2-month-old control (CTRL) and microglial *Cyfip1* conditional knock-out (*Cyfip1* cKO) mice were used in this experiment. Mice were sacrificed by cervical dislocation. Brains were rapidly removed, rinsed and transferred into ice-cold PBS (Life Technologies, cat# 14190169). Before processing brain tissue, enzyme mix 1 (50 µl enzyme P and 1900 µl buffer Z) (Miltenyi Biotec, cat# 130-042-108) was prepared and added into a C tube (Miltenyi Biotec, cat# 130-093-237). Each brain tissue was cut sagitally into 8 pieces with a blade, and placed into a C tube containing enzyme mix 1, followed by the addition of enzyme mix 2 (20 µl buffer A and 10 µl enzyme A). C tubes containing brain tissue were loaded onto a Miltenyi Octodissociator (Miltenyi Biotec, cat# 130-096-427), and the 37°C ABDK program was run for 30 minutes to homogenize the tissue. After the dissociation, cell suspension was collected to the bottom of the tubes by spinning the tubes at 500 g for 1 minute. Cell suspension was filtered through a 70 µm cell strainer to remove tissue chunks, and 10 ml of ice-cold PBS was added to the C tubes and filtered through the same 70 µm cell strainer to collect the remaining cells. The samples were centrifuged at 500 g for 10 minutes at 4 °C, and the supernatant was discarded. Cell pellets were resuspended in 3 ml of ice-cold PBS, and 900 µl debris removal solution (Miltenyi Biotec, cat# 130-109-398) was added. The samples were mixed well and transferred into 15 ml falcon tubes. 4 ml of ice-cold PBS was very carefully added on top of the cell suspension without mixing. The border between phases with different densities should be very clear. The samples were centrifuged at 3000 g for 10 min at 4 °C, and the top and middle layers containing myelin and debris were removed. Additional PBS was added into 15 ml falcon tubes to wash out the remaining debris removal solution. The samples were again centrifuged at 1000 g for 10 min at 4 °C, and the supernatant was completely discarded. For microglia isolation, 80 µl ice-cold PB buffer (0.5 % BSA (Sigma Aldrich, cat# A4503) in 1x PBS) was added to resuspend the pellets and transferred to a 5 ml FACS tube. The pellets were then incubated with 20 µl anti-CD11b magnetic beads (Miltenyi Biotec, cat# 130-093-634) at 4 °C for 15 min in the dark. For isolation of astrocytes, pellets were resuspended in 90 µl ice-cold PB buffer containing 10 µl Fc blocking buffer (Miltenyi Biotec, cat# 130-092-575), and incubated for 15

minutes. To prevent false-positive selection of microglia in the astrocyte fraction, Fc blocking was utilized to prevent erroneous binding of antibody Fc domain to Fc receptors on microglia. After Fc blocking, 10 µl of anti-ACSA2 microbeads (Miltenyi Biotec, cat# 130-123-284) were added and incubated with the sample for 10 minutes in the dark at 4 °C. After incubation with antibodies, 1 ml of ice-cold PB buffer was added and mixed well with the pellets to wash away unbound antibodies. The samples were centrifuged at 500 g for 10 minutes at 4 °C, and the supernatant was discarded. During the time of centrifugation, MACS columns (Miltenyi Biotec, cat# 130-042-801) and MACS Separator (Miltenyi Biotec, cat# 130-042-602) were set up. 500 µl ice-cold PB buffer was applied to rinse the MACS column. Following the removal of the supernatant containing unbound antibodies, the pellets were resuspended in 500 µl of ice-cold PB buffer and flown through the MACS column. Microbead-labeled cells were constrained in the column. The column then was washed 3 times with 500 µl of ice-cold PB buffer. After washing, the column was removed from the MACS separator, and 1 ml of ice-cold PB buffer was applied to elute the labelled cells from the column. Lastly, the samples were centrifuged at 500 g for 10 minutes at 4 °C to collect the target cells.

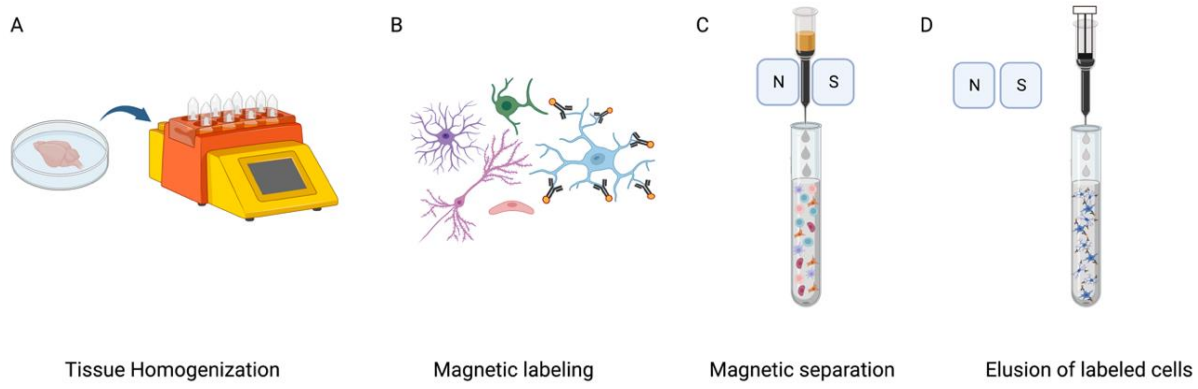

Figure 4.2: Experimental procedure of MACS
(A) Freshly extracted brain tissue was divided into 8 pieces and placed into a MACS C tube containing an enzyme mix. Tissue was enzymatically dissociated at 37 °C using MACS octodissociator. **(B)** Following the removal of tissue debris and myelin, the target cell population was labelled with specific antibodies coupled with magnetic beads. **(C)** MACS column was inserted in magnet-based MACS separator. Cell suspension was added and flowed through the MACS column. During the separation, magnetically labelled cells (target cell population) were restrained within the column, whereas unlabelled cells flew past. **(D)** After the cell suspension had completely flown through the MACS column, the column was removed from the separator, and the target cell population confined inside the column was eluted out.

We confirmed the purity of the target cells isolated using MACS through fluorescence-activated cell sorting (FACS). Microglial cells were incubated with anti-CD11b (Biozol Diagnostica, cat# BLD-101208) and anti-CD45 antibodies (Biozol Diagnostica, cat# BLD-

103112), and the viable microglial cell population was identified based on high CD11b and low CD45 levels. Astrocytic cells were incubated with anti-ACSA2 (Miltenyi Biotec, cat# 130-097-678) and anti-CD11b antibodies, and viable astrocytic cell population was determined by high ACSA2 and low CD11b levels. Low CD11b level was an indicator of minimal microglial contamination in astrocytic cell population. Both microglia and astrocytes isolated via MACS have more than 90 % purity (Figure 4.3).

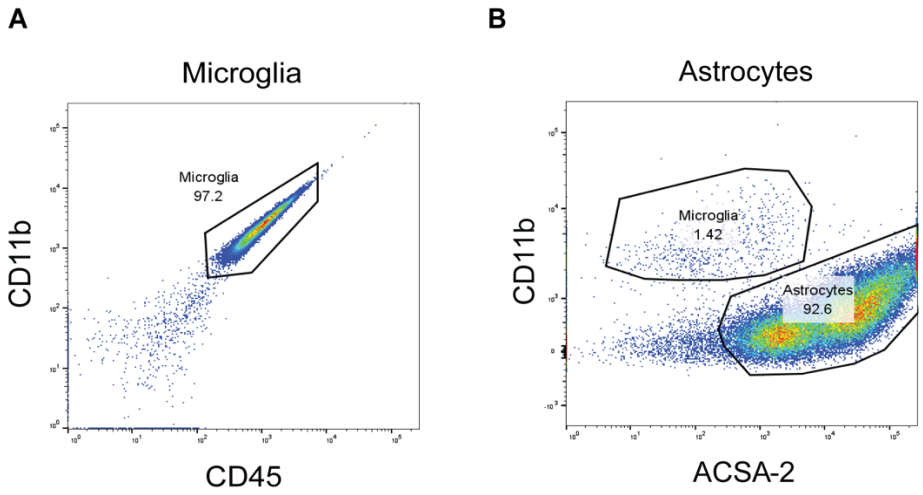

Figure 4.3: MACS purity validation
The purity of freshly-isolated microglia and astrocytes from brain tissues using MACS was validated by FACS. **(A)** The purity of microglia isolated using MACS is around 97 %. **(B)** The purity of astrocytes isolated using MACS is around 93 %.

4.2.2.2. Neuronal synaptosome isolation

Synaptosomes were isolated from wild-type adult mouse cortices (*Nagy and Delçªgado,1984*). Two cortices from each mouse were homogenized in 12 ml homogenizing buffer (0.32 M sucrose, 1 mM EDTA, 1 mg/ml BSA, 5 mM HEPES pH7.4) at 4 °C. The buffer containing homogenized tissue was centrifuged at 3,000 g for 10 minutes at 4 °C. Supernatant containing cytoplasm and synaptosomes was recovered, transferred to fresh falcon tubes, and centrifuged at 14,000 g for 12 minutes at 4 °C. After discarding the supernatant, the pelleted synaptosomes were carefully resuspended in 500 µl ice-cold Krebs-Ringer buffer (140 mM NaCl, 5 mM KCl, 5 mM glucose, 1 mM EDTA, 10 mM HEPES pH7.4) in each tube without generating bubbles. The resuspension was transferred into 2 ml tubes, and 450 µl of ice-cold Percoll was added to each tube (final concentration 45%). The samples were gently inverted and centrifuged at 14,000 rpm for 2 minutes at 4°C. By gently removing the underlying solution with a 5 ml syringe equipped with a 22 G needle, the enriched synaptosomes on the surface of the floating

gradient were recovered. 1 ml of ice-cold Krebs-Ringer buffer was added to resuspend the synaptosomes, and the samples were spun at 14,000 rpm for 30 seconds at 4 °C. The supernatant was discarded, and the synaptosomes were recovered in 600 µl of HEPES-Krebs buffer (147 mM NaCl, 3 mM KCl, 10 mM glucose, 2 mM $MgSO_4$, 2 mM CaCl2, 20 mM HEPES pH 7.4) in each tube.

Following that, samples were kept on ice for pHrodo indicator conjugation or snap-frozen in liquid N_2 for CYFIP1 quantification by western blot. The concentration of synaptosomal protein was determined using the Bradford assay, and the synaptosomes were conjugated with a pH indicator (pHrodo^{TM} Red succinimidyl ester) (Thermal Fisher Scientific, cat# P36600) at the ratio of 1 µl : 0.3 mg protein. The conjugation method was based on a published protocol (Byun & Chung, 2018). Synaptosomes were centrifuged at 21,000 g for 4 minutes at 4 °C. Because succinimidyl ester reacts more efficiently with primary amines at a slightly alkaline pH, 200 µl of 0.1 M Na_2CO_3 was added to raise the pH. 2 µl of pH indicator was added to the tube and gently mixed with the sample by pipetting carefully. Synaptosomes were incubated with pH indicator at room temperature for 2 hours in a twist shaker with 30 – 40 rpm agitation. The tubes were covered with aluminum foil to avoid exposure of light. Following the incubation, 1 ml of DPBS was added to the tube to wash out the unbound pH indicator, and the sample was centrifuged at 21,000 g for 2 minutes at room temperature. The supernatant was discarded and this washing step was repeated 7 times to ensure the unbound pH indicator was removed. Finally, pHrodo-conjugated synaptosomes were resuspended in 200 µl of DPBS containing 5 % DMSO (Sigma-Aldrich, cat# 41639).

4.2.2.3. *In vitro* wound healing assay

DIV 13-17 CTRL and *Cyfip1* cKO primary microglia cells were resuspended in ACM and seeded onto µ-Slide 8-well glass-bottom plates (ibidi, cat# 80827). Cells were seeded in 300 µl of ACM at the density of 200,000 per well and incubated at 37 °C overnight. ACM was changed the next day. On the second day, a 3 mm wide vertical wound was created in the centre of the well with a pipette tip. Live-cell imaging was conducted to monitor wound closure by primary microglia over 72 hours. The images were taken every three hours. The live-cell imaging was carried out at 37 °C with a 5 % CO_2 supply.

4.2.2.4. *In vitro* synaptosome phagocytosis assay

DIV 13-17 CTRL and *Cyfip1* cKO primary microglia were harvested and resuspended in ACM. Cells were seeded at the density of 35,000 cells per well in µ-Slide 8-well glass-bottom plates (ibidi, cat# 80827), and incubated overnight at 37 °C. PHrodo-conjugated synaptosomes were diluted in ACM to the concentration of 0.5 µg/µl. On the second day, 300 µl of the diluted synaptosomes were added into each well and incubated for 90 minutes at 37 °C to allow synaptosomes to precipitate. After 90 minutes of incubation, microglial phagocytic activity was recorded for 24 hours using live-cell imaging. Live-cell imaging was conducted at 37 °C with 5% CO_2 supply in both bright-field and 555 nm (for pHrodo signal) (see chapter 4.2.6.1). After live-cell imaging, the wells were washed three times with PBS to remove unengulfed synaptosomes, and the cells were fixed for 10 minutes at 37 °C with 1.5 % PFA (Sigma-Aldrich, cat# 252549) containing 0.25% glutaraldehyde (Sigma-Aldrich, cat# G5882) in PHEM buffer (60 mM PIPES, 25 mM HEPES, 10 mM EGTA, 2mM $MgCl_2$). After the fixation, the PFA solution was removed and the wells were washed 3 times with PBS. Finally, 300 µl of PBS was added to each well, and the plates were stored at 4 °C.

4.2.3. Molecular biology methods

4.2.3.1. Genomic DNA extraction

For genomic DNA extraction, ear punches from mice or cell suspension from brain homogenate were utilized. To lyse the tissue or cells, 150 µl lysis buffer (Life Technologies, cat# 89900) containing 0.5 mg/ml proteinase K was added to 10 µl of samples, and the samples were digested overnight at 55 °C. On the next day, the samples were heated for 45 minutes at 85 °C to deactivate proteinase K (QIAGEN, cat# 19131), and centrifuged at 10,000 g for 2 minutes under room temperature. The amount of material required for PCR was determined by the target gene and primers.

4.2.3.2. Polymerase chain reaction (PCR)

PCR is a fundamental method in molecular biology, which enables rapid amplification of certain segment of DNA through several cycles of temperature changes with addition of DNA polymerase, nucleotides and specific primers (Garibyan & Avashia, 2013). The PCR reaction is carried out in a thermal cycler. DNA extracted from ear punches was denatured for 5 minutes at 95 °C, and the DNA from cells was denatured for 30 seconds at 94 °C. During the denaturing process, the double-stranded DNA was separated into 2 single-stranded DNA, and the single-

stranded DNA served as the DNA template for the PCR reaction. The temperature was reduced to 60 °C for 30 seconds during the annealing stage to allow the designed primers to anneal to the target region on DNA. The designed primers (primer mix) contained both forward and reverse primers, which attached to the stop codon and start codon of the template DNA respectively. The DNA was then polymerised by Taq polymerase for 30 seconds at 72 °C. Taq polymerase extended the primer by incorporating free deoxynucleotide triphosphates (dNTPs) from the PCR master mix, which led to the synthesis of new DNA strand. The components of PCR master mix were indicated in Table 4.1 (*Cyfip1*-flx) and Table 4.4 (*Cx3cr1*-cre). The process of DNA denaturation, annealing and elongation of primers was repeated 32 to 35 times to amplify the target gene.

Cyfip1-flx PCR

Cyfip1-flx PCR was performed to investigate if the mice carried the floxed *Cyfip1* gene. The volume of each component in *Cyfip1*-flx PCR master mix is indicated in Table 4.1 and the primers for *Cyfip1*-flx PCR are indicated in Table 4.2 and Figure 4.4. The Red load Taq Master mix (Jena Bioscience, cat# 11828012) contained DNA polymerase, dNTPs, KCl, $MgCl_2$, red dye, gel loading buffer and stabilizers.

1 µl of sample was mixed with 49 µl of *Cyfip1*-flx PCR master mix for the PCR procedure. The PCR program for *Cyfip1*-flx gene is shown in Table 4.3.

Table 4.1: *Cyfip1*-flx PCR reaction

PCR master mix	Concentration	Amount
Milli-Q H_2O		37 µl
dNTP mix (Red Load Taq Master mix)	5x	10 µl
Cyfip1-flx1 forward primer	20 µM	1 µl
Cyfip1-flx1 reverse primer	20 µM	1 µl
Total		49 µl

Table 4.2: Primers used for *Cyfip1*-flx PCR

Primer		Primer sequence 5’ → 3’
Cyfip1-flx1 (#262)	forward	GTTTTAAGGAAGTCTTTGCC
Cyfip1-flx1 (#266)	reverse	TAACTAAAAGAGGTACC

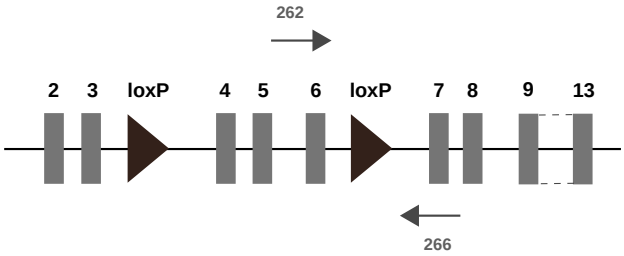

Figure 4.4: Primers for *Cyfip1*-flx PCR
One forward primer (262) and one reverse primer (266) were employed to examine *Cyfip1* loxP site.

Table 4.3: PCR program for *Cyfip1*-flx1

Temperature	Duration	Cycle
95°C	3 min	
94°C	30 sec	x 35
50°C	1 min	
72°C	1 min	
72°C	5 min	
16°C	1 min	

Cx3cr1-cre PCR

Cx3cr1-cre PCR was conducted to determine whether the mice had expression of cre recombinase directed by *Cx3cr1* gene. The volume of each component in Cx3cr1-cre PCR master mix and the primer mix for *Cx3cr1*-cre PCR are listed in Table 4.4 and Table 4.5.

Table 4.4: *Cx3cr1*-cre PCR reaction

PCR master mix	Concentration	Amount
Milli-Q H_2O		10 µl
dNTP mix (GoTaq G2 Green Master Mix)	2x	12.5 µl
Cx3cr1-cre wild-type forward primer	20 µM	0.5
Cx3cr1-cre common reverse primer	20 µM	0.5
Cx3cr1-cre mutant forward primer	20 µM	0.5
Total		24 µl

Table 4.5: Primers used for *Cx3cr1*-cre PCR

Primer		Primer sequence 5' → 3'
Cx3cr1-cre wild-type (#247)	forward	CCT CAG TGT GAC GGA GAC AG
Cx3cr1-cre common (#248)	reverse	GCA GGG AAA TCT GAT GCA AG
Cx3cr1-cre mutant (#249)	forward	GAC ATT TGC CTT GCT GGA C

GoTaq G2 Green Master Mix (Promega, cat# M7822) contained DNA polymerase, dNTPs, $MgCl_2$ and reaction buffer. 2 µl of sample was mixed with 24 µl of *Cx3cr1*-cre PCR master mix for the PCR procedure. The PCR program for *Cx3cr1*-cre gene is shown in Table 4.6.

Table 4.6: PCR program for *Cx3cr1*-cre

Temperature	Duration	Cycle
95°C	3 min	
94°C	30 sec	x 32
60°C	30 sec	
72°C	1 min	
72°C	3 min	
16°C	1 min	

Agarose gel electrophoresis

Gel electrophoresis is a common technique used in biochemistry to separate DNA, RNA or proteins based on their size. Agarose gel electrophoresis is used in DNA, RNA and sometimes large protein separation. The nucleotides and the phosphate backbones of DNA contribute to the negative charge of DNA. It results in DNA running towards the cathode (+) when an electrical current was applied. The moving speed of DNA is negatively correlated to its size.

1.5 to 2 % agarose gel with 0.04% MIDORI Green (Biozym Scientific, cat# 617004) was freshly prepared in 1x Tris-acetate EDTA (TAE) buffer during the PCR program. MIDORI Green was the nucleic acid stain. It was chosen over ethidium bromide for detecting DNA in this experiment due to its non-carcinogenicity and good signal-to-noise ratio.

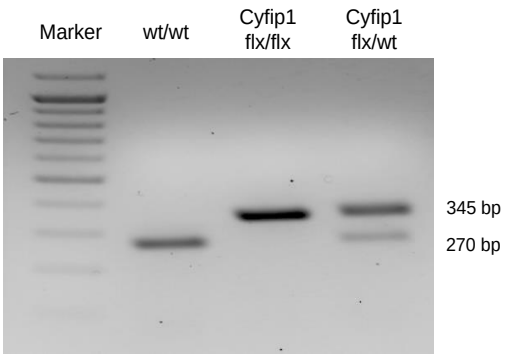

Figure 4.5: *Cyfip1*-flx genotyping PCR result
A wt band for *Cyfip1* at 270 bp and a loxP1 band at 345 bp were produced by combining primers 262 and 266.

To run the agarose gel electrophoresis, 10 µl of sample was loaded into each well, and the electrophoresis was run for 50 minutes. When the electrophoresis was finished, the agarose gel was imaged with UV light. Inside the agarose gel, ethidium bromide intercalated between the base pairs in DNA, producing fluorescence allowing the visualization of the DNA fragment under a UV light source. A DNA ladder was used to help identify the target DNA by its approximate size. The PCR results of *Cyfip1*-flx and *Cx3cr1*-cre are shown in Figure 4.5 and Figure 4.6.

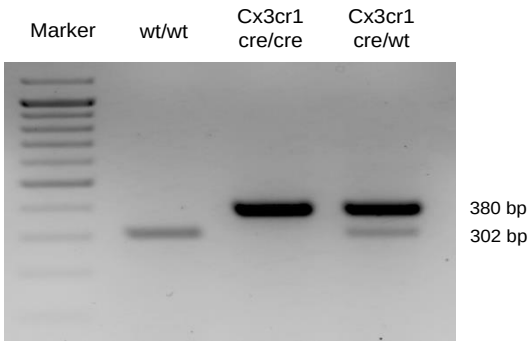

Figure 4.6: *Cx3cr1*-cre genotyping PCR result
A wt band for *Cx3cr1*-cre at 302 bp was produced by combining primers 247 and 248. Pairing primers 249 and 248 resulted in a mutant band for *Cx3cr1*-cre at around 380 bp.

4.2.4. Histology methods

4.2.4.1. Immunofluorescent staining

2-month-old CTRL and microglial *Cyfip1* cKO mice were sacrificed by cervical dislocation. Brains were quickly taken out from the heads, and rinsed with ice-cold DPBS. Brains were separated into 2 hemispheres. The right hemisphere was fixed in 4 % PFA for 1 day, transferred into 0.04 % PFA on the next day and stored at 4 °C until further use. The left hemisphere was immediately frozen in isopentane (VWR, cat# 24872.298) on dry ice, and stored at - 80 °C.

The right hemisphere was sectioned with a vibratome, and the slices were used for immunofluorescent staining. The hemisphere was mounted with glue and sectioned sagitally at a thickness of 50 µm. Sagittal slices were kept in 24-well plates with PBS containing 0.1 % sodium azide. Floating staining of brain tissue was performed in a 24-well plate. Before the staining process started, slices were washed 3 times in PBS to remove the sodium azide from the previous storage solution. Each wash took 5 minutes. To reduce non-specific antibody binding, the sections were incubated in a blocking buffer containing 10 % goat serum (Sigma-Aldrich, cat# G9023) for 2 hours at room temperature. The composition of blocking buffer is listed in Table 4.7. After blocking, the slices were briefly washed with PBS before being incubated with primary antibody in 10 % blocking buffer at 4 °C overnight. On the next day, the slices were washed 3 times with 10 % blocking buffer to remove the unbound primary antibodies. Secondary antibodies diluted in 10 % blocking buffer were incubated with the slices for 2 hours at room temperature. Slices were washed 3 times with PBS before being stained with DAPI (Life Technologies, cat# D1306) for nuclei at room temperature for 5 minutes. After staining, slices were transferred to adhesive microscope slides and mounted in Aqua-poly/Mount (Polysciences, cat# 18606).

Table 4.7: Composition of blocking buffer

Components	Concentration (%; mass/volume, volume/volume)
Goat serum	10% (v/v)
BSA	2% (m/v)
Triton X-100	2% (v/v)
1x PBS	88% (v/v)

Staining of primary microglia following phagocytosis assay was done directly in the 8-well plates. Cells were fixed as described in chapter 4.2.2.4. The cells were permeabilized using 0.2 % Triton-X (Sigma-Aldrich, cat# X100) in PBS for 20 minutes at room temperature, and the washed briefly with PBS before staining with primary antibody. Afterwards, the cells were incubated with anti-CD11b antibody overnight at 4 °C. The following day, cells were washed 3 times with PBS to remove unbound primary antibody, and the secondary antibody was added and incubated with the cells for 1 hour at room temperature. After washing the cells 3 times with PBS to remove excessive secondary antibody, the cells were stained with phalloidin

overnight at 4 °C. On the third day, the cells were washed 3 times with PBS to remove excess phalloidin, and the cell nuclei were stained with DAPI for 1 minute at room temperature. Cells were rinsed briefly and kept in 1x PBS at 4 °C until imaging. Table 4.7, Table 4.8 and Table 4.9 show the primary, secondary antibodies and dyes used in immunofluorescent staining.

Table 4.8: Primary antibodies used for immunofluorescent staining

Antigen	Host species	Dilution	Source
IBA1	Rabbit	1:200, 1:400	WAKO
CD68	Rat	1:400	Bio-Rad
NeuN	Mouse	1:200	MerckMillipore
Bassoon	Mouse	1:200	Enzo
Homer1	Chicken	1:500	Synaptic system
CD11b	Rat	1:500	Biozol Diagnostica

Table 4.9: Secondary antibodies used for immunofluorescent staining

Target species	Host species	Dilution	Fluorescence	Source
Anti-rabbit	goat	1:400	Alexa 555	Life Technologies
Anti-rat	goat	1:400,	Alexa 488,	Invitrogen
		1:500	Alexa 674	Life Technologies
Anti-mouse	goat	1:200,	Alexa 647,	Life Technologies
		1:1000	Alexa 488	Life Technologies
Anti-chicken	goat	1:750	Alexa 647	Life Technologies

Table 4.10: Dyes used for immunofluorescent staining

Name	Target	Dilution	Source
DAPI	Nuclei	1:1000	Life Technologies
Phalloidin	F-actin	1:50	Cytoskeleton

4.2.4.2. Golgi staining

Golgi staining was invented by Camillo Golgi and improved by Ramón y Cajal. It is one of the most effective techniques in studying neuronal morphology. Using Golgi staining, neurons in brain tissue are stained by the formation of silver chromate crystals, which can be visualized

as black structures. The random precipitation of silver chromate crystals only stains a random subset of the neurons rather than the entire population. This allows a better visualization of the complex neuronal morphology in brain tissue. In order to analyze neuronal morphology in adult mouse brain tissue, a kit for Golgi staining from FD NeuroTechnologies was used in this study. The Golgi staining impregnation solution was prepared (15 ml/ mouse brain) at least 24 hours and stored at room temperature in the dark without agitation before collecting the brain tissue from the animals. The Golgi impregnation solution was composed of $HgCl_2$, K_2CrO_4 and $K_2Cr_2O_7$. 2-month-old CTRL and *Cyfip1* cKO mice were sacrificed and their brains were used for neuronal morphology analysis in this study. The brains extracted from the mouse skulls were rinsed with Milli-Q water, and then were immersed in the impregnation solution (7,5 ml / brain). The impregnation solution was changed the next day, and the brains were impregnated in the dark for 2 weeks at room temperature. During the impregnation period, the samples were gently swirled every 2 – 3 days. After 2 weeks of impregnation, the brains were transferred into tissue-protectant solution (7 ml / brain) and kept in the dark at 4 °C for 3 days. The tissue-protectant solution was replaced on the second day.

After the 3-day tissue protection period was finished, the samples were prepared for sectioning with a vibratome. Prior to sectioning, the olfactory bulbs and cerebellum were removed from the brain tissue. The brains were sectioned coronally at the thickness of 200 µm in cold PBS. The 200 µm coronal slices were placed on gelatin-coated slides with a drop of tissue protectant solution. The excessive solution on the slides was dried with a pipette and gently absorbed with a filter paper. Afterwards, the slices were air-dried in the dark overnight. The next day, the staining solution was prepared right before use, and the slices were rinsed in cold Milli-Q water twice for 1 minute each time. After rinsing, the slices were stained in a staining jar containing 100 ml of freshly prepared staining solution for 10 minutes at room temperature with agitation. When the staining was completed, slices were rinsed again with cold Milli-Q water twice, 1 min each, and were dehydrated in 50 %, 75 %, 95 % and 100 % ethanol (Sigma-Aldrich, cat# 51976) in the sequential order. Each dehydration step took 4 min. At last, the slices were cleaned with xylene (Roth, cat# CN80.1) 3 times for 4 minutes each and mounted in Entellan (Merck, cat# 107960). The slides were stored at room temperature until further imaging was performed. Table 4.11 shows the composition and volume of impregnation, tissue protection and staining solutions.

Table 4.11: Solutions from FD Rapid GolgiStain ™Kit used for Golgi staining

	Solution	Ratio	Volume
Impregnation	A + B	1 : 1	7.5 ml / brain
Tissue protection	C	1	7 ml / brain
Staining	D + E + H_2O	1 : 1 : 2	100 ml / staining jar

4.2.4.3. Hematoxylin and eosin (H&E) staining

H&E staining is an approach widely used in histology to study the anatomical changes in the tissue. It is a combination of hematoxylin and eosin staining. Hematoxylin stains the nucleotides in DNA and RNA purplish blue, and eosin stains proteins existing in cytoplasm and extracellular matrix pink. Natively frozen brains from 2-month-old mice were sectioned sagittally with 12 µm thickness using a cryostat. The chamber temperature of the cryostat was between -18 °C and -20 °C, and the object temperature was between -17 °C and -19 °C. After sectioning, the slices were placed onto slides and kept at – 80 °C until further use for staining. 12 µm-thick slices were first fixed with 4 % PFA (Histofix) for 5 minutes, and rinsed with demineralized water briefly. Following that, the slices were stained in hematoxylin solution for 2 minutes with gentle agitation. The unbound stain was washed away 5 times with warm tap water for 1 minute each time, and the nuclei appeared purplish blue after this step. The slices were then stained for 10 minutes with eosin solution, and the excessive stain was washed off with warm water for 1 minute. This washing step was repeated for 5 times as well. The stained slices were air-dried and mounted in Entellan.

4.2.5. Biochemistry methods

4.2.5.1. Protein extraction

Total extracts from MACS–isolated cells

Freshly sorted cells from adult mouse brains by MACS were washed with 500 µl of ice-cold PBS and centrifuged at 500 g at 4 °C for 10 minutes in order to remove the BSA from PB buffer. The supernatant was discarded, the pellets were lysed and the proteins were extracted in 50 µl of 1x SDS loading buffer (5x: 110mM Tris-HCl pH 6.8, 20 % Glycerol, 3.8 % SDS, 8 % β-mercaptoethanol, 0.03 % Bromophenol blue). The lysates were then boiled for 10 minutes at 100 °C. During the boiling process, the samples were vortexed twice to shear DNA. The samples were then cooled down on ice and stored at – 20 °C until further use.

Separation of F and G–actin from cultured microglia

DIV 13 - 17 CTRL and *Cyfip1* cKO primary microglia were harvested from flasks and resuspended in ACM. Cells were separated into 2 groups: unstimulated and *E.coli* stimulated. All cells were first plated in 6 cm diameter petri dishes at the density of 2.5 million/dish for 2 days. For the *E.coli* stimulation group, pHrodo Ecoli (Life Technologies, cat# P35361) was given to the petri dish at the concentration of 0.1 mg/ml in ACM, and incubated with the cells for 1 hr before the further lysing step. For the unstimulated group, cells were rinsed and lysed directly after 2 days of plating. Before being lysed, cells were rinsed with cold DPBS to remove remaining ACM. Afterwards, cells were lysed in 500 µl of ice-cold 1x PHEM buffer (60 mM PIPES, 25 mM HEPES, 10 mM EGTA, 2 mM $MgCl_2$) containing 1 % Triton 100-X by manually scraping. The whole washing and lysing steps were performed on ice to preserve protein quality.

Cell suspension was collected into a 1.5 ml tube and spun at 300 g for 10 minutes at 4 °C. To avoid disrupting the pellets at the bottom, which contain stable actin filaments (F-actin), 400 µl rather than 500 µl of the supernatant was collected and transferred into another 1.5 ml tube. The remaining 100 µl of supernatant was discarded and the pellets were resuspended in 625 µl 1x SDS buffer. The collected supernatant was centrifuged at 10,000 g for 10 minutes at 4 °C, and 300 µl of the resulting supernatant was collected into another fresh 1.5 ml tube. After removing the remaining 100 µl pf supernatant, 500 µl of 1x SDS buffer was used to resuspend the small fraction of pellets containing dynamic F-actin. 75 µl of 5x SDS buffer was added to the 300 µl supernatant containing the soluble fraction of cell components and actin monomers (G-actin), resulting in a concentration of SDS buffer of 1x. Pipetting and sonication were employed to thoroughly mix the samples in the tubes containing insoluble fractions of cell components. Following that, all samples were heated at 100 °C for 10 minutes to denature proteins, and the tubes containing insoluble cell components were vortexed once during the heating to shear DNA. All samples were cooled down on ice after heating and stored at – 20 °C.

4.2.5.2. Preparation of SDS polyacrylamide gels

Sodium dodecyl sulfates – polyacrylamide gel electrophoresis (SDS-PAGE) is a common method in molecular biology used to separate proteins. SDS and polyacrylamide gel can remove the influence of charge and structure, and the protein separation is based on the differences of molecular weight.

Table 4.12: Composition of SDS – polyacrylamide gels (40 ml for 4 gels)

Component	Resolving		Stacking
	10 %	8%	4%
H_2O	18.6 ml	21.4 ml	12.2 ml
30 % Acrylamide (1:38)	13.4 ml	10.6 ml	2.6 ml
2M Tris/HCl pH8.8	7.6 ml	7.6 ml	-
20 % SDS	200 µl	200 µl	100 µl
0.5 M Tris/HCl pH 6.8	-	-	5 ml
10% APS	280 µl	280 µl	140 µl
TEMED	20 µl	20 µl	10 µl

Polyacrylamide gels were composed of stacking gel and resolving gel. Stacking gels were used to line up the proteins, so the protein could enter the resolving gels at the same time. Resolving gels were used to separate the proteins. They had bigger pole size and higher pH (8.8) than stacking gels (pH 6.8). The concentration of resolving gels was determined according to the molecular weight of the target proteins. 8 % acrylamide gels were used for identifying WRC components, and 10 % gels were used for the F – and G- actin separation experiment. Table 4.11 lists the components of polyacrylamide gels used in this study.

4.2.5.3. SDS-PAGE

SDS – polyacrylamide gel electrophoresis (SDS-PAGE) was conducted in a gel-running chamber using SDS running buffer (25 mM Tris, 190 mM glycine, 1 % SDS pH 8.8). For proteins to run through 4 % stacking gel, 70 V or 80 V voltage was applied for 30 min (70 V for 10 % gel, 80 V for 8 % gel). After the proteins had passed through the stacking gel, the voltage was raised to 130 V for the proteins to separate and run through the resolving gel. The entire duration for gel running was roughly 1.5 hours. The SDS-PAGE was completed when the bromophenol was detected near the bottom of the gel.

4.2.5.4. Western blotting

Western blotting is a common technique used in biochemistry and molecular biology for detecting certain proteins in tissue extracts or cells. It consists of 3 major steps – separation of proteins by size, transfer of proteins to a solid membrane and protein detection using antibodies. After SDS-PAGE was completed, samples were transferred to a polyvinylidene fluoride

(PVDF) membrane (Millipore, cat# IPVH00010) for further identification of specific proteins using antibodies. The standard wet transfer system was employed in this study. Prior to the transfer, PVDF membranes were briefly activated with MeOH (VWR, cat# 152505N), and the sponges and Whatman papers (GE Healthcare, cat# 9.950 371) were soaked in ice-cold transfer buffer (25 mM Tris, 190 mM glycine, 20 % methanol). When the gel running was completed, the gels were taken out from the running chamber, and the transfer sandwiches were carefully prepared by placing a sponge, 2 Whatman papers, resolving gel, activated PVDF membrane, 2 more Whatman papers and another sponge in the sequential order. Air bubbles were gently removed when placing the resolving gel and PVDF membrane to prevent them from disturbing the protein transfer. The transfer sandwich was placed in between a cassette, and the cassettes were inserted into a transfer chamber with the gel orientated towards the cathode. To prevent overheating during transfer, the ice-cold transfer buffer and an ice block were filled and placed in the transfer chamber.

The transfer for WRC identification was carried out at 20 V at room temperature overnight, while the transfer for F- and G-actin separation required only 70 minutes at 110 V at room temperature. When the transfer was finished, membranes for WRC identification were taken out and blocked in 5 % BSA in 1x NCP (10 mM Tris/HCl (pH 8.0 – 8.4), 150 mM NaCl, 0.05% Tween-20) for a few hours at room temperature. Primary antibodies for individual WRC members were diluted in blocking solution (Table 4.13) and membranes were incubated overnight at 4 °C with gentle agitation. Membranes for F– and G–actin separation were directly incubated with primary antibody, which was diluted in 5 % skim milk (Roth, cat# T145) overnight at 4 °C with gentle agitation.

On the next day, membranes were washed 3 times with 1x NCP, each time for 15 minutes. HRP-conjugated secondary antibodies (Jackson ImmunoResearch) were diluted in 1x NCP and incubated with the membranes for 1 hour at room temperature with gentle agitation. After being washed 3 times with 1x NCP, each wash 5 minutes, the membranes were developed using enhanced chemical luminescence (ECL) solution right before imaging. ECL solution was composed of reagent A (0.1 mM Tris/HCl (pH 8.6), 0.05 % p-hydroxy-coumarin, 2 % luminol) and B (0.1 mM Tris/HCl (pH 8.6), 0.03 % H_2O_2) at the ratio of 1:1. The H_2O_2 in reagent B oxidized the luminol in reagent A, and this process was catalyzed by the HRP on secondary antibodies. Once luminol was oxidized, it emitted a signal at 450 nm, which was captured by a luminescent image analyzer with CCD camera (LAS 4000 mini).

Table 4.13: Antibodies used for western blotting

	Species	Dilution	Source
CYFIP1	Mouse	undiluted	AG Witke
CYFIP2	Mouse	undiluted	AG Witke
NCAKP1	Rabbit	1:400	Sigma-Aldrich
HEM1	Rabbit	1:1000 (BSA)	Stradal Lab
WAVE1	Rabbit	1:1000	Upstate
WAVE2	Rabbit	1:1000 (BSA)	Cell Signaling
WAVE3	Rabbit	1:1000	Cell Signaling
ABI1	Rabbit	1:1000	Sigma-Aldrich
ABI2	Rabbit	1:1000 (BSA)	Abcam
ABI3	Rabbit	1:1000 (BSA)	Cell Signaling
β-actin	Mouse	1:5000	MP Biomedicals

(The antibodies were diluted in either 5 % skimmed milk or 5 % BSA in NCP)

4.2.5.5. Protein quantification by Coomassie-stained PVDF membrane

Membrane Coomassie staining was used to calibrate the actual loading of each sample in the western blotting experiments. The conventional loading calibration method by measuring standard proteins (e.g. actin, gamma tubulin and GADPH) is not ideal for this study because the loss of CYFIP1 very likely influences the expression of these proteins. Thus, Coomassie staining of membranes provided a more direct and reliable means of determining the total protein loading from each sample. Following the measurement of target protein expression, the membranes were first fixed in 40 % methanol (40 % methanol, 10 % acetic acid) for 5 min before being placed in Coomassie staining solution (0.2 % Coomassie brilliant blue R-250 (BioRad, cat# 1610436), 50 % methanol and 10 % acetic acid (VWR)) for another 5 minutes with gentle agitation under room temperature. After Coomassie staining, the membranes were washed with 40 % methanol (40 % methanol, 10 % acetic acid) with moderate agitation under room temperature to remove excessive Coomassie. The membranes were washed 3 times, with each wash lasting 5 minutes. In the final washing step, the membranes were washed twice in 20 % methanol (20 % methanol, 10 % acetic acid) for 5 minutes each. Finally, the membranes

were air-dried in a fume hood until the background turned white and the contrast between the stained protein and the background increased. The dried membranes were imaged using the LAS 4000 mini. The total protein loading was determined by measuring the Coomassie-stained protein in each sample lane after subtracting the background signal (Figure 4.7). The signal of target protein was in the end calibrated by normalizing it to the total protein loading.

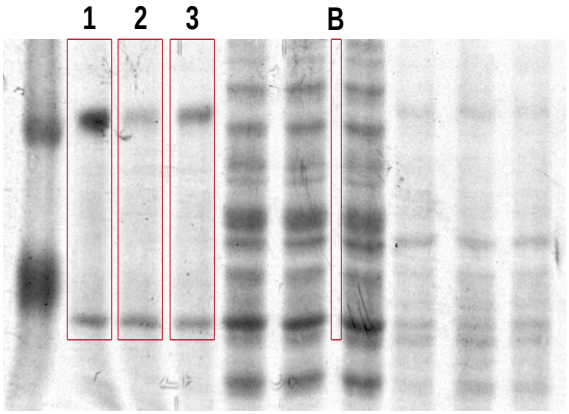

Figure 4.7: Protein quantification by Coomassie-stained PVDF membrane
The total protein loading was calculated after Coomassie staining of the PVDF membranes by defining the Coomassie-stained protein in each sample lane (as shown in lane 1, 2 and 3). The area between the lanes was chosen as background (B in the image). The background signal was deducted from the signal in each lane, yielding the real signal of the total protein.

4.2.6. Microscopy

4.2.6.1. Live-cell imaging

All live-cell imaging experiments were conducted at 37°C with 5 % CO_2. Imaging parameters were the same for every individual experiment in each assay. *In vitro* synaptosome phagocytosis and wound healing assays were recorded using the Epi-fluorescence scope 2 (Epi-scope 2) from Zeiss. The Epi-scope 2 is an inverted microscope equipped with definite focus (hardware-based focus drift-correction), a seven-line LED combiner (385 nm, 430 nm, 475 nm, 511 nm, 555 nm, 590 nm, 630 nm) and transmitted light source (bright-field). Besides, Episcope 2 also had a small incubation chamber, which provides constant 5 % CO_2 and whose temperature is maintained at 37°C. The above conditions made Episcope 2 an ideal microscope for the live-cell experiments. *In vitro* synaptosome phagocytosis was recorded at 20x in both fluorescent (555 nm) and bright-field channels. Images were captured every hour for total 24 hours. *In vitro* wound healing assay was recorded at 20x using the bright-field channel every 3 hours for 72 hours. The Zeiss LSM 780 confocal microscope was used to continuously record membrane ruffling of primary microglia at 40x for in total 150 images for around 15 minutes. LSM 780 is an inverted confocal microscope equipped with a transmission detector in addition to 34-channel GaAsP detector. The setup also includes an incubator with stable control of CO_2 and temperature, which allows live-cell imaging to be conducted.

4.2.6.2. Confocal imaging

Mouse brain tissue and primary microglial cells stained with fluorescent antibodies or dyes were imaged with Zeiss LSM 980 and 700 confocal microscopes. Zeiss LSM 980 and LSM 700 are inverted confocal microscopes with several excitation lasers (LSM 980: 405 nm, 445 nm, 488 nm, 514 nm, 561 nm, 594 nm, 639 nm; LSM 700: 405 nm, 488 nm, 555 nm, 639 nm), ideal for multi-color fluorescence imaging.

For *in vivo* microglial morphology and CD68 analysis, microglia were stained with Iba1 and CD68 antibodies. Slices were imaged with LSM 980 at 20x and 63x, and 16 µm z-stacks with 0.6 µm interval were taken. For excitatory synapse analysis, tissue was stained with anti-Bassoon and Homer1 antibodies. Imaging was carried out using the LSM 700 confocal microscope at 63x, 1.5 µm z-stacks were taken with 0.3 µm interval. Neuronal cell number was also investigated by staining the tissue with NeuN antibody. 20 µm z-stacks with 1 µm intervals were taken with LSM 980 at 20x. Phalloidin and CD11b were used to stain primary microglial cells after *in vitro* phagocytosis assay. Cells were imaged at 20x at a single plane using LSM 980.

4.2.6.3. Bright-field imaging

Bright-field imaging with KEYENCE all-in-one microscope was conducted for the visualization of dendritic spines. The KEYENCE all-in-one microscope was equipped with a fully-motorized control system for instant target acquisition. It had a large motorized stage, high-speed auto-focusing and automatic capture conditions.

The layer V somatosensory cortex was first scanned at 20x. Pyramidal neurons with intact basal structures were selected and their positions were marked. Basal primary branches of dendrites were then imaged at 90x (60x objective with a 1.5x digital zoom). Z-stacks with 0.5 µm intervals were taken. Thinner intervals allowed a better resolution for spine structure, and it improved the quality of the analysis of dendritic length, morphology and spine number.

H&E - stained sections were imaged at 0.8x using a Olympus stereo microscope.

4.2.7. Image analysis

4.2.7.1. 3D microglial morphology analysis

To explore morphological features of microglia in adult mouse tissue, we employed MotiQ, an imageJ-based open source plugin (Hansen *et al.*, 2022) developed in our lab. MotiQ can

perform automated analysis of cell morphology. It has an automated pipeline for thresholding to distinguish cells from the background and generates binary images for 3D reconstruction. It also provides analysis based on numerous morphological parameters. Anti-Iba1 antibody was used to stain microglial cells in sagittal brain slices, and 20x confocal Z-stack images were employed for microglial 3D morphological analysis. The background of the confocal images was subtracted with a rolling ball radius of 30 pixels, and the images were processed with MotiQ thresholder to compute the intensity threshold using the "Li" method. Following that, binary images were created and employed in the MotiQ 3D analyzer to automatically reconstitute and evaluate the morphological characteristics of microglial cells. In this study, the particle filter in the MotiQ 3D analyzer was set to 3500 voxels. Particles with less than 3500 voxels were excluded from 3D reconstruction.

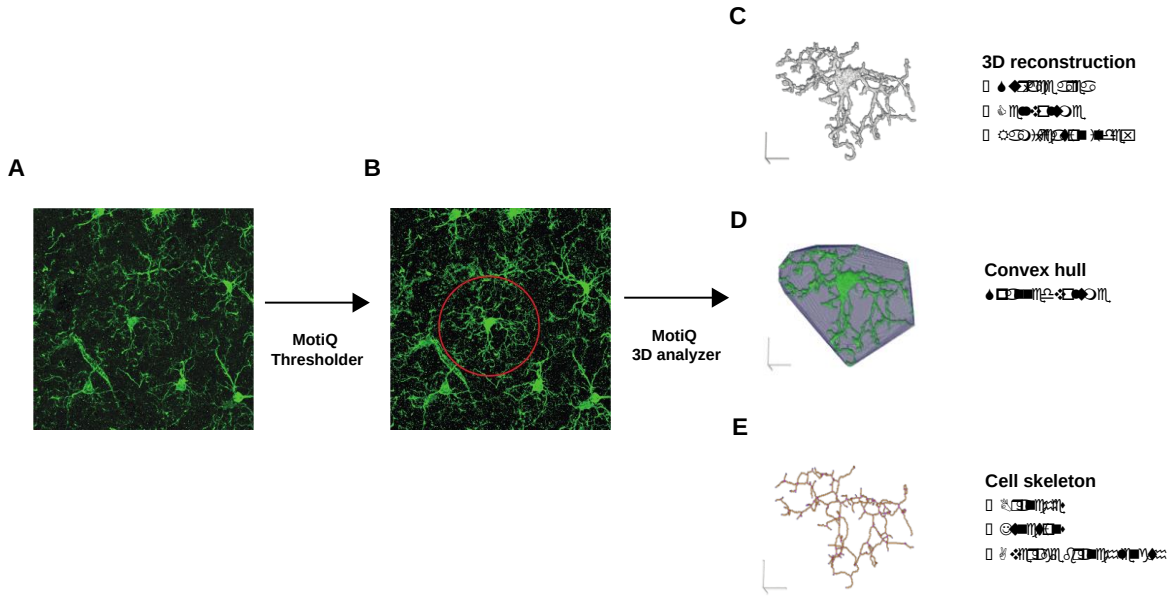

Figure 4.8: MotiQ workflow for 3D microglial morphology analysis
(A) 20x confocal Z-stack image whose background was subtracted was processed with MotiQ thresholder. **(B)** Following the intensity thresholding, a binary image was generated for automatic morphological analysis of microglial cells using MotiQ 3D analyzer. **(C)** MotiQ 3D analyzer reconstructed microglial cells, and determined their surface area, cell volume and ramification index. **(D)** The spanned volume of each microglial cell was also generated. It represents the area scanned by each microglial cell. **(E)** The parameters of cell skeleton, including numbers of branches and junction, and average branch length were also evaluated. A cell with more branches and junctions was more ramified, but its average branch length would be shorter.

Figure 4.8 depicts the MotiQ workflow for 3D microglial morphology analysis. Microglial surface area, cell volume and ramification index were assessed after 3D reconstruction of microglial cells. The ramification index was derived by dividing the cell's surface area by the surface area of a minimally ramified cell. It reflected the cell's branching level. The spanned volume of microglial cells was estimated by measuring the volume of a convex three-dimensional hull surrounding the cell, representing the territory surveyed by that microglial cell. MotiQ 3D analyzer was also used to analyze parameters of the cell skeleton. The number of microglial branches, junctions and the average branch length were quantified. These parameters were in concert with the cell ramification index. A cell with higher ramification had a greater number of branches and junctions, but its average branch length was shorter.

4.2.7.2. Analysis of microglial CD68

The CD68 level in microglia was measured using IMARIS according to a published methodology (Schafer *et al*, 2014). CD68 is expressed in all microglial cells but is increased in activated microglia. Sagittal brain sections from adult mice were stained with anti-Iba1 and anti-CD68 antibodies to label microglial cells and CD68. IMARIS 3D surface rendering was performed using 63x confocal Z-stack images. The background in the confocal images was first subtracted. The filter width for the Iba1 channel was 5 µm, whereas the filter width for CD68 channel was 1 µm. To begin, the Iba1 channel was employed to reconstruct microglial cells using the surface rendering function in IMARIS. Regions of interest (ROIs) were selected by choosing the intact microglial cells in each image. 2 ROIs were selected from each image, for a total of 4 ROIs utilized for analysis per animal. The threshold for microglial surface creation was set at absolute intensity 45 to remove the noise and undesired fluorescence. At the last step of microglial surface rending process, the filter "volume" was chosen, and the unconnected particles were filtered out. Following the reconstruction of the selected microglia, its CD68 was also reconstituted using the surface rendering function. The CD68 channel's thresholding was tuned to the absolute intensity 15, and the shortest distance of the reconstituted CD68 to the corresponding microglia was set to 0 at the end of the rendering process in order to filter out the CD68 signal outside of the microglia. The CD68 level was calculated by normalizing the volume of CD68 inside the microglia to the corresponding microglial cell volume. The surface rendering condition was the same for all of the images.

4.2.7.3. Analysis of primary microglial migration

Cell movement in migration assays was tracked following the ibidi migration analysis protocol (Chemotaxis and Migration Tool Version 1.01). The position of the chosen cell from the right side of the wound was pinpointed and followed over time. The cumulative distance was calculated and the cell velocity was determined by dividing the total distance by the duration of movement.

References

Abd-el-Basset EM, Fedoroff S (1994) Dynamics of actin filaments in microglia during Fc receptor-mediated phagocytosis. *Acta Neuropathol* 88: 527-537

Abekhoukh S, Sahin HB, Grossi M, Zongaro S, Maurin T, Madrigal I, Kazue-Sugioka D, Raas-Rothschild A, Doulazmi M, Carrera P *et al* (2017) New insights into the regulatory function of CYFIP1 in the context of WAVE- and FMRP-containing complexes. *Dis Model Mech* 10: 463-474

Abercrombie M, Heaysman JE, Pegrum SM (1971) The locomotion of fibroblasts in culture. IV. Electron microscopy of the leading lamella. *Exp Cell Res* 67: 359-367

Acharya D, Reis R, Volcic M, Liu G, Wang MK, Chia BS, Nchioua R, Groß R, Münch J, Kirchhoff F *et al* (2022) Actin cytoskeleton remodeling primes RIG-I-like receptor activation. *Cell* 185: 3588-3602.e3521

Ajami B, Bennett JL, Krieger C, McNagny KM, Rossi FMV (2011) Infiltrating monocytes trigger EAE progression, but do not contribute to the resident microglia pool. *Nature Neuroscience* 14: 1142-1149

Alberts B, Bray D, Lewis J, Raff M, Roberts M, and Watson J (2008) *Molecular biology of the cell*. Garland Science, New York, NY u.a.

Allen NJ, Bennett ML, Foo LC, Wang GX, Chakraborty C, Smith SJ, Barres BA (2012) Astrocyte glypicans 4 and 6 promote formation of excitatory synapses via GluA1 AMPA receptors. *Nature* 486: 410-414

Alliot F, Godin I, Pessac B (1999) Microglia derive from progenitors, originating from the yolk sac, and which proliferate in the brain. *Brain Res Dev Brain Res* 117: 145-152

Alliot F, Lecain E, Grima B, Pessac B (1991) Microglial progenitors with a high proliferative potential in the embryonic and adult mouse brain. *Proc Natl Acad Sci U S A* 88: 1541-1545

Aloisi F (2001) Immune function of microglia. *Glia* 36: 165-179

Andoh M, Koyama R (2021) Microglia regulate synaptic development and plasticity. *Dev Neurobiol* 81: 568-590

Andoh M, Shibata K, Okamoto K, Onodera J, Morishita K, Miura Y, Ikegaya Y, Koyama R (2019) Exercise Reverses Behavioral and Synaptic Abnormalities after Maternal Inflammation. *Cell Rep* 27: 2817-2825.e2815

Askew K, Li K, Olmos-Alonso A, Garcia-Moreno F, Liang Y, Richardson P, Tipton T, Chapman MA, Riecken K, Beccari S *et al* (2017) Coupled Proliferation and Apoptosis Maintain the Rapid Turnover of Microglia in the Adult Brain. *Cell Rep* 18: 391-405

Atri C, Guerfali FZ, Laouini D (2018) Role of Human Macrophage Polarization in Inflammation during Infectious Diseases. *Int J Mol Sci* 19

Attaai A, Neidert N, von Ehr A, Potru PS, Zöller T, Spittau B (2018) Postnatal maturation of microglia is associated with alternative activation and activated TGFβ signaling. *Glia* 66: 1695-1708

Bamburg JR (1999) Proteins of the ADF/cofilin family: essential regulators of actin dynamics. *Annu Rev Cell Dev Biol* 15: 185-230

Barger SR, Vorselen D, Gauthier NC, Theriot JA, Krendel M (2022) F-actin organization and target constriction during primary macrophage phagocytosis is balanced by competing activity of myosin-I and myosin-II. *Mol Biol Cell* 33: br24

Barron KD (1995) The microglial cell. A historical review. *Journal of the Neurological Sciences* 134: 57-68

Beers DR, Henkel JS, Xiao Q, Zhao W, Wang J, Yen AA, Siklos L, McKercher SR, Appel SH (2006) Wild-type microglia extend survival in PU.1 knockout mice with familial amyotrophic lateral sclerosis. *Proc Natl Acad Sci U S A* 103: 16021-16026

Bernardet M, Crusio WE (2006) Fmr1 KO mice as a possible model of autistic features. *ScientificWorldJournal* 6: 1164-1176

Bernier LP, Bohlen CJ, York EM, Choi HB, Kamyabi A, Dissing-Olesen L, Hefendehl JK, Collins HY, Stevens B, Barres BA *et al* (2019) Nanoscale Surveillance of the Brain by Microglia via cAMP-Regulated Filopodia. *Cell Rep* 27: 2895-2908.e2894

Bernstein BW, Bamburg JR (2010) ADF/cofilin: a functional node in cell biology. *Trends Cell Biol* 20: 187-195

Bertrand JY, Jalil A, Klaine M, Jung S, Cumano A, Godin I (2005) Three pathways to mature macrophages in the early mouse yolk sac. *Blood* 106: 3004-3011

Biswas SK, Mantovani A (2010) Macrophage plasticity and interaction with lymphocyte subsets: cancer as a paradigm. *Nat Immunol* 11: 889-896

Block MR, Badowski C, Millon-Fremillon A, Bouvard D, Bouin AP, Faurobert E, Gerber-Scokaert D, Planus E, Albiges-Rizo C (2008) Podosome-type adhesions and focal adhesions, so alike yet so different. *Eur J Cell Biol* 87: 491-506

Boczkowska M, Rebowski G, Petoukhov MV, Hayes DB, Svergun DI, Dominguez R (2008) X-ray scattering study of activated Arp2/3 complex with bound actin-WCA. *Structure* 16: 695-704

Borm B, Requardt RP, Herzog V, Kirfel G (2005) Membrane ruffles in cell migration: indicators of inefficient lamellipodia adhesion and compartments of actin filament reorganization. *Exp Cell Res* 302: 83-95

Bosworth AP, Contreras M, Novak SW, Sancho L, Salas IH, Manor U, Allen NJ (2023) Astrocyte glypican 5 regulates synapse maturation and stabilization. *bioRxiv*: 2023.2003. 2002.529949

Brown GC, Neher JJ (2014) Microglial phagocytosis of live neurons. *Nature Reviews Neuroscience* 15: 209-216

Burbach JP, van der Zwaag B (2009) Contact in the genetics of autism and schizophrenia. *Trends Neurosci* 32: 69-72

Byun YG, Chung WS (2018) A Novel In Vitro Live-imaging Assay of Astrocyte-mediated Phagocytosis Using pH Indicator-conjugated Synaptosomes. *J Vis Exp*

Cai L, Marshall TW, Uetrecht AC, Schafer DA, Bear JE (2007) Coronin 1B coordinates Arp2/3 complex and cofilin activities at the leading edge. *Cell* 128: 915-929

Campellone KG, Welch MD (2010) A nucleator arms race: cellular control of actin assembly. *Nat Rev Mol Cell Biol* 11: 237-251

Charabati M, Rabanel JM, Ramassamy C, Prat A (2020) Overcoming the Brain Barriers: From Immune Cells to Nanoparticles. *Trends Pharmacol Sci* 41: 42-54

Chen B, Chou HT, Brautigam CA, Xing W, Yang S, Henry L, Doolittle LK, Walz T, Rosen MK (2017) Rac1 GTPase activates the WAVE regulatory complex through two distinct binding sites. *Elife* 6

Chen Z, Borek D, Padrick SB, Gomez TS, Metlagel Z, Ismail AM, Umetani J, Billadeau DD, Otwinowski Z, Rosen MK (2010) Structure and control of the actin regulatory WAVE complex. *Nature* 468: 533-538

Chereau D, Kerff F, Graceffa P, Grabarek Z, Langsetmo K, Dominguez R (2005) Actin-bound structures of Wiskott-Aldrich syndrome protein (WASP)-homology domain 2 and the implications for filament assembly. *Proc Natl Acad Sci U S A* 102: 16644-16649

Chesarone MA, Goode BL (2009) Actin nucleation and elongation factors: mechanisms and interplay. *Curr Opin Cell Biol* 21: 28-37

Chhabra ES, Higgs HN (2007) The many faces of actin: matching assembly factors with cellular structures. *Nature Cell Biology* 9: 1110-1121

Chi Q, Yin T, Gregersen H, Deng X, Fan Y, Zhao J, Liao D, Wang G (2014) Rear actomyosin contractility-driven directional cell migration in three-dimensional matrices: a mechano-chemical coupling mechanism. *J R Soc Interface* 11: 20131072

Chitu V, Stanley ER (2017) Regulation of Embryonic and Postnatal Development by the CSF-1 Receptor. *Curr Top Dev Biol* 123: 229-275

Chung L, Wang X, Zhu L, Towers AJ, Cao X, Kim IH, Jiang YH (2015) Parental origin impairment of synaptic functions and behaviors in cytoplasmic FMRP interacting protein 1 (Cyfip1) deficient mice. *Brain Res* 1629: 340-350

Clarke LE, Barres BA (2013) Emerging roles of astrocytes in neural circuit development. *Nat Rev Neurosci* 14: 311-321

Correll CU, Schooler NR (2020) Negative Symptoms in Schizophrenia: A Review and Clinical Guide for Recognition, Assessment, and Treatment. *Neuropsychiatr Dis Treat* 16: 519-534

Crapser JD, Arreola MA, Tsourmas KI, Green KN (2021) Microglia as hackers of the matrix: sculpting synapses and the extracellular space. *Cellular & Molecular Immunology* 18: 2472-2488

Crespi B, Stead P, Elliot M (2010) Evolution in health and medicine Sackler colloquium: Comparative genomics of autism and schizophrenia. *Proc Natl Acad Sci U S A* 107 Suppl 1: 1736-1741

Cunningham CL, Martínez-Cerdeño V, Noctor SC (2013) Microglia regulate the number of neural precursor cells in the developing cerebral cortex. *J Neurosci* 33: 4216-4233

Dani A, Huang B, Bergan J, Dulac C, Zhuang X (2010) Superresolution imaging of chemical synapses in the brain. *Neuron* 68: 843-856

Davenport EC, Szulc BR, Drew J, Taylor J, Morgan T, Higgs NF, Lopez-Domenech G, Kittler JT (2019) Autism and Schizophrenia-Associated CYFIP1 Regulates the Balance of Synaptic Excitation and Inhibition. *Cell Rep* 26: 2037-2051 e2036

de Groot CJ, Huppes W, Sminia T, Kraal G, Dijkstra CD (1992) Determination of the origin and nature of brain macrophages and microglial cells in mouse central nervous system, using non-radioactive in situ hybridization and immunoperoxidase techniques. *Glia* 6: 301-309

De Rubeis S, Pasciuto E, Li KW, Fernandez E, Di Marino D, Buzzi A, Ostroff LE, Klann E, Zwartkruis FJ, Komiyama NH *et al* (2013) CYFIP1 coordinates mRNA translation and cytoskeleton remodeling to ensure proper dendritic spine formation. *Neuron* 79: 1169-1182

del Rio-Hortega P (1939) THE MICROGLIA. *The Lancet* 233: 1023-1026

DeMali KA, Burridge K (2003) Coupling membrane protrusion and cell adhesion. *J Cell Sci* 116: 2389-2397

Di Marino D, Chillemi G, De Rubeis S, Tramontano A, Achsel T, Bagni C (2015) MD and Docking Studies Reveal That the Functional Switch of CYFIP1 is Mediated by a Butterfly-like Motion. *J Chem Theory Comput* 11: 3401-3410

Ding B, Yang S, Schaks M, Liu Y, Brown AJ, Rottner K, Chowdhury S, Chen B (2022) Structures reveal a key mechanism of WAVE regulatory complex activation by Rac1 GTPase. *Nature Communications* 13: 5444

Dissing-Olesen L, LeDue JM, Rungta RL, Hefendehl JK, Choi HB, MacVicar BA (2014) Activation of neuronal NMDA receptors triggers transient ATP-mediated microglial process outgrowth. *J Neurosci* 34: 10511-10527

Dominguez R (2016) The WH2 Domain and Actin Nucleation: Necessary but Insufficient. *Trends Biochem Sci* 41: 478-490

Dominguez R, Holmes KC (2011) Actin structure and function. *Annu Rev Biophys* 40: 169-186

Domínguez-Iturza N, Lo AC, Shah D, Armendáriz M, Vannelli A, Mercaldo V, Trusel M, Li KW, Gastaldo D, Santos AR *et al* (2019) The autism- and schizophrenia-associated protein CYFIP1 regulates bilateral brain connectivity and behaviour. *Nature Communications* 10: 3454

Doornbos M, Sikkema-Raddatz B, Ruijvenkamp CAL, Dijkhuizen T, Bijlsma EK, Gijsbers ACJ, Hilhorst-Hofstee Y, Hordijk R, Verbruggen KT, Kerstjens-Frederikse WS *et al* (2009) Nine patients with a microdeletion 15q11.2 between breakpoints 1 and 2 of the Prader–Willi critical region, possibly associated with behavioural disturbances. *European Journal of Medical Genetics* 52: 108-115

Dubielecka PM, Ladwein KI, Xiong X, Migeotte I, Chorzalska A, Anderson KV, Sawicki JA, Rottner K, Stradal TE, Kotula L (2011) Essential role for Abi1 in embryonic survival and WAVE2 complex integrity. *Proc Natl Acad Sci U S A* 108: 7022-7027

Eden S, Rohatgi R, Podtelejnikov AV, Mann M, Kirschner MW (2002) Mechanism of regulation of WAVE1-induced actin nucleation by Rac1 and Nck. *Nature* 418: 790-793

Elder LM, Dawson G, Toth K, Fein D, Munson J (2008) Head circumference as an early predictor of autism symptoms in younger siblings of children with autism spectrum disorder. *J Autism Dev Disord* 38: 1104-1111

Elliott MR, Ravichandran KS (2010) Clearance of apoptotic cells: implications in health and disease. *J Cell Biol* 189: 1059-1070

Espinoza-Sanchez S, Metskas LA, Chou SZ, Rhoades E, Pollard TD (2018) Conformational changes in Arp2/3 complex induced by ATP, WASp-VCA, and actin filaments. *Proc Natl Acad Sci U S A* 115: E8642-e8651

Facci L, Barbierato M, Marinelli C, Argentini C, Skaper SD, Giusti P (2014) Toll-Like Receptors 2, -3 and -4 Prime Microglia but not Astrocytes Across Central Nervous System Regions for ATP-Dependent Interleukin-1β Release. *Scientific Reports* 4: 6824

Faix J, Grosse R (2006) Staying in shape with formins. *Dev Cell* 10: 693-706

Färber K, Cheung G, Mitchell D, Wallis R, Weihe E, Schwaeble W, Kettenmann H (2009) C1q, the recognition subcomponent of the classical pathway of complement, drives microglial activation. *J Neurosci Res* 87: 644-652

Fedoroff S, Zhai R, Novak JP (1997) Microglia and astroglia have a common progenitor cell. *J Neurosci Res* 50: 477-486

Fernandez-Arjona MDM, Grondona JM, Granados-Duran P, Fernandez-Llebrez P, Lopez-Avalos MD (2017) Microglia Morphological Categorization in a Rat Model of Neuroinflammation by Hierarchical Cluster and Principal Components Analysis. *Front Cell Neurosci* 11: 235

Firat-Karalar EN, Welch MD (2011) New mechanisms and functions of actin nucleation. *Current Opinion in Cell Biology* 23: 4-13

Flannagan RS, Jaumouillé V, Grinstein S (2012) The Cell Biology of Phagocytosis. *Annual Review of Pathology: Mechanisms of Disease* 7: 61-98

Franco-Bocanegra DK, George B, Lau LC, Holmes C, Nicoll JAR, Boche D (2019) Microglial motility in Alzheimer's disease and after Abeta42 immunotherapy: a human post-mortem study. *Acta Neuropathol Commun* 7: 174

Fraser DA, Pisalyaput K, Tenner AJ (2010) C1q enhances microglial clearance of apoptotic neurons and neuronal blebs, and modulates subsequent inflammatory cytokine production. *Journal of neurochemistry* 112: 733-743

Freeman SA, Grinstein S (2014) Phagocytosis: receptors, signal integration, and the cytoskeleton. *Immunol Rev* 262: 193-215

Freeman SA, Uderhardt S, Saric A, Collins RF, Buckley CM, Mylvaganam S, Boroumand P, Plumb J, Germain RN, Ren D *et al* (2020) Lipid-gated monovalent ion fluxes regulate endocytic traffic and support immune surveillance. *Science* 367: 301-305

Frost JL, Schafer DP (2016) Microglia: Architects of the Developing Nervous System. *Trends Cell Biol* 26: 587-597

Garey LJ, Ong WY, Patel TS, Kanani M, Davis A, Mortimer AM, Barnes TRE, Hirsch SR (1998) Reduced dendritic spine density on cerebral cortical pyramidal neurons in schizophrenia. *Journal of Neurology, Neurosurgery & Psychiatry* 65: 446

Garibyan L, Avashia N (2013) Polymerase chain reaction. *J Invest Dermatol* 133: 1-4

Gautreau A, Ho HY, Li J, Steen H, Gygi SP, Kirschner MW (2004) Purification and architecture of the ubiquitous Wave complex. *Proc Natl Acad Sci U S A* 101: 4379-4383

Gildawie KR, Orso R, Peterzell S, Thompson V, Brenhouse HC (2020) Sex differences in prefrontal cortex microglia morphology: Impact of a two-hit model of adversity throughout development. *Neuroscience Letters* 738: 135381

Ginhoux F, Lim S, Hoeffel G, Low D, Huber T (2013) Origin and differentiation of microglia. *Front Cell Neurosci* 7: 45

Giulian D, Baker TJ (1986) Characterization of ameboid microglia isolated from developing mammalian brain. *J Neurosci* 6: 2163-2178

Glantz LA, Lewis DA (2000) Decreased Dendritic Spine Density on Prefrontal Cortical Pyramidal Neurons in Schizophrenia. *Arch Gen Psychiatry* 57

Gold ES, Underhill DM, Morrissette NS, Guo J, McNiven MA, Aderem A (1999) Dynamin 2 is required for phagocytosis in macrophages. *J Exp Med* 190: 1849-1856

Goley ED, Welch MD (2006) The ARP2/3 complex: an actin nucleator comes of age. *Nat Rev Mol Cell Biol* 7: 713-726

Goode BL, Rodal AA, Barnes G, Drubin DG (2001) Activation of the Arp2/3 complex by the actin filament binding protein Abp1p. *J Cell Biol* 153: 627-634

Grafodatskaya D, Chung B, Szatmari P, Weksberg R (2010) Autism spectrum disorders and epigenetics. *J Am Acad Child Adolesc Psychiatry* 49: 794-809

Guo S, Wang H, Yin Y (2022) Microglia Polarization From M1 to M2 in Neurodegenerative Diseases. *Front Aging Neurosci* 14: 815347

Haan N, Westacott LJ, Carter J, Owen MJ, Gray WP, Hall J, Wilkinson LS (2021) Haploinsufficiency of the schizophrenia and autism risk gene Cyfip1 causes abnormal postnatal hippocampal neurogenesis through microglial and Arp2/3 mediated actin dependent mechanisms. *Transl Psychiatry* 11: 313

Habela CW, Yoon KJ, Kim NS, Taga A, Bell K, Bergles DE, Maragakis NJ, Ming GL, Song H (2020) Persistent Cyfip1 Expression Is Required to Maintain the Adult Subventricular Zone Neurogenic Niche. *J Neurosci* 40: 2015-2024

Haber M, Zhou L, Murai KK (2006) Cooperative astrocyte and dendritic spine dynamics at hippocampal excitatory synapses. *J Neurosci* 26: 8881-8891

Haimon Z, Volaski A, Orthgiess J, Boura-Halfon S, Varol D, Shemer A, Yona S, Zuckerman B, David E, Chappell-Maor L *et al* (2018) Re-evaluating microglia expression profiles using RiboTag and cell isolation strategies. *Nat Immunol* 19: 636-644

Hansen JN, Brückner M, Pietrowski MJ, Jikeli JF, Plescher M, Beckert H, Schnaars M, Fülle L, Reitmeier K, Langmann T (2022) MotiQ: an open-source toolbox to quantify the cell motility and morphology of microglia. *Molecular biology of the cell* 33: ar99

Hao C, Richardson A, Fedoroff S (1991) Macrophage-like cells originate from neuroepithelium in culture: characterization and properties of the macrophage-like cells. *Int J Dev Neurosci* 9: 1-14

Hardan AY, Muddasani S, Vemulapalli M, Keshavan MS, Minshew NJ (2006) An MRI study of increased cortical thickness in autism. *Am J Psychiatry* 163: 1290-1292

Harris HE, Weeds AG (1984) Plasma gelsolin caps and severs actin filaments. *FEBS Lett* 177: 184-188

Harrison Jeffrey K, Jiang Yan, Chen Shizong, Xia Yiyang, Maciejewski Dominique, Mcnamara Robert K, Streiti Wolfgang J, Salafranca Mina N, Adhikari Soumya, Thompson

Darren A *et al* (1998) Role for neuronally derived fractalkine in mediating interactions between neurons and CX3CR1-expressing microglia. *Proc Natl Acad Sci USA* 95

Hauck S, 2021. Function of CYFIP2 in spinal motor neuron during embryonic development.

Haynes SE, Hollopeter G, Yang G, Kurpius D, Dailey ME, Gan WB, Julius D (2006) The P2Y12 receptor regulates microglial activation by extracellular nucleotides. *Nat Neurosci* 9: 1512-1519

Hinton VJ, Brown WT, Wisniewski K, Rudelli RD (1991) Analysis of neocortex in three males with the fragile X syndrome. *Am J Med Genet* 41: 289-294

Hinwood M, Morandini J, Day TA, Walker FR (2012) Evidence that microglia mediate the neurobiological effects of chronic psychological stress on the medial prefrontal cortex. *Cereb Cortex* 22: 1442-1454

Hinwood M, Tynan RJ, Charnley JL, Beynon SB, Day TA, Walker FR (2013) Chronic stress induced remodeling of the prefrontal cortex: structural re-organization of microglia and the inhibitory effect of minocycline. *Cereb Cortex* 23: 1784-1797

Hirayama-Kurogi M, Takizawa Y, Kunii Y, Matsumoto J, Wada A, Hino M, Akatsu H, Hashizume Y, Yamamoto S, Kondo T *et al* (2017) Downregulation of GNA13-ERK network in prefrontal cortex of schizophrenia brain identified by combined focused and targeted quantitative proteomics. *Journal of Proteomics* 158: 31-42

Honda S, Sasaki Y, Ohsawa K, Imai Y, Nakamura Y, Inoue K, Kohsaka S (2001) Extracellular ATP or ADP induce chemotaxis of cultured microglia through Gi/o-coupled P2Y receptors. *J Neurosci* 21: 1975-1982

Hong S, Beja-Glasser VF, Nfonoyim BM, Frouin A, Li S, Ramakrishnan S, Merry KM, Shi Q, Rosenthal A, Barres BA *et al* (2016) Complement and microglia mediate early synapse loss in Alzheimer mouse models. *Science* 352

Hosseini SA, Molla M (2023) Asperger Syndrome. In: *StatPearls*, StatPearls Publishing Copyright © 2023, StatPearls Publishing LLC.: Treasure Island (FL)

Hu Y, Gao Z (2021) The role of purinergic signaling in microglial responses. *Stress and Brain* 1: 46-58

Hughes PM, Botham MS, Frentzel S, Mir A, Perry VH (2002) Expression of fractalkine (CX3CL1) and its receptor, CX3CR1, during acute and chronic inflammation in the rodent CNS. *Glia* 37: 314-327

Hutsler JJ, Zhang H (2010) Increased dendritic spine densities on cortical projection neurons in autism spectrum disorders. *Brain Res* 1309: 83-94

Iijima M, Huang YE, Devreotes P (2002) Temporal and spatial regulation of chemotaxis. *Dev Cell* 3: 469-478

Innocenti M (2018) New insights into the formation and the function of lamellipodia and ruffles in mesenchymal cell migration. *Cell Adh Migr* 12: 401-416

Inoue K (2007) UDP facilitates microglial phagocytosis through P2Y6 receptors. *Cell Adh Migr* 1: 131-132

Insall RH, Machesky LM (2009) Actin dynamics at the leading edge: from simple machinery to complex networks. *Dev Cell* 17: 310-322

Irwin SA, Patel B, Idupulapati M, Harris JB, Crisostomo RA, Larsen BP, Kooy F, Willems PJ, Cras P, Kozlowski PB *et al* (2001) Abnormal Dendritic Spine Characteristics in the Temporal and Visual Cortices of Patients With Fragile-X Syndrome-A Quantitative Examination *American Journal of Medical Genetics* 98

Ishihara D, Dovas A, Park H, Isaac BM, Cox D (2012) The chemotactic defect in wiskott-Aldrich syndrome macrophages is due to the reduced persistence of directional protrusions. *PLoS One* 7: e30033

Jaumouillé V, Cartagena-Rivera AX, Waterman CM (2019) Coupling of β(2) integrins to actin by a mechanosensitive molecular clutch drives complement receptor-mediated phagocytosis. *Nat Cell Biol* 21: 1357-1369

Jaumouillé V, Waterman CM (2020) Physical Constraints and Forces Involved in Phagocytosis. *Front Immunol* 11: 1097

Jawaid S, Kidd GJ, Wang J, Swetlik C, Dutta R, Trapp BD (2018) Alterations in CA1 hippocampal synapses in a mouse model of fragile X syndrome. *Glia* 66: 789-800

Jiang LH, Roger S (2020) Targeting the P2X7 receptor in microglial cells to prevent brain inflammation. *Neural Regen Res* 15: 1245-1246

Jurga AM, Paleczna M, Kuter KZ (2020) Overview of General and Discriminating Markers of Differential Microglia Phenotypes. *Front Cell Neurosci* 14: 198

Kabrawala S, Zimmer MD, Campellone KG (2020) WHIMP links the actin nucleation machinery to Src-family kinase signaling during protrusion and motility. *PLoS Genet* 16: e1008694

Kabsch W, Mannherz HG, Suck D, Pai EF, Holmes KC (1990) Atomic structure of the actin: DNase I complex. *Nature* 347: 37-44

Kage F, Doring H, Mietkowska M, Schaks M, Gruner F, Stahnke S, Steffen A, Musken M, Stradal TEB, Rottner K (2022a) Lamellipodia-like actin networks in cells lacking WAVE regulatory complex. *J Cell Sci* 135

Kage F, Döring H, Mietkowska M, Schaks M, Grüner F, Stahnke S, Steffen A, Müsken M, Stradal TEB, Rottner K (2022b) Lamellipodia-like actin networks in cells lacking WAVE regulatory complex. *Journal of Cell Science* 135

Karahan H, Smith DC, Kim B, Dabin LC, Al-Amin MM, Wijeratne HRS, Pennington T, Viana di Prisco G, McCord B, Lin PB *et al* (2021) Deletion of Abi3 gene locus exacerbates neuropathological features of Alzheimer's disease in a mouse model of Aβ amyloidosis. *Sci Adv* 7: eabe3954

Kawasaki T, Kawai T (2014) Toll-like receptor signaling pathways. *Front Immunol* 5: 461

Kerschman J (1939) GENESIS OF MICROGLIA IN THE HUMAN BRAIN. *Archives of Neurology & Psychiatry* 41: 24-50

Kettenmann H, Hanisch UK, Noda M, Verkhratsky A (2011) Physiology of microglia. *Physiol Rev* 91: 461-553

Kettenmann H, Kirchhoff F, Verkhratsky A (2013) Microglia: new roles for the synaptic stripper. *Neuron* 77: 10-18

Kheir WA, Gevrey JC, Yamaguchi H, Isaac B, Cox D (2005) A WAVE2-Abi1 complex mediates CSF-1-induced F-actin-rich membrane protrusions and migration in macrophages. *J Cell Sci* 118: 5369-5379

Kierdorf K, Erny D, Goldmann T, Sander V, Schulz C, Perdiguero EG, Wieghofer P, Heinrich A, Riemke P, Holscher C *et al* (2013) Microglia emerge from erythromyeloid precursors via Pu.1- and Irf8-dependent pathways. *Nat Neurosci* 16: 273-280

Kigerl KA, Gensel JC, Ankeny DP, Alexander JK, Donnelly DJ, Popovich PG (2009) Identification of two distinct macrophage subsets with divergent effects causing either neurotoxicity or regeneration in the injured mouse spinal cord. *J Neurosci* 29: 13435-13444

Kirov G, Gumus D, Chen W, Norton N, Georgieva L, Sari M, O'Donovan MC, Erdogan F, Owen MJ, Ropers HH *et al* (2008) Comparative genome hybridization suggests a role for NRXN1 and APBA2 in schizophrenia. *Hum Mol Genet* 17: 458-465

Kobayashi K, Kuroda S, Fukata M, Nakamura T, Nagase T, Nomura N, Matsuura Y, Yoshida-Kubomura N, Iwamatsu A, Kaibuchi K (1998) p140Sra-1 (specifically Rac1-associated protein) is a novel specific target for Rac1 small GTPase. *J Biol Chem* 273: 291-295

Koestler SA, Rottner K, Lai F, Block J, Vinzenz M, Small JV (2009) F-and G-actin concentrations in lamellipodia of moving cells. *PloS one* 4: e4810

Koizumi S, Shigemoto-Mogami Y, Nasu-Tada K, Shinozaki Y, Ohsawa K, Tsuda M, Joshi BV, Jacobson KA, Kohsaka S, Inoue K (2007) UDP acting at P2Y6 receptors is a mediator of microglial phagocytosis. *Nature* 446: 1091-1095

Konopaske GT, Lange N, Coyle JT, Benes FM (2014) Prefrontal cortical dendritic spine pathology in schizophrenia and bipolar disorder. *JAMA Psychiatry* 71: 1323-1331

Korn ED, Carlier MF, Pantaloni D (1987) Actin polymerization and ATP hydrolysis. *Science* 238: 638-644

Koronakis V, Hume PJ, Humphreys D, Liu T, Hørning O, Jensen ON, McGhie EJ (2011) WAVE regulatory complex activation by cooperating GTPases Arf and Rac1. *Proc Natl Acad Sci U S A* 108: 14449-14454

Kovar DR (2006) Molecular details of formin-mediated actin assembly. *Curr Opin Cell Biol* 18: 11-17

Koyama R, Ikegaya Y (2015) Microglia in the pathogenesis of autism spectrum disorders. *Neuroscience Research* 100: 1-5

Kueh HY, Charras GT, Mitchison TJ, Brieher WM (2008) Actin disassembly by cofilin, coronin, and Aip1 occurs in bursts and is inhibited by barbed-end cappers. *J Cell Biol* 182: 341-353

Kumaravelu P, Hook L, Morrison AM, Ure J, Zhao S, Zuyev S, Ansell J, Medvinsky A (2002) Quantitative developmental anatomy of definitive haematopoietic stem cells/long-term repopulating units (HSC/RUs): role of the aorta-gonad-mesonephros (AGM) region and the yolk sac in colonisation of the mouse embryonic liver. *Development* 129: 4891-4899

Lauffenburger DA, Horwitz AF (1996) Cell migration: a physically integrated molecular process. *Cell* 84: 359-369

Lawson LJ, Perry VH, Gordon S (1992) Turnover of resident microglia in the normal adult mouse brain. *Neuroscience* 48: 405-415

Lehnardt S (2010) Innate immunity and neuroinflammation in the CNS: the role of microglia in Toll-like receptor-mediated neuronal injury. *Glia* 58: 253-263

Lehrman EK, Wilton DK, Litvina EY, Welsh CA, Chang ST, Frouin A, Walker AJ, Heller MD, Umemori H, Chen C *et al* (2018) CD47 Protects Synapses from Excess Microglia-Mediated Pruning during Development. *Neuron* 100: 120-134.e126

Lelli A, Gervais A, Colin C, Chéret C, Ruiz de Almodovar C, Carmeliet P, Krause KH, Boillée S, Mallat M (2013) The NADPH oxidase Nox2 regulates VEGFR1/CSF-1R-mediated microglial chemotaxis and promotes early postnatal infiltration of phagocytes in the subventricular zone of the mouse cerebral cortex. *Glia* 61: 1542-1555

Li X, Zhou W, Yi Z (2022) A glimpse of gender differences in schizophrenia. *Gen Psychiatr* 35: e100823

Liddelow SA, Guttenplan KA, Clarke LE, Bennett FC, Bohlen CJ, Schirmer L, Bennett ML, Münch AE, Chung WS, Peterson TC *et al* (2017) Neurotoxic reactive astrocytes are induced by activated microglia. *Nature* 541: 481-487

Lim SH, Park E, You B, Jung Y, Park AR, Park SG, Lee JR (2013) Neuronal synapse formation induced by microglia and interleukin 10. *PLoS One* 8: e81218

Litschko C, Linkner J, Bruhmann S, Stradal TEB, Reinl T, Jansch L, Rottner K, Faix J (2017) Differential functions of WAVE regulatory complex subunits in the regulation of actin-driven processes. *Eur J Cell Biol* 96: 715-727

Marchand JB, Kaiser DA, Pollard TD, Higgs HN (2001) Interaction of WASP/Scar proteins with actin and vertebrate Arp2/3 complex. *Nat Cell Biol* 3: 76-82

Marie-Anaïs F, Mazzolini J, Herit F, Niedergang F (2016) Dynamin-Actin Cross Talk Contributes to Phagosome Formation and Closure. *Traffic* 17: 487-499

Marín-Teva JL, Cuadros MA, Martín-Oliva D, Navascués J (2011) Microglia and neuronal cell death. *Neuron Glia Biol* 7: 25-40

Marín-Teva JL, Dusart I, Colin C, Gervais A, van Rooijen N, Mallat M (2004) Microglia promote the death of developing Purkinje cells. *Neuron* 41: 535-547

Martinez-Cerdeno V (2017) Dendrite and spine modifications in autism and related neurodevelopmental disorders in patients and animal models. *Dev Neurobiol* 77: 393-404

Massimi M, 2008. Characterization of Profilin2 Complexes in the Mouse.

Matsudaira P (1994) Actin crosslinking proteins at the leading edge. *Semin Cell Biol* 5: 165-174

Matsui H, Ohgomori T, Natori T, Miyamoto K, Kusunoki S, Sakamoto K, Ishiguro N, Imagama S, Kadomatsu K (2013) Keratan sulfate expression in microglia is diminished in the spinal cord in experimental autoimmune neuritis. *Cell Death Dis* 4: e946

McDonough A, Lee RV, Weinstein JR (2017) Microglial Interferon Signaling and White Matter. *Neurochem Res* 42: 2625-2638

McGrath KE, Koniski AD, Malik J, Palis J (2003) Circulation is established in a stepwise pattern in the mammalian embryo. *Blood* 101: 1669-1676

McKercher SR, Torbett BE, Anderson KL, Henkel GW, Vestal DJ, Baribault H, Klemsz M, Feeney AJ, Wu GE, Paige CJ *et al* (1996) Targeted disruption of the PU.1 gene results in multiple hematopoietic abnormalities. *Embo j* 15: 5647-5658

Meucci O, Fatatis A, Simen AA, Miller RJ (2000) Expression of CX3CR1 chemokine receptors on neurons and their role in neuronal survival. *Proc Natl Acad Sci U S A* 97: 8075-8080

Mittelbronn M, Dietz K, Schluesener HJ, Meyermann R (2001) Local distribution of microglia in the normal adult human central nervous system differs by up to one order of magnitude. *Acta Neuropathol* 101: 249-255

Miyamoto A, Wake H, Ishikawa AW, Eto K, Shibata K, Murakoshi H, Koizumi S, Moorhouse AJ, Yoshimura Y, Nabekura J (2016) Microglia contact induces synapse formation in developing somatosensory cortex. *Nature Communications* 7: 12540

Miyamoto A, Wake H, Moorhouse AJ, Nabekura J (2013) Microglia and synapse interactions: fine tuning neural circuits and candidate molecules. *Front Cell Neurosci* 7: 70

Mizutani M, Pino PA, Saederup N, Charo IF, Ransohoff RM, Cardona AE (2012) The fractalkine receptor but not CCR2 is present on microglia from embryonic development throughout adulthood. *J Immunol* 188: 29-36

Moreau-Gachelin F (1994) Spi-1/PU.1: an oncogene of the Ets family. *Biochimica et Biophysica Acta (BBA) - Reviews on Cancer* 1198: 149-163

Morgan JT, Chana G, Pardo CA, Achim C, Semendeferi K, Buckwalter J, Courchesne E, Everall IP (2010) Microglial activation and increased microglial density observed in the dorsolateral prefrontal cortex in autism. *Biol Psychiatry* 68: 368-376

Mosser CA, Baptista S, Arnoux I, Audinat E (2017) Microglia in CNS development: Shaping the brain for the future. *Prog Neurobiol* 149-150: 1-20

Mullins RD, Heuser JA, Pollard TD (1998) The interaction of Arp2/3 complex with actin: nucleation, high affinity pointed end capping, and formation of branching networks of filaments. *Proc Natl Acad Sci U S A* 95: 6181-6186

Mylvaganam S, Freeman SA, Grinstein S (2021) The cytoskeleton in phagocytosis and macropinocytosis. *Curr Biol* 31: R619-R632

Naito M, Takahashi K, Nishikawa S (1990) Development, differentiation, and maturation of macrophages in the fetal mouse liver. *J Leukoc Biol* 48: 27-37

Napoli I, Mercaldo V, Boyl PP, Eleuteri B, Zalfa F, De Rubeis S, Di Marino D, Mohr E, Massimi M, Falconi M *et al* (2008) The fragile X syndrome protein represses activity-dependent translation through CYFIP1, a new 4E-BP. *Cell* 134: 1042-1054

Navascués J, Calvente R, Marín-Teva JL, Cuadros MA (2000) Entry, dispersion and differentiation of microglia in the developing central nervous system. *An Acad Bras Cienc* 72: 91-102

Newton K, Dixit VM (2012) Signaling in innate immunity and inflammation. *Cold Spring Harb Perspect Biol* 4

Nguyen PT, Dorman LC, Pan S, Vainchtein ID, Han RT, Nakao-Inoue H, Taloma SE, Barron JJ, Molofsky AB, Kheirbek MA *et al* (2020) Microglial Remodeling of the Extracellular Matrix Promotes Synapse Plasticity. *Cell* 182: 388-403.e315

Nguyen TTM, Gillet G, Popgeorgiev N (2021) Caspases in the Developing Central Nervous System: Apoptosis and Beyond. *Front Cell Dev Biol* 9: 702404

Nikodemova M, Kimyon RS, De I, Small AL, Collier LS, Watters JJ (2015) Microglial numbers attain adult levels after undergoing a rapid decrease in cell number in the third postnatal week. *J Neuroimmunol* 278: 280-288

Nimmerjahn A, Kirchhoff F, Helmchen F (2005) Resting microglial cells are highly dynamic surveillants of brain parenchyma in vivo. *Science* 308: 1314-1318

Nishida H, Okabe S (2007) Direct astrocytic contacts regulate local maturation of dendritic spines. *J Neurosci* 27: 331-340

Noroozi R, Omrani MD, Sayad A, Taheri M, Ghafouri-Fard S (2018) Cytoplasmic FMRP interacting protein 1/2 (CYFIP1/2) expression analysis in autism. *Metabolic Brain Disease* 33: 1353-1358

Novak IL, Slepchenko BM, Mogilner A (2008) Quantitative analysis of G-actin transport in motile cells. *Biophys J* 95: 1627-1638

Oguro-Ando A, Rosensweig C, Herman E, Nishimura Y, Werling D, Bill BR, Berg JM, Gao F, Coppola G, Abrahams BS *et al* (2015) Increased CYFIP1 dosage alters cellular and dendritic morphology and dysregulates mTOR. *Mol Psychiatry* 20: 1069-1078

Orkin SH, Zon LI (2008) Hematopoiesis: an evolving paradigm for stem cell biology. *Cell* 132: 631-644

Özer I, 2020. Analyzing the Role of CyFIP2 in the Mouse Brain.

Palis J, Robertson S, Kennedy M, Wall C, Keller G (1999) Development of erythroid and myeloid progenitors in the yolk sac and embryo proper of the mouse. *Development* 126: 5073-5084

Paolicelli RC, Bolasco G, Pagani F, Maggi L, Scianni M, Panzanelli P, Giustetto M, Ferreira TA, Guiducci E, Dumas L *et al* (2011) Synaptic pruning by microglia is necessary for normal brain development. *Science* 333: 1456-1458

Paolicelli RC, Ferretti MT (2017) Function and Dysfunction of Microglia during Brain Development: Consequences for Synapses and Neural Circuits. *Front Synaptic Neurosci* 9: 9

Park H, Staehling-Hampton K, Appleby MW, Brunkow ME, Habib T, Zhang Y, Ramsdell F, Liggitt HD, Freie B, Tsang M *et al* (2008) A point mutation in the murine Hem1 gene reveals an essential role for Hematopoietic protein 1 in lymphopoiesis and innate immunity. *J Exp Med* 205: 2899-2913

Parker EM, Sweet RA (2017) Stereological Assessments of Neuronal Pathology in Auditory Cortex in Schizophrenia. *Front Neuroanat* 11: 131

Parkhurst CN, Yang G, Ninan I, Savas JN, Yates JR, 3rd, Lafaille JJ, Hempstead BL, Littman DR, Gan WB (2013) Microglia promote learning-dependent synapse formation through brain-derived neurotrophic factor. *Cell* 155: 1596-1609

Pathania M, Davenport EC, Muir J, Sheehan DF, Lopez-Domenech G, Kittler JT (2014) The autism and schizophrenia associated gene CYFIP1 is critical for the maintenance of dendritic complexity and the stabilization of mature spines. *Transl Psychiatry* 4: e374

Perry VH, Hume DA, Gordon S (1985) Immunohistochemical localization of macrophages and microglia in the adult and developing mouse brain. *Neuroscience* 15: 313-326

Piccinini AM, Midwood KS (2010) DAMPening inflammation by modulating TLR signalling. *Mediators Inflamm* 2010

Pils S, Kopp K, Peterson L, Delgado Tascon J, Nyffenegger-Jann NJ, Hauck CR (2012) The adaptor molecule Nck localizes the WAVE complex to promote actin polymerization during CEACAM3-mediated phagocytosis of bacteria. *PLoS One* 7: e32808

Platanias LC (2005) Mechanisms of type-I- and type-II-interferon-mediated signalling. *Nature Reviews Immunology* 5: 375-386

Pollard TD (2016) Actin and Actin-Binding Proteins. *Cold Spring Harb Perspect Biol* 8

Pollard TD, Borisy GG (2003) Cellular motility driven by assembly and disassembly of actin filaments. *Cell* 112: 453-465

Prinz M, Priller J (2014) Microglia and brain macrophages in the molecular age: from origin to neuropsychiatric disease. *Nat Rev Neurosci* 15: 300-312

Qualmann B, Kessels MM (2009) New players in actin polymerization – WH2-domain-containing actin nucleators. *Trends in Cell Biology* 19: 276-285

Raftopoulou M, Hall A (2004) Cell migration: Rho GTPases lead the way. *Dev Biol* 265: 23-32

Ransohoff RM (2016) A polarizing question: do M1 and M2 microglia exist? *Nature Neuroscience* 19: 987-991

Rasmussen I, Pedersen LH, Byg L, Suzuki K, Sumimoto H, Vilhardt F (2010) Effects of F/G-actin ratio and actin turn-over rate on NADPH oxidase activity in microglia. *BMC Immunology* 11: 44

Reemst K, Noctor SC, Lucassen PJ, Hol EM (2016) The Indispensable Roles of Microglia and Astrocytes during Brain Development. *Front Hum Neurosci* 10: 566

Reinke M, 2021. Profilin 2 threonine 90 phosphorylation: a regulatory mechanism.

Remedios CGD, Chhabra D, Kekic M, Dedova IV, Tsubakihara M, Berry DA, Nosworthy NJ (2003) Actin Binding Proteins: Regulation of Cytoskeletal Microfilaments. *Physiological Reviews* 83: 433-473

Rezaie P, Male D (2002) Mesoglia & microglia–a historical review of the concept of mononuclear phagocytes within the central nervous system. *Journal of the History of the Neurosciences* 11: 325-374

Rice RA, Pham J, Lee RJ, Najafi AR, West BL, Green KN (2017) Microglial repopulation resolves inflammation and promotes brain recovery after injury. *Glia* 65: 931-944

Ricotti L, das Neves RP, Ciofani G, Canale C, Nitti S, Mattoli V, Mazzolai B, Ferreira L, Menciassi A (2014) Boron nitride nanotube-mediated stimulation modulates F/G-actin ratio and mechanical properties of human dermal fibroblasts. *Journal of Nanoparticle Research* 16: 2247

Ridley AJ (2011) Life at the leading edge. *Cell* 145: 1012-1022

Ridley AJ, Schwartz MA, Burridge K, Firtel RA, Ginsberg MH, Borisy G, Parsons JT, Horwitz AR (2003) Cell migration: integrating signals from front to back. *Science* 302: 1704-1709

Romero S, Le Clainche C, Didry D, Egile C, Pantaloni D, Carlier MF (2004) Formin is a processive motor that requires profilin to accelerate actin assembly and associated ATP hydrolysis. *Cell* 119: 419-429

Rottner K, Hänisch J, Campellone KG (2010) WASH, WHAMM and JMY: regulation of Arp2/3 complex and beyond. *Trends Cell Biol* 20: 650-661

Rottner K, Stradal TEB, Chen B (2021) WAVE regulatory complex. *Curr Biol* 31: R512-R517

Rotty JD, Brighton HE, Craig SL, Asokan SB, Cheng N, Ting JP, Bear JE (2017) Arp2/3 Complex Is Required for Macrophage Integrin Functions but Is Dispensable for FcR Phagocytosis and In Vivo Motility. *Dev Cell* 42: 498-513 e496

Rotty JD, Wu C, Bear JE (2013) New insights into the regulation and cellular functions of the ARP2/3 complex. *Nature Reviews Molecular Cell Biology* 14: 7-12

Rougerie P, Miskolci V, Cox D (2013) Generation of membrane structures during phagocytosis and chemotaxis of macrophages: role and regulation of the actin cytoskeleton. *Immunol Rev* 256: 222-239

Sachs NA, Sawa A, Holmes SE, Ross CA, DeLisi LE, Margolis RL (2005) A frameshift mutation in Disrupted in Schizophrenia 1 in an American family with schizophrenia and schizoaffective disorder. *Mol Psychiatry* 10: 758-764

Saller E, Tom E, Brunori M, Otter M, Estreicher A, Mack DH, Iggo R (1999) Increased apoptosis induction by 121F mutant p53. *Embo j* 18: 4424-4437

Santos AM, Calvente R, Tassi M, Carrasco MC, Martín-Oliva D, Marín-Teva JL, Navascués J, Cuadros MA (2008) Embryonic and postnatal development of microglial cells in the mouse retina. *J Comp Neurol* 506: 224-239

Sauer A, Stanton J, Hans S, Grabrucker A (2021) Autism Spectrum Disorders: Etiology and Pathology. In: AMEthology G. (ed.)Exon Publications: Brisbane (AU):

Schafer DP, Lehrman EK, Heller CT, Stevens B (2014) An engulfment assay: a protocol to assess interactions between CNS phagocytes and neurons. *J Vis Exp*

Schafer Dorothy P, Lehrman Emily K, Kautzman Amanda G, Koyama R, Mardinly Alan R, Yamasaki R, Ransohoff Richard M, Greenberg Michael E, Barres Ben A, Stevens B (2012) Microglia Sculpt Postnatal Neural Circuits in an Activity and Complement-Dependent Manner. *Neuron* 74: 691-705

Schafer DP, Stevens B (2015) Microglia Function in Central Nervous System Development and Plasticity. *Cold Spring Harb Perspect Biol* 7: a020545

Schaks M, Singh SP, Kage F, Thomason P, Klünemann T, Steffen A, Blankenfeldt W, Stradal TE, Insall RH, Rottner K (2018) Distinct Interaction Sites of Rac GTPase with WAVE Regulatory Complex Have Non-redundant Functions in Vivo. *Curr Biol* 28: 3674-3684.e3676

Schenck A, Bardoni B, Moro A, Bagni C, Mandel JL (2001) A highly conserved protein family interacting with the fragile X mental retardation protein (FMRP) and displaying selective interactions with FMRP-related proteins FXR1P and FXR2P. *Proc Natl Acad Sci U S A* 98: 8844-8849

Schulz C, Gomez Perdiguero E, Chorro L, Szabo-Rogers H, Cagnard N, Kierdorf K, Prinz M, Wu B, Jacobsen SE, Pollard JW *et al* (2012) A lineage of myeloid cells independent of Myb and hematopoietic stem cells. *Science* 336: 86-90

Scott-Hewitt N, Perrucci F, Morini R, Erreni M, Mahoney M, Witkowska A, Carey A, Faggiani E, Schuetz LT, Mason S *et al* (2020) Local externalization of phosphatidylserine mediates developmental synaptic pruning by microglia. *Embo j* 39: e105380

Sekar A, Bialas AR, de Rivera H, Davis A, Hammond TR, Kamitaki N, Tooley K, Presumey J, Baum M, Van Doren V *et al* (2016) Schizophrenia risk from complex variation of complement component 4. *Nature* 530: 177-183

Sellers JR (2000) Myosins: a diverse superfamily. *Biochim Biophys Acta* 1496: 3-22

Sellgren CM, Gracias J, Watmuff B, Biag JD, Thanos JM, Whittredge PB, Fu T, Worringer K, Brown HE, Wang J *et al* (2019) Increased synapse elimination by microglia in schizophrenia patient-derived models of synaptic pruning. *Nature Neuroscience* 22: 374-385

Shutova M, Yang C, Vasiliev JM, Svitkina T (2012) Functions of nonmuscle myosin II in assembly of the cellular contractile system. *PLoS One* 7: e40814

Sierra A, Abiega O, Shahraz A, Neumann H (2013) Janus-faced microglia: beneficial and detrimental consequences of microglial phagocytosis. *Front Cell Neurosci* 7: 6

Sierra A, de Castro F, Del Rio-Hortega J, Rafael Iglesias-Rozas J, Garrosa M, Kettenmann H (2016) The "Big-Bang" for modern glial biology: Translation and comments on Pio del Rio-Hortega 1919 series of papers on microglia. *Glia* 64: 1801-1840

Silva AI, Haddon JE, Ahmed Syed Y, Trent S, Lin TE, Patel Y, Carter J, Haan N, Honey RC, Humby T *et al* (2019) Cyfip1 haploinsufficient rats show white matter changes, myelin thinning, abnormal oligodendrocytes and behavioural inflexibility. *Nat Commun* 10: 3455

Smolders S, Smolders SM, Swinnen N, Gärtner A, Rigo JM, Legendre P, Brône B (2015) Maternal immune activation evoked by polyinosinic:polycytidylic acid does not evoke microglial cell activation in the embryo. *Front Cell Neurosci* 9: 301

Smolders SM, Kessels S, Vangansewinkel T, Rigo JM, Legendre P, Brône B (2019) Microglia: Brain cells on the move. *Prog Neurobiol* 178: 101612

Sokolowski JD, Chabanon-Hicks CN, Han CZ, Heffron DS, Mandell JW (2014) Fractalkine is a "find-me" signal released by neurons undergoing ethanol-induced apoptosis. *Front Cell Neurosci* 8: 360

Sorokin SP, Hoyt RF, Jr., Blunt DG, McNelly NA (1992) Macrophage development: II. Early ontogeny of macrophage populations in brain, liver, and lungs of rat embryos as revealed by a lectin marker. *Anat Rec* 232: 527-550

Spittau B, Dokalis N, Prinz M (2020) The Role of TGFβ Signaling in Microglia Maturation and Activation. *Trends Immunol* 41: 836-848

Stahnke S, Doring H, Kusch C, de Gorter DJJ, Dutting S, Guledani A, Pleines I, Schnoor M, Sixt M, Geffers R *et al* (2021) Loss of Hem1 disrupts macrophage function and impacts migration, phagocytosis, and integrin-mediated adhesion. *Curr Biol* 31: 2051-2064 e2058

Stefansson H, Rujescu D, Cichon S, Pietiläinen OPH, Ingason A, Steinberg S, Fossdal R, Sigurdsson E, Sigmundsson T, Buizer-Voskamp JE *et al* (2008) Large recurrent microdeletions associated with schizophrenia. *Nature* 455: 232-236

Stefansson H, Steinthorsdottir V, Thorgeirsson TE, Gulcher JR, Stefansson K (2004) Neuregulin 1 and schizophrenia. *Ann Med* 36: 62-71

Steffen A, Faix J, Resch GP, Linkner J, Wehland J, Small JV, Rottner K, Stradal TE (2006) Filopodia formation in the absence of functional WAVE- and Arp2/3-complexes. *Mol Biol Cell* 17: 2581-2591

Steffen A, Rottner K, Ehinger J, Innocenti M, Scita G, Wehland J, Stradal TE (2004) Sra-1 and Nap1 link Rac to actin assembly driving lamellipodia formation. *Embo j* 23: 749-759

Stöcker S, 2015. Function of the Cytoplasmic FMRP interacting protein 1.

Suetsugu S, Yamazaki D, Kurisu S, Takenawa T (2003) Differential Roles of WAVE1 and WAVE2 in Dorsal and Peripheral Ruffle Formation for Fibroblast Cell Migration. *Developmental Cell* 5: 595-609

Sun HQ, Wooten DC, Janmey PA, Yin HL (1994) The actin side-binding domain of gelsolin also caps actin filaments. Implications for actin filament severing. *J Biol Chem* 269: 9473-9479

Suraneni P, Fogelson B, Rubinstein B, Noguera P, Volkmann N, Hanein D, Mogilner A, Li R (2015) A mechanism of leading-edge protrusion in the absence of Arp2/3 complex. *Mol Biol Cell* 26: 901-912

Suraneni P, Rubinstein B, Unruh JR, Durnin M, Hanein D, Li R (2012) The Arp2/3 complex is required for lamellipodia extension and directional fibroblast cell migration. *J Cell Biol* 197: 239-251

Suwankitwat N, Libby S, Liggitt HD, Avalos A, Ruddell A, Rosch JW, Park H, Iritani BM (2021) The actin-regulatory protein Hem-1 is essential for alveolar macrophage development. *Journal of Experimental Medicine* 218

Svitkina TM, Borisy GG (1999) Arp2/3 complex and actin depolymerizing factor/cofilin in dendritic organization and treadmilling of actin filament array in lamellipodia. *J Cell Biol* 145: 1009-1026

Swanson JA, Johnson MT, Beningo K, Post P, Mooseker M, Araki N (1999) A contractile activity that closes phagosomes in macrophages. *J Cell Sci* 112 (Pt 3): 307-316

Takenawa T, Suetsugu S (2007) The WASP-WAVE protein network: connecting the membrane to the cytoskeleton. *Nat Rev Mol Cell Biol* 8: 37-48

Taylor SE, Morganti-Kossmann C, Lifshitz J, Ziebell JM (2014) Rod microglia: a morphological definition. *PLoS One* 9: e97096

Thion MS, Ginhoux F, Garel S (2018) Microglia and early brain development: An intimate journey. *Science* 362: 185-189

Tremblay ME, Lowery RL, Majewska AK (2010) Microglial interactions with synapses are modulated by visual experience. *PLoS Biol* 8: e1000527

Trepat X, Chen Z, Jacobson K (2012) Cell migration. *Compr Physiol* 2: 2369-2392

Truman LA, Ford CA, Pasikowska M, Pound JD, Wilkinson SJ, Dumitriu IE, Melville L, Melrose LA, Ogden CA, Nibbs R *et al* (2008) CX3CL1/fractalkine is released from apoptotic lymphocytes to stimulate macrophage chemotaxis. *Blood* 112: 5026-5036

Tur-Gracia S, Martinez-Quiles N (2021) Emerging functions of cytoskeletal proteins in immune diseases. *J Cell Sci* 134

Uhlen M, Fagerberg L, Hallstrom BM, Lindskog C, Oksvold P, Mardinoglu A, Sivertsson A, Kampf C, Sjostedt E, Asplund A *et al* (2015) Proteomics. Tissue-based map of the human proteome. *Science* 347: 1260419

Uruno T, Liu J, Zhang P, Fan Y, Egile C, Li R, Mueller SC, Zhan X (2001) Activation of Arp2/3 complex-mediated actin polymerization by cortactin. *Nat Cell Biol* 3: 259-266

Uzman A (2001) Molecular Cell Biology (4th edition): Harvey Lodish, Arnold Berk, S. Lawrence Zipursky, Paul Matsudaira, David Baltimore and James Darnell; Freeman & Co., New York, NY, 2000, 1084 pp., list price $102.25, ISBN 0-7167-3136-3. *Biochemistry and Molecular Biology Education* 29: 126-128

Veenstra-Vanderweele J, Christian SL, Cook EH, Jr. (2004) Autism as a paradigmatic complex genetic disorder. *Annu Rev Genomics Hum Genet* 5: 379-405

Verstraelen P, Garcia-Diaz Barriga G, Verschuuren M, Asselbergh B, Nuydens R, Larsen PH, Timmermans JP, De Vos WH (2020) Systematic Quantification of Synapses in Primary Neuronal Culture. *iScience* 23: 101542

Vidal-Itriago A, Radford RAW, Aramideh JA, Maurel C, Scherer NM, Don EK, Lee A, Chung RS, Graeber MB, Morsch M (2022) Microglia morphophysiological diversity and its implications for the CNS. *Front Immunol* 13: 997786

Vilhardt F (2005) Microglia: phagocyte and glia cell. *Int J Biochem Cell Biol* 37: 17-21

Wake H, Moorhouse AJ, Jinno S, Kohsaka S, Nabekura J (2009) Resting microglia directly monitor the functional state of synapses in vivo and determine the fate of ischemic terminals. *J Neurosci* 29: 3974-3980

Wakselman S, Béchade C, Roumier A, Bernard D, Triller A, Bessis A (2008) Developmental neuronal death in hippocampus requires the microglial CD11b integrin and DAP12 immunoreceptor. *J Neurosci* 28: 8138-8143

Wassink TH, Piven J, Patil SR (2001) Chromosomal abnormalities in a clinic sample of individuals with autistic disorder. *Psychiatr Genet* 11: 57-63

Watson AES, de Almeida MMA, Dittmann NL, Li Y, Torabi P, Footz T, Vetere G, Galleguillos D, Sipione S, Cardona AE *et al* (2021) Fractalkine signaling regulates oligodendroglial cell genesis from SVZ precursor cells. *Stem Cell Reports* 16: 1968-1984

Weaver AM, Karginov AV, Kinley AW, Weed SA, Li Y, Parsons JT, Cooper JA (2001) Cortactin promotes and stabilizes Arp2/3-induced actin filament network formation. *Current Biology* 11: 370-374

Wegner A (1976) Head to tail polymerization of actin. *J Mol Biol* 108: 139-150

Weinhard L, di Bartolomei G, Bolasco G, Machado P, Schieber NL, Neniskyte U, Exiga M, Vadisiute A, Raggioli A, Schertel A *et al* (2018) Microglia remodel synapses by presynaptic trogocytosis and spine head filopodia induction. *Nature Communications* 9: 1228

Welch MD, DePace AH, Verma S, Iwamatsu A, Mitchison TJ (1997) The human Arp2/3 complex is composed of evolutionarily conserved subunits and is localized to cellular regions of dynamic actin filament assembly. *J Cell Biol* 138: 375-384

Weston L, Coutts AS, La Thangue NB (2012) Actin nucleators in the nucleus: an emerging theme. *J Cell Sci* 125: 3519-3527

Wheeler AP, Ridley AJ (2007) RhoB affects macrophage adhesion, integrin expression and migration. *Exp Cell Res* 313: 3505-3516

Whitelaw JA, Swaminathan K, Kage F, Machesky LM (2020) The WAVE Regulatory Complex Is Required to Balance Protrusion and Adhesion in Migration. *Cells* 9

Winder SJ, Ayscough KR (2005) Actin-binding proteins. *Journal of Cell Science* 118: 651-654

Witke W (2004) The role of profilin complexes in cell motility and other cellular processes. *Trends Cell Biol* 14: 461-469

Witke W, Podtelejnikov AV, Di Nardo A, Sutherland JD, Gurniak CB, Dotti C, Mann M (1998) In mouse brain profilin I and profilin II associate with regulators of the endocytic pathway and actin assembly. *Embo j* 17: 967-976

Wong AH, Van Tol HH (2003) Schizophrenia: from phenomenology to neurobiology. *Neurosci Biobehav Rev* 27: 269-306

Wu C, Asokan SB, Berginski ME, Haynes EM, Sharpless NE, Griffith JD, Gomez SM, Bear JE (2012) Arp2/3 is critical for lamellipodia and response to extracellular matrix cues but is dispensable for chemotaxis. *Cell* 148: 973-987

Wu S, Xue R, Hassan S, Nguyen TML, Wang T, Pan H, Xu J, Liu Q, Zhang W, Wen Z (2018) Il34-Csf1r Pathway Regulates the Migration and Colonization of Microglial Precursors. *Developmental Cell* 46: 552-563.e554

Wurm J, Konttinen H, Andressen C, Malm T, Spittau B (2021) Microglia Development and Maturation and Its Implications for Induction of Microglia-Like Cells from Human iPSCs. *Int J Mol Sci* 22

Xiong XY, Liu L, Yang QW (2016) Functions and mechanisms of microglia/macrophages in neuroinflammation and neurogenesis after stroke. *Prog Neurobiol* 142: 23-44

Yamasaki R, Lu H, Butovsky O, Ohno N, Rietsch AM, Cialic R, Wu PM, Doykan CE, Lin J, Cotleur AC *et al* (2014) Differential roles of microglia and monocytes in the inflamed central nervous system. *J Exp Med* 211: 1533-1549

Yan C, Martinez-Quiles N, Eden S, Shibata T, Takeshima F, Shinkura R, Fujiwara Y, Bronson R, Snapper SB, Kirschner MW *et al* (2003) WAVE2 deficiency reveals distinct roles in embryogenesis and Rac-mediated actin-based motility. *Embo j* 22: 3602-3612

Yan M, Collins RF, Grinstein S, Trimble WS (2005) Coronin-1 function is required for phagosome formation. *Mol Biol Cell* 16: 3077-3087

Yona S, Kim KW, Wolf Y, Mildner A, Varol D, Breker M, Strauss-Ayali D, Viukov S, Guilliams M, Misharin A *et al* (2013) Fate mapping reveals origins and dynamics of monocytes and tissue macrophages under homeostasis. *Immunity* 38: 79-91

Yu F, Wang Y, Stetler AR, Leak RK, Hu X, Chen J (2022) Phagocytic microglia and macrophages in brain injury and repair. *CNS Neurosci Ther* 28: 1279-1293

Zeidan J, Fombonne E, Scorah J, Ibrahim A, Durkin MS, Saxena S, Yusuf A, Shih A, Elsabbagh M (2022) Global prevalence of autism: A systematic review update. *Autism Res* 15: 778-790

Zhang Y, Chen K, Sloan SA, Bennett ML, Scholze AR, O'Keeffe S, Phatnani HP, Guarnieri P, Caneda C, Ruderisch N *et al* (2014a) An RNA-sequencing transcriptome and splicing database of glia, neurons, and vascular cells of the cerebral cortex. *J Neurosci* 34: 11929-11947

Zhang Y, Chen K, Sloan SA, Bennett ML, Scholze AR, O'Keeffe S, Phatnani HP, Guarnieri P, Caneda C, Ruderisch N *et al* (2014b) An RNA-Sequencing Transcriptome and Splicing Database of Glia, Neurons, and Vascular Cells of the Cerebral Cortex. *The Journal of Neuroscience* 34: 11929-11947

Zhang Y, Kang H, Lee Y, Kim Y, Lee B, Kim JY, Jin C, Kim S, Kim H, Han K (2018) Smaller Body Size, Early Postnatal Lethality, and Cortical Extracellular Matrix-Related Gene Expression Changes of Cyfip2-Null Embryonic Mice. *Front Mol Neurosci* 11: 482

Zhang Y, Sloan SA, Clarke LE, Caneda C, Plaza CA, Blumenthal PD, Vogel H, Steinberg GK, Edwards MS, Li G *et al* (2016) Purification and Characterization of Progenitor and Mature Human Astrocytes Reveals Transcriptional and Functional Differences with Mouse. *Neuron* 89: 37-53

Ziebell JM, Taylor SE, Cao T, Harrison JL, Lifshitz J (2012) Rod microglia: elongation, alignment, and coupling to form trains across the somatosensory cortex after experimental diffuse brain injury. *J Neuroinflammation* 9: 247

Zöller T, Schneider A, Kleimeyer C, Masuda T, Potru PS, Pfeifer D, Blank T, Prinz M, Spittau B (2018) Silencing of TGFβ signalling in microglia results in impaired homeostasis. *Nature Communications* 9: 4011

Acknowledgements

First of all, I would like to thank my supervisor Dr. Annett Halle for giving me the opportunity to pursue my PhD in her lab, and for her support and professional guidance throughout this project. I am also thankful to all the members in AG Halle for their companionship and support along this journey. I would like give my thanks to Bertrand Tambe for his enriching scientific contributions and the joy he brought to the group, to Marie Mittag for her expert advice on MotiQ and her consideration for all the colleagues, to Silvia Letmathe for being an amazing student, who was a great help in the project and a joyful companion, to Riccardo Maruccia for the delightful conversations professionally and personally, to Stanislav Kozlov for his scientific input, and to Amr Gabr for the professional discussion and his inspiring spirit in life. I want to also thank our technicians, Yvonne Biederbick for her high quality of work and her assistance in this project, and Eduard Schmidt for optimizing the lab work.

Additionally, I am grateful for the scientific support and valuable input from Prof. Dr. Gabor Petzold and for Dr. Nicole Reichenbach's and Jan Peter's contribution for the synapse imaging and staining. I would like to give my heartfelt gratitude to Nancy El Deiry for her kindness and all the support throughout my PhD journey. On top of that, I want to thank all the friends I have made at DZNE, for the shared memories I deeply cherish.

Second, I would like to express my appreciation to Prof. Dr. Walter Witke for his generous support and guidance in our collaboration, allowing me to perform experiments in his lab, and to his group members for their warm reception and their contribution to this project. I am deeply grateful to Dr. Pietro Pilo Boyl for all the fruitful discussions, his patient guidance in science, and his mentorship which provided me invaluable support in both scientific and personal life. I also extend my thanks to Dr. Carina Beuck for her friendship, her encouragement and the scientific exchanges, and to Dr. Michael Reinke for his experimental suggestions and uplifting conversations. I also thank Melli Jokwitz for her assistance with biochemistry experiments and to Gerda Hetig for sharing her lab bench and assistance in the cryo-sectioning of brain tissues.

Finally, I would like to express my deepest gratitude to my family for their unreserved support in every aspect of my PhD journey. To my husband, Clemens Pollak, I am thankful for his love and always having my back, which empowered me to overcome every challenge. I am also deeply grateful to my parents, my sisters - Naomi and Wendy, and my parents-in-law - Ulrike und Karl-Heinz, for their unconditional love, their encouragement and their believe in me, which has been the source of my strength throughout this journey.